POLYTECHNIC UNIVERSITY OF TURIN

Master's degree in Aerospace Engineering

Master Thesis

Analysis of solar array power-mass budget for a Sunshade concept

Supervisor:
Prof. Dr. rer. nat. Lorenzo Casalino

Candidate:
Leonardo Baso

a.y. 2024/2025

A man's dream will never die
(Marshall D. Teach)

Ringraziamenti

Ho pensato veramente a lungo chi ringraziare o come scrivere questa parte della mia tesi, probabilmente la più personale tra tutte, una delle parti più lette o quella che io sono sempre stato più curioso di leggere nelle tesi degli altri, e forse anche per questo la sto scrivendo per ultima, proprio perchè non volevo sbagliarla.

Quindi per prima cosa ringrazio te che stai leggendo in questo momento perchè se stai tenendo in mano la mia tesi sei sicuramente una persona che devo ringraziare perchè mi sei stato o stata vicina in questo pezzo di vita o in tanti pezzi di vita e questo sicuramente è un tassello importante che aggiungo al mio puzzle.

Probabilmente oggi avrò detto mille volte che non sto realizzando o non mi è chiaro cosa sia successo ancora, visto il cammino intenso che è stato questa magistrale, con momenti di stanchezza in cui mi sono seduto trovando sempre un fuoco caldo e dei canti e delle voci amiche che mi accogliessero, luoghi e persone che ho avuto il dono di poter chiamare casa.

Voglio che sappiate e sentiate davvero che ogni passo lascia la sua impronta, non importa quanto grande o quanto piccola, l'importante è poterle vedere tutte insieme.

Un ringraziamento particolare va a mamma e papà, che mi hanno insegnato il valore della resilienza e della fatica attraverso l'esempio, ma soprattutto che la felicità più grande, che è quella di essere amati, non si guadagna con la fatica, anzi non si guadagna proprio, si riceve e basta.

Vi voglio bene e so che voi siete fieri di me quanto io lo sono di voi.

Il secondo ringraziamento va alla mia seconda famiglia, a tutti i miei amici che negli anni sono arrivato a chiamare fratelli. Siamo cresciuti insieme, nella pioggia a cercare l'arcobaleno e nel buio a guardare le stelle. Sono chi sono grazie a voi, perchè nessuno diventa grande da solo. Non posso scrivere i nomi di tutti ma se ti ho chiamato fratello, fratellino, vecchio bib o bro almeno una volta, sei rappresentato da questa categoria.

Voglio ringraziare Stoccarda e Torino e tutte le persone che ho incontrato lì. Mi hanno accolto in una terra lontana aiutandomi a identificarla come casa. Il freddo e la neve sono stati compagni e amici calorosi lungo l'inverno.

Ringrazio chi si è sorbito i miei "non so niente" prima di ogni esame e mi ha atteso nelle mie assenze e nei miei ritardi, con la pazienza di chi resta.

Ringrazio tutti quelli che mi hanno chiesto "ma quando ti laurei" tenendo la mia testa sulla consapevolezza di questo cammino.

E infine ringrazio Dio, l'Amore o la Bellezza, chiamatelo come volete, che mi ha donato tutto per potermelo godere fino in fondo.

Acknowledgements

I've really been thinking for a long time about who to thank or how to write this part of my thesis. It's probably the most personal of all, one of the most read parts, or the one that I've always been most curious to read in other people's theses. Maybe that's also why I'm writing it last, because I didn't want to get it wrong.

So, first of all, I want to thank you, the reader, because if you're holding my thesis, you're someone I have to thank. You've been a part of my life, or you've been close to me in so many ways, and this piece is an important part of my path.

I probably can't tell you how many times today I've said that I'm still wrapping my head around everything that's happened, especially given the intense journey that has been this master's degree. There have been moments of fatigue where I've sat by a warm fire and found some friendly songs and voices to greet me, places and people that I've been blessed to call home.

I want you to really know and feel that every step leaves its mark, no matter how big or small. The important thing is to be able to see them all together.

I'd like to say a big thank you to Mom and Dad, who taught me the value of resilience and hard work through example, but, most of all, that the greatest happiness, which is to be loved, is not earned through hard work, in fact it is not earned, it is given.

I love you, and I know that you are as proud of me as I am of you.

I'd like to say a big thank you to my second family, all my friends who have become like brothers to me over the years. We grew up together, in the rain looking for the rainbow and in the dark looking at the stars. I am who I am today because of you, because no one grows up alone. I don't remember everyone's names, but if I've ever called you my brother, little brother, old man bib or bro, you're in this category.

I just want to say a big thank you to Stuttgart and Turin, and all the lovely people I met there. They welcomed me to a faraway land by helping me identify it as home. Even though it was cold and snowy, they made it warm and worthwhile.

I want to thank those who put up with my "I don't know anything" before every exam and waited for me in my absences and delays, with the patience of those who stay.

I'm also very grateful to everyone who asked me when I was going to graduate, because it made me think about where I was going in life.

And last but not least, I thank God, Love or Beauty, call it what you will, who stand always by my side and gave me everything I needed to enjoy it to the fullest.

Abstract

The urgent need to find solutions to the problem of climate change has prompted the exploration of large-scale geoengineering solutions, including a planetary sunshade. This space-based system, composed partly of photovoltaic panels and partly of aluminium panels, is designed to reduce the Earth's temperature by 1 K by blocking a fraction of the incoming solar radiation at the Sun-Earth Lagrange point 1 (SEL1). This space construction is designed to give the human population more time to find a lasting and effective climate solution directly on Earth.It differs from traditional space projects because it favors production on the Moon, using the resources that can be found on our satellite instead of those on Earth. This minimizes terrestrial air pollution and launch costs.

It has been conducted a detailed comparative analysis of silicon and perovskite solar cells, evaluating their efficiency, durability and suitability for the space environment. This analysis enabled us to determine the most suitable solar cells for the project in both phases.We have proposed a multi-phase roadmap, with key milestones from 2028 to 2060 and beyond. This roadmap includes lunar infrastructure development, material extraction, panel assembly and deployment via coilgun. A power-to-mass balance model has been developed to assess the energy requirements of each phase and the long-term energy return of the sunshade itself.

The results of the study indicate that in-situ production on the Moon is a viable and more sustainable option when compared with terrestrial production. The number of launches required is significantly reduced compared to previous proposals. However, several critical challenges remain, which would require further investigation, including degradation of the solar cells in space, thermal management, in-orbit sunshade assembly, long-term maintenance of the sunshade at the SEL1 point, and storage of the energy produced. This research, in conjunction with the work conducted by S. Fix and T. Maheswaran, seeks to establish a robust foundation for future studies investigating the feasibility of large-scale space geoengineering projects. It also contributes to the broader discourse on mitigating the climate crisis through innovative aerospace solutions.

Contents

List of symbols

Abbreviations

AIAA	American Institute of Aeronautics and Astronautics
AM	Air Mass
AOCS	Attitude and Orbit Control System
AR5	Fifth Assessment Report
ASTM	American Society for Testing and Materials standard
CNSA	China National Space Administration
DR	Degradation Rate
DSSC	Dye-Sensitized Solar Cell
EML1	Earth-Moon Lagrange Point 1
EML2	Earth-Moon Lagrange Point 2
ESA	European Space Agency
ETL	Electron Transport Layer
ETM	Electron Transport Material
EVA	Ethylene Vinyl Acetate
FF	Fill Factor
FLOAT	Flexible Levitation system on a Track
FTO	Fluorine doped Tin Oxide
GHG	GreenHouse Gasses
HEO	Human Exploration Activities
HTL	Hole Transport Layer
HTM	Hole Transport Material
IPCC	Intergovernmental Panel on Climate Change
ISRO	Indian Space Research Organisation
ISRU	In-Situ Resource Utilization
ITO	Indium doped Tin Oxide
IZO	Indium Zinc Oxide
JSC	Short-Circuit Current Density

LM	Light Management
LSP	Lunar Solar Park
MRE	Molten Regolith Electrolysis
MOE	Molten Oxide Electrolysis
NASA	National Aeronautics and Space Administration
NIAC	Nasa Innovative Advanced Concepts
NR	Natural Rubber
OMHP	Organo-Metal Halide Perovskites
OSC	Organic Solar Cell
OTR	Oxygen Transmission Rate
OxPS	Oxygen Production and Storage
PE3D	Pulsed Electrical Discharge Addictive Manufacturing
PECVD	Plasma-Enhanced Chemical Vapor Deposition
PILS	Photovoltaic Investigation on the Lunar Surface
ppm	parts per million
PSC	Perovskite Solar Cell
PV	Photo-Voltaic
QDSC	Quantum Dot Solar Cell
R2R	Roll to Roll
RCP	Representative Concentration Pathway
RF	Radio Frequency
SEL1	Sun-Earth Lagrange Point 1
S-Q	Shockley-Queisser limit
SRM	Solar Radiation Management
SRP	Solar Radiation Pressure
TRL	Technology Readiness Level
VOC	Open Circuit Voltage
VSAT	Vertical Solar Array Technology
UV	UltraViolet
WVTR	Water Vapor Transmission Rate

Chemical Symbols and Nomenclature

ABS_3	Chalcogenide chemical formula (A: Alkaline earth metal, B: Early transition metal)
AlF_3	Aluminum Fluoride
Al_2O_3	Aluminum Oxide
$BaSnO_3$	Barium Stannate

$BaZrTiS_3$	Barium Zirconium Titanium Trisulfide
$BaZrS_3$	Barium Zirconium Trisulfide - chalcogenide perovskite
$BaHfS_3$	Barium Hafnium Trisulfide - chalcogenide perovskite
$CaTiO_3$	Calcium Titanate
$CdTe$	Cadmium Telluride
CH_4	Methane
CO_2	Carbon Dioxide
$CsSn_{0.5}Ge_{0.5}I_3$	Cesium Tin Germanium Iodide
Cs_2TiX_6	Cesium Titanium Halide Perovskite
Cs_2TiBr_6	Cesium Titanium Bromide
CuI	Copper(I) Iodide
F_2	Fluorine
FeF_3	Iron(III) Fluoride
$GaAs$	Gallium Arsenide
$GaInP_2$	Gallium Indium Phosphide
KF	Potassium Fluoride
$MAPbI_3$	Methylammonium Lead Iodide
PbI_2	Lead(II) Iodide
S	Sulfur
Se	Selenium
Si	Silicon
SiF_4	Silicon Tetrafluoride
SiO_2	Silicon Dioxide
SO_2	Sulphur Dioxide
$SrHfS_3$	Strontium Hafnium Trisulfide
$SrZrS_3$	Strontium Zirconium Trisulfide - chalcogenide perovskite
TiO_2	Titanium Dioxide
ZnO	Zinc Oxide
$ZnO-NP$	Zinc Oxide Nanoparticles
Zn_2SnO_4	Zinc Tin Oxide (ZTO)
$ZnTiO_3$	Zinc Titanate

Constants

AU	Astronomical Unit	km	$1.496 \cdot 10^8$
d_{SEL1}	Sun-Earth L1 distance from Earth	km	$1.588 \cdot 10^6$
h	Planck's costant	Js	$6.626 \cdot 10^{-34}$
k	Boltzmann constant	J/K	$1.380 \cdot 10^{-23}$

q	Electron charge	C	$1.602 \cdot 10^{-19}$
r	Sun-Earth distance	m	$1.496 \cdot 10^{11}$
R_S	Radius of the Sun	km	696340
S	Average Solar Insulation	W/m^2	342.75
T_S	Temperature of the Sun as a black body	K	5800
α_p	Earth albedo		0.313
σ	Stefan-Boltzmann constant	$W/(m^2K^4)$	$5.670 \cdot 10^{-8}$
π	Pi		3.1416

Mathematical and Physical Symbols

A_{sh}	Sunshade Area required
e	Daily Efficiency Loss
f	Fraction of light to be reduced
I	Current produced by a solar cell (Chapter 3)
I	Solar Intensity (Section 3.1.2)
I_L	Photogeneration Current
I_0	Reverse Saturation Current (Chapter 3)
I_0	Solar Intensity at 1 AU (Section 3.1.2)
k	Temperature Coefficient of Efficiency
n	sigmoidicity coefficient
n_{pan}	number of panels
P	Power
Q_c	Flux of Blackbody photons above the Band Gap energy
R_{sh}	Sunshade Radius required
T	Temperature [K]
v	Frequency of Electromagnetic Radiation
V_{oc}	Open Circuit Voltage
α	Absorptivity
ΔS	Reduction in solar insolation due to counter radiative forcing
ϵ	Thermal Emissivity (Section 3.1.2)
ϵ	Power generated by one panel on the Moon (Chapter 6.2)
η	Conversion Efficiency
η_0	Linearly Extrapolated Efficiency
Φ	Work Function of the Material
ϕ	Solar Radiation to be absorbed
Θ	Zenith Angle

Chapter 1: Introduction

In recent years, a significant number of national and international associations, operating both in the public and private spheres, have devoted their efforts to addressing the issue of growing climate problems. This attention stems from the realization that climate change poses an existential threat to the biosphere, the global socioeconomic balance, but mainly the life on our planet. Government organizations, academic institutions and private companies are trying to collaborate to develop innovative solutions that can mitigate the negative effects of global warming and ensure the sustainability of the planet for future generations, but the feeling is that not enough is being done.

The efforts have been driven by the urgent need to identify a common global solution to the damage caused to the Earth by humanity's current lifestyle. Strategies have ranged from reducing greenhouse gas emissions to promoting renewable energy to bolder geoengineering projects. Among these, one of the most innovative and ambitious solution is the Planetary Sunshade, also called Sunshield, a mission designed to reduce Earth's temperature by 1 K by regulating incoming solar radiation, without perceptibly reducing the amount of light reaching our planet.

The Planetary Sunshield is an ambitious project originated by Ross Center from Colorado School of Mines and Uwe Brauer from Boeing. This work is also linked to two other master's theses, Sebastian Fix's, an ESA trainee, Tharshan Maheswaran's, a research assistant at the Institute for Space Systems at the University of Stuttgart. The goal of the project is to create a space sunshade consisting of a series of reflective aluminum panels and high-efficiency photovoltaic panels, to be placed at the Sun-Earth Lagrange Gravitational Equilibrium Point 1 (SEL1). This point, located about 1.5 million kilometers from Earth in the direction of the Sun, offers a unique opportunity to install a structure capable of deflecting a fraction of solar radiation before it reaches the planet to reduce its temperature without affecting the light radiation.

From a geoengineering perspective, the project is distinguished by the choice to produce all components directly in situ on the Moon. The main motivation for this choice lies in the desire to reduce as much as possible the environmental impact and costs associated with launching materials from Earth. Mining and processing lunar resources, such as aluminum and silicon, could enable sustainable production, drastically reducing the need to transport materials through Earth's gravity. The primary goal of the Planetary Sunshade is to lower the global temperature by about 1K, thus providing humanity with a larger window of opportunity to implement definitive

and sustainable solutions against climate change directly on Earth.

In addition to its primary function of temperature regulation, the project has a significant secondary function. Due to its perennial exposure to sunlight, the system could be used for the generation of photovoltaic power intended for laser or microwave transmission to the lunar bases or maybe even to the Earth itself. This additional energy could power critical infrastructure, support maintenance of the system and ensure the efficiency of orbital control maneuvers.

The purpose of this thesis is to analyze a number of fundamental aspects for the design of a planetary solar shield. In particular, the selection of the most suitable type of perovskite cell will be examined, considering parameters such as efficiency, durability, resistance to space conditions, mass and material availability. The research will also include the development of a sustainable power balance model aimed at ensuring the long-term operation of the system. A further part of the study will involve the analysis of the masses involved in the construction and transportation of the system, with a focus on optimizing resources to minimize costs and operational risks.

So my personal contribution to this project will begin with a detailed description of the mission, its needs, technical requirements and engineering constraints. Next, an in-depth analysis will be developed on the types of perovskite cells available and their suitability for space application. At this stage, key aspects such as chemical stability in the space environment, sensitivity to cosmic radiation, and effectiveness in converting solar energy into electricity will be considered.

Another key focus will be the study of potential lunar infrastructure that could support direct production of perovskite cells and other essential system components. Facilities planned for future lunar missions will be examined, as well as technologies that could be exploited to extract and process local resources. Among the facilities analyzed will be those planned under NASA's Artemis program, China's lunar base, and private initiatives such as those of Blue Origin and SpaceX.

Finally, the concluding section will include a comprehensive analysis of the power budget related to all aspects of the mission. It will assess the energy required for the extraction and processing of materials, the energy costs associated with the launch and production processes, the energy requirements of the lunar infrastructure involved, and the energy absorbed and redirected to the Moon or Earth. This study will provide a clear picture of the energy sustainability of the entire project and possible strategies to improve its efficiency.

More complete information about the project and the two master's theses mentioned above can be found on the Planetary Sunshade Foundation website. The contribution of this research is part of a larger context of studies and initiatives aimed at countering the effects of climate change through innovative and technologically advanced solutions. If successfully implemented, the Planetary Sunshade could represent a decisive breakthrough in the fight against global warming, offering a complementary solution to emission reduction and sustainable energy transition strategies.

Chapter 2: Background

The idea of a space-based solar shading system originated as a potentially effective solution for climate change mitigation through Solar Radiation Management (SRM). The research conducted by Sebastian Fix (2021) explored some points of feasibility of a solar umbrella positioned in the vicinity of the Sun-Earth Lagrange point L1 (SEL1), with the goal of reducing the Earth's temperature by approximately 1 K by partially shielding incoming solar radiation. The results indicate that many of the technologies required for building satellites in space and for sustainable lunar exploration are compatible with the realization of a solar shading system, and part of the results to be obtained were used as input for this work. However, there remained some critical challenges related to the choice of which type of solar cells to use and, above all, whether it was energetically feasible and what kind of mass quantities it would involve specifically. In other words, a concrete technological demonstration is required to be able to think about implementing this project on a large scale.

Another key aspect for the realization of the project concerns the logistics of construction and transport of materials. In this regard, Tharshan Maheswaran's (2021) research analyzed the material transfer strategies and construction logistics of a space umbrella in SEL1. The study proposed a roadmap based on past and future lunar exploration missions, outlining optimal trajectories in the Sun-Earth-Moon system by establishing a logistics hub at the Earth-Moon Lagrange Point 2 (EML2). This logistical hub would represent a collection and sorting point for the resources extracted from the Moon prior to their shipment to SEL1. To ensure the efficient transport of the large quantities of materials needed to build the shielding system, the concept of a lunar coilgun, located in the Shackleton crater, is introduced. The thermal environment of the lunar polar region offers ideal conditions for the use of superconductive technologies, reducing the energy consumption of the launch system.

A further key aspect analyzed by Maheswaran concerns the orbital and attitude control of the solar umbrella. To ensure the stability of the system at SEL1, an advanced Attitude and Orbit Control System (AOCS) is required that can compensate for perturbations due to solar radiation pressure and gravitational effects. The research suggests that existing technologies for the control of satellite fleets could be adapted and optimized to ensure the long-term stability of the structure, although this point should certainly be further investigated.

Fix and Maheswaran's research provided a solid basis for the development of the planetary

sunshade concept and for this thesis, demonstrating that a space infrastructure built with lunar resources is technologically feasible in the long term. The combination of in-situ production, advanced lunar logistics and orbital control technologies form the foundation upon which this thesis develops a detailed assessment of the project's practical feasibility.

We now start with a brief background analysis on the climate scenarios, the logistical location of the sunshade and proceed to define some needs, requirements and constraints concerning the mission.

2.1 Climate scenarios

For the planetary Sunshade mission, the different climate scenarios used by the Intergovernmental Panel on Climate Change (IPCC) for the Fifth Assessment Report (AR5) were taken into account. In particular, the following cases of Representative Concentration Pathway (RCP, is a greenhouse gas concentration trajectory) were analyzed:

- **Decrease the earth's temperature by 1 K**: is our case of interest, the parameter on which we try to model the planetary Sunshade in order to gain time to find a stable solution on Earth;

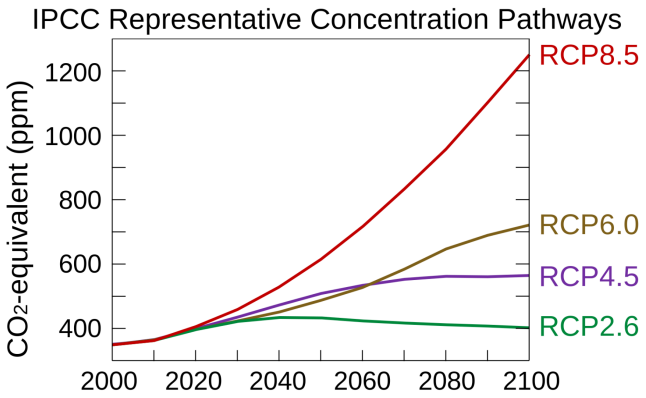

Figure 2.1: Different RCP scenarios result in different GHG concentrations in the atmosphere (from 2000 to 2100)

- **RCP 1.9**: this case is aimed at limiting global warming to a maximum of 1.5 °C, which is the main goal of the Paris Agreement;

- **RCP 2.6**: represents a pathway defined as 'very stringent'. Emissions of carbon dioxide (CO_2) must approach zero by 2100, methane (CH_4) emissions in 2100 must be half of what they were in 2020, and sulphur dioxide (SO_2) emissions must be 10% of what they were in 1980-1990. A CO_2 absorption of 2 Gigatons per year is also required, keeping the increase in the Earth's temperature below 2 °C;

- **RCP 3.4**: it is a middle ground between RCP 2.6 and the less stringent efforts of RCP 4.5. The aim is to reach $2.0-2.4\,^{\circ}C$ by 2100;

- **RCP 4.5**: is a less stringent scenario. Emissions in this case peak around 2040 and then decline. CO_2 emissions decrease from 2040 onwards and fall by half in 2100 (compared to 2050). Methane will need to stop rising in 2050 and fall to 75% of 2040 levels in 2100, while SO_2 emissions will need to fall by around 20% compared to the 1980s-90s. An uptake of 2 Gigatons of CO_2 per year by trees remains confirmed as in RCP 2.6. The rise in mean sea level is 35% higher than in RCP 2.6 and the rise in global temperature is expected to be between 2 and $3\,^{\circ}C$ by 2100. In all likelihood, many species of the animal and plant kingdoms will not be able to adapt to the changes in this climate scenario and those above it;

- **RCP 6.0**: emissions peak is estimated around 2080, then decline. In this scenario, the radiative forcing is stabilized after 2100, with the use of technologies and strategies to reduce GHG emissions. "6.0" stands for W/m^2 of radiative forcing to be achieved by 2100. It predicts continued global warming, with a temperature increase of about $3\text{-}4\,^{\circ}C$ and CO_2 up to 660 ppm;

- **RCP 7.0**: is not really a mitigation objective but more of an outcome;

- **RCP 8.5**: in this scenario, emissions continue to rise uninterruptedly throughout the 21st century. It is the worst case scenario, but fortunately it is also considered less and less plausible every year. It predicts a temperature rise of $4\text{-}5\,^{\circ}C$.

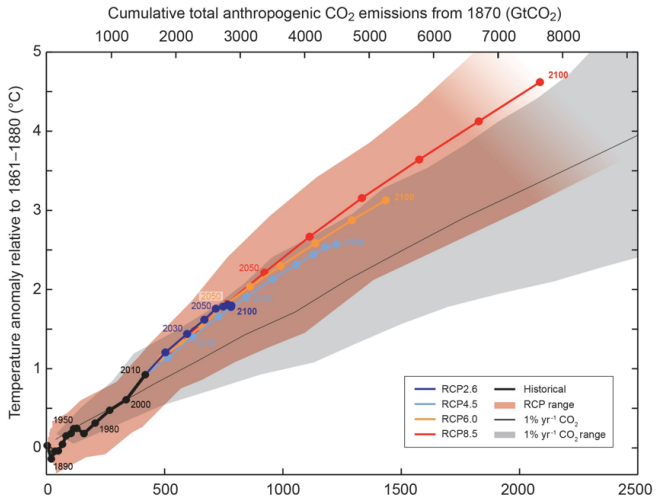

Figure 2.2: Temperature rise in time for the differen RCP scenarios

2.2 Sun-Earth Lagrange Point1

At Lagrange points, the gravitational influence spheres of Hill of the Earth and the Sun are equivalent and create five points of equilibrium. L1, L2 and L3 are unstable equilibrium points, thus requiring small corrections for orbital maintenance, while L4 and L5 are stable points.

For the purpose of this project, L1 point is the most interesting one, because it is the one between Sun and Earth. The L1 point rotates around the Sun with the same angular speed as the Earth, thus allowing a Sunshade to remain in a position where it can casts continuous shade on the Earth just with minor station-keeping maneuvers. The aim of this project is not only to shield solar radiation in order to lower the temperature of the Earth by 1 degree, but also to exploit solar radiation as much as possible as a source of clean and space-based energy that can be used to power possible lunar or Earth infrastructures. When everything will be set and the processes will be running autonomously, it will be almost Earth-independent.

If Solar Radiation Pressure (SRP) were not considered, L1 equilibrium point would be located exactly at $1,5 \cdot 10^6$ km from Earth. For the Sunshade, however, the force exerted by photons impinging on it is not negligible and tends to push it towards the Earth, reducing the gravitational action of the Sun. For this reason, the actual point of equilibrium is shifted Sun-wards, so that a balance between the various forces at work can be found.

Sánchez J-P and McInnes CR in their article say that the optimal position of the Sunshade for the masses calculated would be $2,44 \cdot 10^6$ km from the Earth towards the Sun.

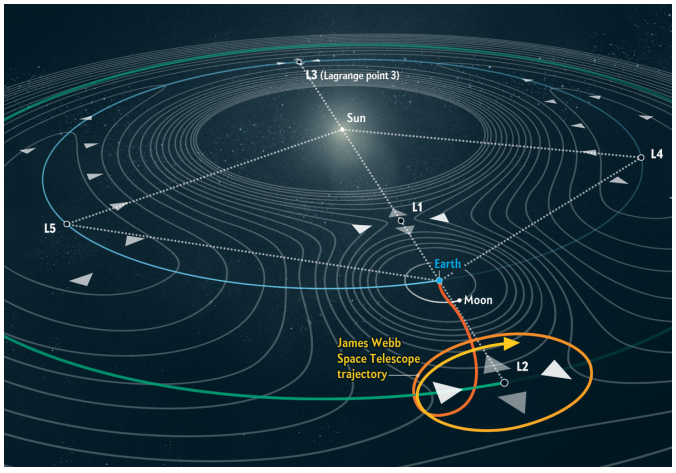

Figure 2.3: Visual illustration of Sun-Earth Lagrange Points and Hill spheres of Sun and Earth

2.3 Mission needs

As with any mission, it is important to analyze the needs before beginning the more detailed study. Some of the general mission needs that are of particular relevance to this thesis are

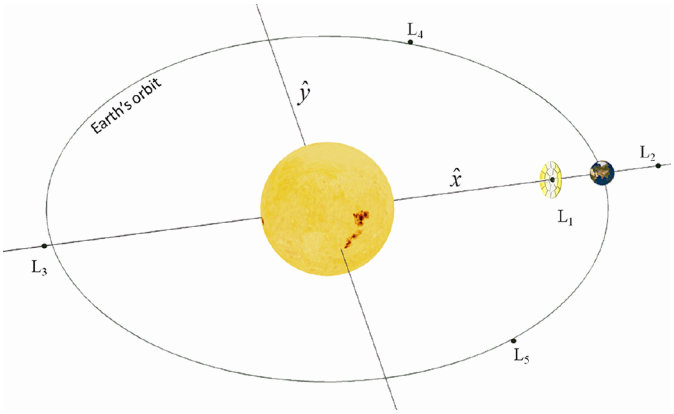

Figure 2.4: Sunshade placed in SEL1

analyzed below.

One of the most important points concerns the energy aspect, which is divided into several more specific subtopics. We need to know the power required to extract the materials for the planetary Sunshade, so that we can make the best use of resources from Earth and on the Moon, to meet the requirements of the chosen climate scenario. Initially, the first launches will have to be carried out from Earth, in order to launch basic materials for the construction of bases and infrastructures on the Moon, as it will be shown later. Therefore another need is identified by the minimum number of launches we will have to do from Earth so that most of the energy associated with the mission to create, launch, assemble, operate and maintain the Sunshade is sustainable. The use of sustainable energy is also relevant for minimizing operating costs in the long term. A further important aspect is energy efficiency: the project must maximize the use of the energy generated, minimize waste and ensure optimal management of energy resources.

So we need to know also the power required to produce and send the Sunshade modules to the Earth-Sun Lagrange point 1 by the lunar coilgun and consequently the model of the growing amount of power we will receive back by the working modules in SEL1. This Power beam back to the Moon is essential for lowering production costs over time, and part of that could also be used as renewable energy back to Earth.

The development of lunar technologies is another fundamental need of this mission, without which it will be impossible to start large-scale production of panels on the Moon itself. It is essential to use materials that effectively reflect solar radiation and materials that absorb it (the choice of perovskite photovoltaic panels will be explained later). Both must have a long service life to ensure that the Sunshade can operate without the need for frequent maintenance or replacement. In addition, the implementation of monitoring systems will be crucial to assess the effectiveness of the shading system and its long-term climate impact. These systems will need to be able to collect and analyze data in real time, allowing operational adjustments to be made to maximize the impact of the project and monitor the health of the Earth's environment.

The third need concerns the economic aspects of the project. It is imperative that the cost of producing and launching the sunshade is affordable to ensure the feasibility of the project. The cost analysis must consider not only the initial investment, but also the long-term operating expenses. In addition, it will be important to establish a clear return on investment by assessing the economic benefits of reduced costs associated with potential climate change damages, such as agricultural losses and recovery costs from avoided natural disasters. Investing in solutions that directly address climate problems could, in fact, lead to significant savings for governments and communities around the world. A cost-benefit analysis will be a determining factor in obtaining the necessary financial support and ensuring the economic viability of the project.

2.4 Mission requirements

One of the main, and probably most complex, requirements will be to guarantee a lifetime of at least 15 years for these panels. Solar cells are subject to a great deal of wear and tear in space, as we will see in the next chapter, so it is necessary to ensure their long-term efficiency. The other, but probably more expensive, option is to continuously replace the panels in orbit. There are different types of solar cells and the focus of this thesis will be on the Silicon and Perovskite ones. Silicon solar cells have been used during the years, but the technology of the Perovskite ones seems to be much more promising.

A part of the material will have to be mined from lunar soil (or maybe from asteroids, but this part will not be developed in this Master Thesis), and this is a fundamental requirement to ensure the green and environmentally sustainable progression of the project. Otherwise, it would pollute and increase Earth's temperature more than it could lower it by shielding it from solar radiation, no longer respecting the settlements reached by the Paris Climate Agreement.

The materials used in the production of solar cells must be as clean as possible, which is why some of them have been ruled out, since even if they were able to provide greater efficiency, or have already been widely tested, their production would create an unsustainable increase in the Earth's temperature.

Another fundamental requirement for the realization of the mission are political collaboration between the different countries and continents, because the salvation of our planet is not and can never be elitist knowledge, but must be born of a common effort of resources, research and money.

Other important requirements are certainly the energy efficiency of the panels, the use of renewable energy and the use of a specific type of launcher (analysed below). Real-time monitoring systems will be required to ensure the continuous effectiveness of the Sunshade.

Finally, the importance of economic requirements is that an upper limit is placed on expenditure and that a positive payback is demonstrated within a certain number of years from the start of the mission.

2.5 Mission constraints

The most important constraint of this mission is undoubtedly the timing. There is an urgent need for action to change the climate situation we are experiencing. For the project to be viable, it needs to be implemented by 2060.

The most pressing time constraint of this mission is undoubtedly the urgency of action to mitigate the effects of climate change. For the project to have a significant impact, it must be completed by 2060. However, this deadline requires precise planning and a structured roadmap that allows for the gradual implementation of the necessary technologies.

The first key milestone is set for 2028, when Phase 1: Technology Development will begin. During this initial phase, the first panels that can be rolled out from Earth will be launched, using the Starship as a transport vehicle. At the same time, the necessary infrastructure for the establishment of the lunar bases will be launched in accordance with the Artemis project. Once this infrastructure is in place and operational on the lunar surface, the process of extracting and separating local materials, such as silicon, from the lunar soil will begin. This phase marks the beginning of the technology development required to build the solar sunshade and supporting infrastructure, laying the foundation for the future operation of the entire system.

The second phase, called Phase 2: Lunar Demonstration, is planned for 2035. During this phase, locally manufactured photovoltaic panels will begin to be assembled on the Moon. In parallel, assembly of the panels that will make up the sunshield will begin. This demonstration phase will be crucial to test the effectiveness of the in-situ assembly and production processes and to verify the operational feasibility of the large-scale project.

In 2045, the mission will enter Phase 3: L1 Production Ramp-Up, which will mark the start of full-scale production and the positioning of the panels in the Lagrange area of SEL1. This phase will see the activation of the Lunar Coilgun, an advanced technology that will allow the panels to be launched directly into SEL1. Once in orbit, the panels will be assembled and the attitude and orbit control mechanisms required to keep the panels in the correct position and at the optimum angle to maximize system efficiency will be activated. In addition to shading the Earth, the photovoltaic panels, once operational, will be able to absorb solar energy and transfer it as electricity to the Moon or Earth via laser transfer through microwaves, generating additional energy return.

From 2060, with the start of Phase 4: Orbit, the system will reach a stable state of energy equilibrium. Once the sunshield assembly is complete and operations have stabilized, regular maintenance of the system will begin, including the repair or replacement of malfunctioning or worn panels. Work will also be carried out on the orbital and lunar infrastructure to ensure the longevity and efficiency of the system. This phase marks the transition to stable and continuous operations management, which is necessary to maintain the integrity of the project and maximize the climate and energy benefits of the solar sunshade.

Another fundamental constraint on this project concerns the environmental impact of the

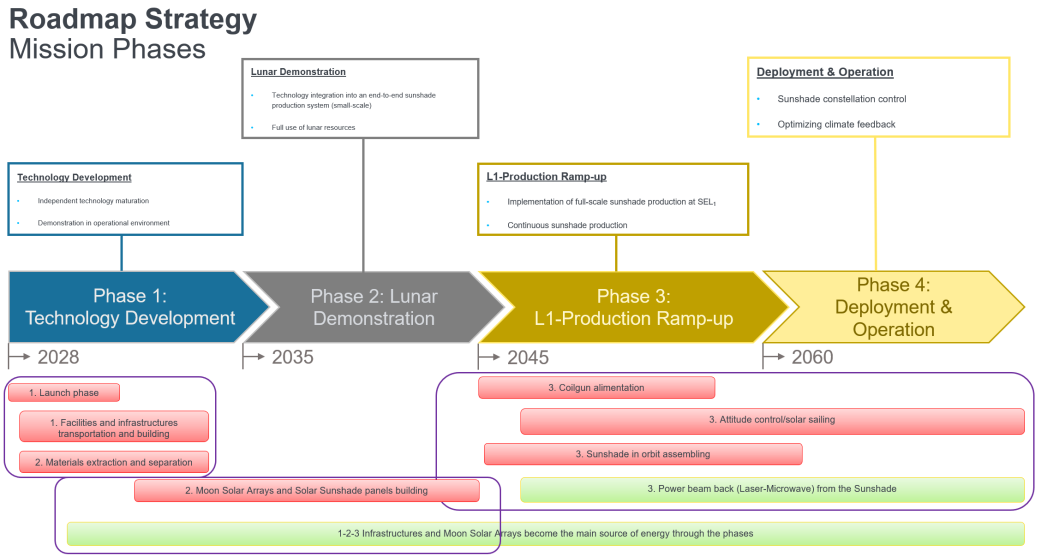

Figure 2.5: Timeline strategy: processes requiring energy are in red, processes generating energy are in green

activities associated with the production and launch of the solar Sunshade. As the project is designed to be a sustainable solution to climate change, it is imperative that emissions and pollution from the production and logistics processes, including the transport of the necessary materials from Earth to the Moon, are kept to a minimum. The transfer of resources for the construction, assembly and subsequent positioning of the Sunshade at the Lagrange point SEL1 must be carried out according to strict criteria of energy efficiency and minimization of environmental impact.

For example, launching a fully loaded spacecraft from Earth to the Moon has a significant energy impact. SpaceX's Starship, with a payload capacity of about 100 tonnes in low Earth orbit, requires a fuel consumption of about 1,200 tonnes of liquid oxygen and methane for a single launch. This results in the release of greenhouse gases into the atmosphere, as methane (CH_4) is a hydrocarbon and although less polluting than conventional fuels, it still produces CO_2 when burned. A Starship launch is estimated to have a climate impact of several hundred tonnes of CO_2 equivalent, in addition to other effects such as local temperature increases in the upper troposphere and stratosphere.

Therefore, despite the use of more advanced technologies than conventional rockets, a large number of launches required to transport materials could neutralize the expected climate benefits of solar shading. It is therefore crucial to integrate production and launch strategies that use advanced low-emission technologies, recyclable or low-impact materials, and minimize the number of launches required by maximizing the use of locally available resources, such as lunar material for possible structural parts. This would avoid the paradox of worsening the global cli-

mate situation by releasing more emissions into the Earth's atmosphere than the Solar Sunshade is designed to reduce.

Chapter 3: Solar cells

Photovoltaics is one of the most innovative and promising technologies for generating electricity from renewable sources. It is based on the principle of the direct conversion of sunlight into electricity through the photoelectric effect, a physical phenomenon that has revolutionized our understanding of the interaction between light and matter. Over the last few decades, PV has played a central role in the global energy transition due to its ability to provide clean and sustainable energy, helping to reduce greenhouse gas emissions and mitigate climate change. This technology is characterized by the simplicity of the conversion process and the absence of moving parts, making it reliable and requiring minimal maintenance.

The photoelectric effect, the basis of solar cell operation, was discovered in the late 19th century and first observed by Heinrich Hertz in 1887. However, it was Albert Einstein who, in 1905, was able to explain the phenomenon theoretically using a quantum approach and introduced the concept of the photon. Einstein hypothesized that light is composed of discrete quanta of energy and that the absorption of these quanta by the electrons of a material could cause them to be emitted from the surface of the material. This theory, for which Einstein received the Nobel Prize in Physics in 1921, challenged classical beliefs about the wave nature of light and laid the foundation for the development of quantum mechanics.

The energy of a photon is described by the equation

$$E = hv$$

where h is Planck's constant ($6.626 \cdot 10^{-34}$ Js) and v is the frequency of electromagnetic radiation. When a photon strikes a semiconductor material such as silicon, the photon's energy is transferred to an electron. If this energy is sufficient to overcome the work function of the material (Φ), the electron is ejected, as described by the equation

$$E_k = hv - \Phi$$

The photoelectric effect demonstrates that the interaction between light and matter is not continuous but quantized, allowing light to be converted directly into electrical current.

Photovoltaic panels exploit this physical principle through the use of solar cells, which are solid-state devices made primarily from semiconductor materials such as monocrystalline, poly-

crystalline or amorphous silicon. Photovoltaic cells consist of a p-n junction, which is achieved by doping semiconductors with impurities that change the concentration of free charges in the material. In the p-layer, doping introduces acceptors that create electron gaps, while in the n-layer donors are introduced that provide free electrons. An internal electric field is created at the interface between the two layers, which acts as a potential barrier.

When sunlight strikes the surface of the cell, photons with energy above the forbidden band of the semiconductor excite electrons from the valence band to the conduction band, creating electron-junction pairs. The internal electric field of the p-n junction separates these charges: electrons are pushed towards the n-layer, while holes migrate towards the p-layer. This movement of charges creates a potential difference at the ends of the cell and, if an external circuit is connected, a direct current flows.

The electrical behavior of a photovoltaic cell is described by the diode equation

$$I = I_L - I_0(e^{qV/kT} - 1)$$

which summarises the relationship between the current and voltage produced by the cell. In this equation, I_L represents the photogeneration current, which is proportional to the incident light intensity, while I_0 is the reverse saturation current, a parameter that depends on the properties of the semiconductor material and the operating temperature. The constant q indicates the electron charge ($1.602 \cdot 10^{-19}$ C), while k is the Boltzmann constant and T the absolute temperature in Kelvin.

The first applications of photovoltaic cells date back to the 1950s, when they were developed to power artificial satellites. The space environment required an autonomous, reliable and lightweight power source, and photovoltaics offered an ideal solution due to its ability to generate electricity directly from sunlight without the need for fuel. In the years since, advances in materials research and manufacturing techniques have led to significant efficiency gains and cost reductions, enabling large-scale deployment on Earth.

Today, photovoltaics is one of the most widely used renewable energy technologies, used in both small-scale installations, such as residential rooftops, and large-scale solar power plants. The continuous development of new materials, such as perovskites, and innovations in cell architecture are pushing the limits of efficiency and opening up new perspectives for the integration of photovoltaics in urban and industrial environments. Solar power is therefore not only a response to the growing demand for sustainable energy, but also an ever-evolving frontier of scientific research.

In order to ensure that the Sunshade project functions properly, we must first be sure that we are working with cells that can provide the project with the best safety and success. All solar cells provide clean energy, but some have higher efficiency and much lower production costs. To date, research has mostly focused on silicon (Si) solar cells, with more than 90% of the solar panels on the market using silicon as one of their main components. As their theoretical efficiency limit is

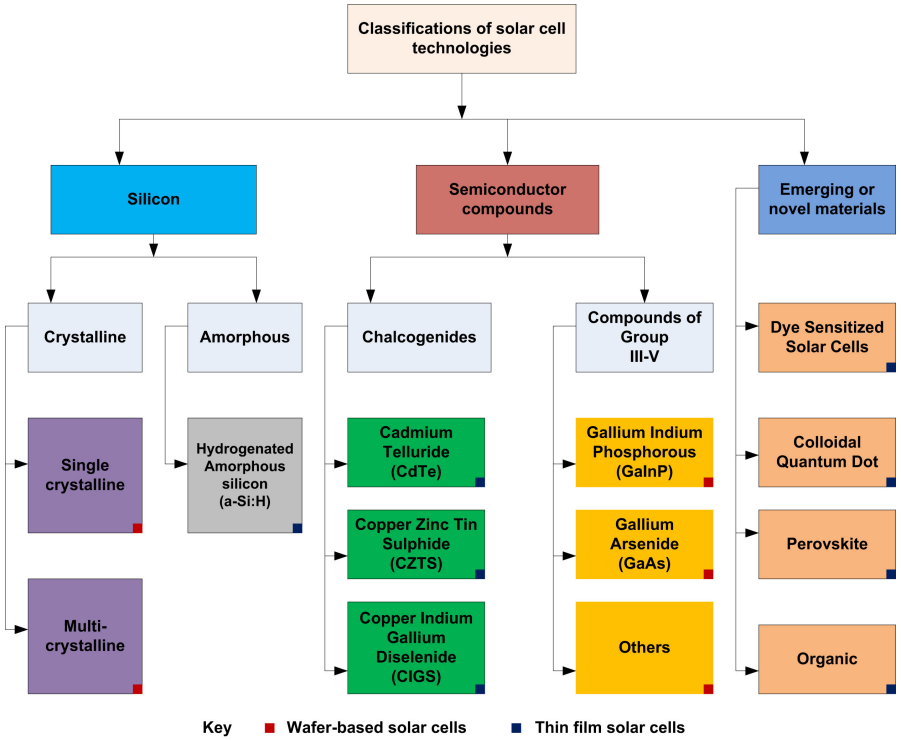

Figure 3.1: Classification of solar cells based on the primary active material

being reached faster and faster, research is now moving on to other cell types.

The direction in which research is moving is undoubtedly that of hybrid perovskitic solar cells. They are called hybrid perovskites because they are composed of organic cations and inorganic cage structures. Development and research on these new cell types is proceeding so fast that conversion efficiencies of up to 25% have been achieved in just ten years. Unfortunately, however, they have serious problems of intrinsic stability when subjected to light illumination, heat (around 100 °C) and even when exposed to air.

This is why new research has been carried out by the *Gifu University* and the *Tokyo Institute of Technology* [7]. Studies are focusing on alternative materials, such as perovskite chalcogenide materials. Chalcogenide represents group-VI atoms, such as sulphur (S) and selenium (Se), and its chemical formula is ABS_3, where A indicates an alkaline earth metal and B an early transition metal.

In [6] is illustrated the fabrication of chalcogenide perovskite alloys containing $BaZrTiS_3$. The maximum theoretical efficiency achievable by this material is astonishing, reaching as high as 38% in Perovskite/Si tandem solar cell architecture. The presence of BaZrTiS3 allows the band gap to be adjusted to a more appropriate value (approximately 1.6 eV).

However, in general, all chalcogenide perovskites, such as $BaZrS_3$, $SrZrS_3$, $BaHfS_3$, and $SrHfS_3$, show great light absorption with a strength exceeding $10^5 cm^{-1}$, which is much higher

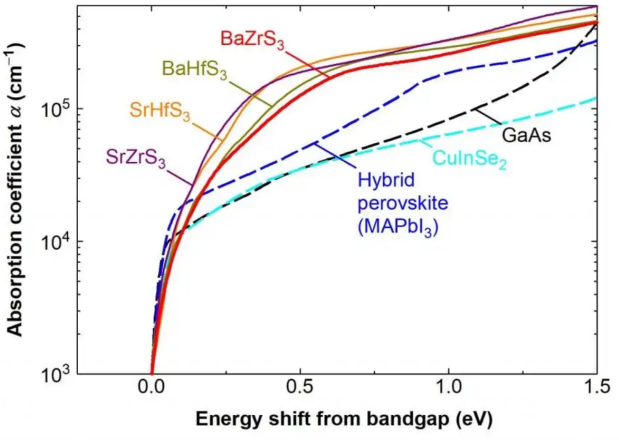

Figure 3.2: Light absorption coefficients of newly fabricated chalcogenide perovskites

than any other existing solar cell material (Fig. 3.2). Thanks to these absorption characteristics, it is possible to create ultra-thin solar cells, facilitating the collection of electrons and holes. This will also increase the final conversion efficiency. This absorption appears to originate from the presence of the unique sulfur orbitals formed in the perovskite structures. The good news is, above all, that these chalcogenic perovskites are composed only of non-toxic elements and therefore, thanks to their stability and superior optical properties, will have a major impact on the future of solar cells. The technology on which the most effort should be put at the moment is the one allows the development of the ultra-thin film. When this too is ready, solar panels will be able to enter a large-scale mass production cycle.

Two main types of solar cells were identified for use in the development of this project. The first is the use of silicon solar cells, while the second is the use of a tandem Perovskite/Si (chalcogenide) architecture together with printable perovskite, for which various studies are continuing.

3.1 Space environment issues

The space environment has always been rightly regarded as one of the most challenging environments in which not only to survive but also to develop technologies and test their functioning. The space environment is not an environment open to life. However, mankind has always been attracted to challenges, and space is one of the greatest challenges we face. For our time, it represents a dream that needs to become reality.

With particularly regard to the production and maintenance of solar panels in SEL1, we face certain challenges.

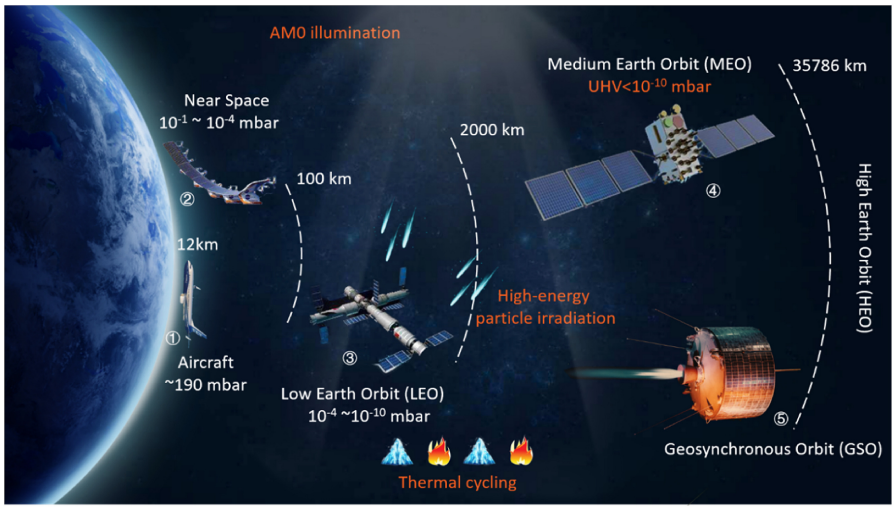

Figure 3.3: UV radiation

3.1.1 Light instability

The first major obstacle (and perhaps the most difficult one) is the stability of solar cells in space.

The first question to ask is the lifetime of a solar cell in space. The minimum lifetime to ensure stability and avoid continuous production of solar cells over time is 15-20 years.

Related to light, the most important parameter for PV solar cells is the Air Mass. It is the path that light takes through the atmosphere, normalized to the shortest possible path (i.e. when the sun is directly overhead) and it is a measure of the reduction in the power of light as it passes through the atmosphere and is absorbed by air and dust. Its formula is:

$$AM = \frac{1}{cos(\Theta)}$$

Solar cells for extraterrestrial use are generally characterized by air mass zero (AM0) solar spectrum. The "0" means that no atmosphere is passed, so the spectrum is the pure spectrum coming from the Sun, neither disturbed nor filtered by the Earth's atmosphere.

Unlike AM1.5G, used for terrestrial applications, AM0 contains larger amounts of UV radiation. A UV filter could protect the PSC more or less easily on Earth, but the problem is that in space applications each addition means more weight at launch and therefore an additional cost in terms of mission.

The UV instability of PSCs arises from the photo-catalysis of inorganic metal oxides, and UV-B radiation (310-317 nm) has been declared more harmful than UV-A (360-380 nm).

Molecular oxygen in the atmosphere has always been thought to be involved in the UV degradation of TiO_2-based PSCs. Oxygen uptake and desorption at oxygen vacancy sites in TiO_2

create deep-level traps that lead to charge recombination and consequently also to photo-current degradation. Studies by Ji et al. have recently revealed the presence of a detailed two-stage UV degradation process of PSCs even in the presence of an inert atmosphere, supporting the possibility that the oxygen-free space environment is the harbor.

In order to avoid such processes (Ti^{3+} defects are transformed into Ti^{4+} due to charge recombination with UV-generated holes in the valence band of TiO_2 and the increase in these defects - Ti^{4+}, leads to the oxidation of I^- and consequently to the irreversible degradation of perovskites with the formation of I_2 or polyiodide I_3), which can also occur with other metal oxides depending on their photocatalysis capacity, the use of UV-inert materials such as Al_2O_3, Zn_2SnO_4, La-doped $BaSnO_3$, $ZnTiO_3$, etc. becomes essential.

Even so, the changes in efficiency of these materials-based PSCs are more than 10% after exposure to only a few hundred hours of UV radiation, which is very little compared to a space mission and, theoretically, the energy of photons in the UV range could be high enough to break chemical bonds in organic materials (especially polymers).

The wavelength of radiation in space can be as short as 120 nm (American Society for Testing and Materials standard: ASTM E490) and with such a high excitation energy, both the stability of the perovskite and the organic charge extraction layers remain unclear.

The studies reported not only highlight the role of conductive holes in the UV stability of PSCs but also indicate the current paucity of information on understanding the mechanism of UV degradation of a complete device.

3.1.2 Temperature range

Another essential component to be considered in the application of perovskitic solar cells is the temperature range.

The application of the space Sunshade is very specific from this point of view, as it requires thermal control without shadowing. The sunshield will always be exposed to direct solar radiation.

However, some studies have been carried out on certain types of solar cells for use in space. They have to pass a thermal cycling test (American Institute of Aeronautics and Astronautics, AIAA S-111A-2014) before being qualified for use in space: extreme cold with temperatures as low as $-185\,°C$ and extreme heat up to $150\,°C$.

The main damage is not caused by high or low temperature, but is dominated by the mechanical component. Inter-facial delamination is the dominant effect in the performance degradation during the different cycles, as the thermal expansion coefficients of the different layers of the device are different. Robust encapsulation is therefore required to prevent this type of damage.

Nevertheless, the effects of extreme temperature ranges on the efficiency of perovskitic solar cells must be considered. High temperatures, such as those exceeding $100\,°C$ in direct sunlight, can lead to significant degradation of the perovskite structure, including ion migration and loss of crystalline stability. This reduces the open circuit voltage (V_{oc}) due to increased non-radiative

recombination, causing a significant drop in efficiency over time.

Conversely, extremely low temperatures, such as those found in shaded space environments (down to $-150\,^{\circ}\mathrm{C}$ or lower), initially reduce ion mobility, potentially improving stability. However, prolonged exposure to such conditions introduces thermo-mechanical stress due to differential thermal expansion between layers. This can lead to micro-fractures or delamination, further contributing to performance degradation.

Studies suggest that perovskitic solar cells typically exhibit peak efficiency at moderate temperatures (between 25 and $50\,^{\circ}\mathrm{C}$), while deviations outside this range (whether heating or cooling) lead to efficiency loss. In the space environment, repeated thermal cycling between extreme temperatures exacerbates these problems, requiring advanced thermal management strategies. These include the use of protective coatings, heat dissipation systems and thermally stabilizing interfaces to minimize damage and maintain cell performance. One solution is to use materials with high band-gaps, such as gallium arsenide (GaAs), which are less sensitive to temperature changes compared to silicon-based cells. Additionally, thermal management techniques, such as heat shields and radiators, can be used to dissipate excess heat and maintain the cells within an optimal temperature range.

The decomposition reaction of a typical mixed perovskite starts at the surface followed by gradual permeation into the bulk, which originates from the intrinsic dangling bonds and defects on the imperfect surface.

Therefore, thermostable perovskites with a passivated surface are much sought after (e.g. emerging inorganic caesium-based perovskites can be stable above $300\,^{\circ}\mathrm{C}$ and two-dimensional layered perovskites up to about $200\,^{\circ}\mathrm{C}$). It has been shown that to improve thermal stability it is very useful to remove the organic hole conductors and to use carbon electrodes.

Cheacharoen et al. conducted comparative tests between two commonly used encapsulants, Ethylene Vinyl Acetate (EVA) and Surlyn. The use of polyolefin with an external butyl rubber seal maintained efficiency between $-40\,^{\circ}\mathrm{C}$ and $85\,^{\circ}\mathrm{C}$ after 200 cycles, which is a good start.

High-performance encapsulation materials must exhibit:

- Low oxygen and moisture permeability, quantified by the Oxygen Transmission Rate (OTR) and Water Vapor Transmission Rate (WVTR), respectively.
- High transparency ($>90\%$) to ensure efficient light absorption.
- Mechanical flexibility and strong adhesion to minimize delamination risks.
- Resistance to UV degradation and thermal oxidation.

The PCE degradation rate (DR) of encapsulated PSCs can be expressed empirically as:

$$\mathrm{DR} = \frac{\mathrm{DR}_{\max} \cdot \mathrm{WVTR}^{n}}{\mathrm{WVTR}_{50}^{n} + \mathrm{WVTR}^{n}}$$

where $\mathrm{DR}_{\max}$ is the maximum degradation rate, WVTR_{50} is the WVTR value at 50% degradation, and n is a sigmoidicity coefficient.

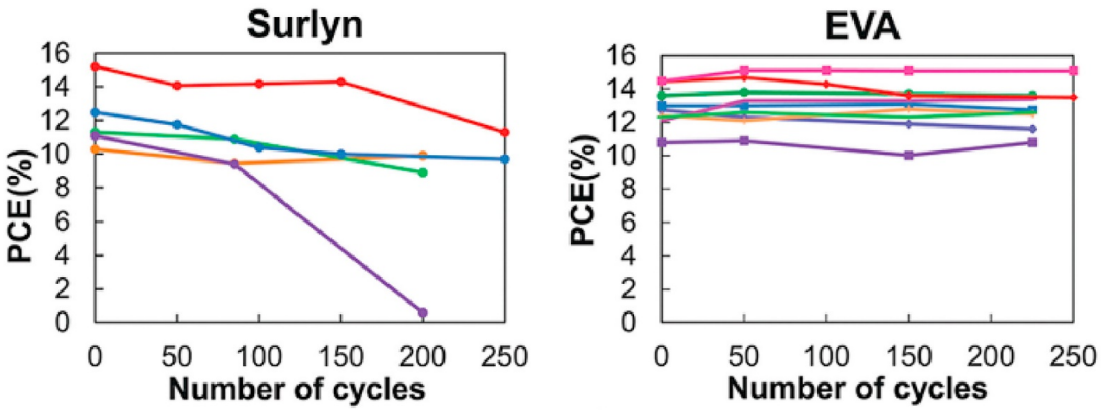

Figure 3.4: Power Conversion Efficiency Percentage (PCE%) in function of the number of cycles for two different types of coating

High-Temperature and Efficiency Challenges The operating temperature (in Kelvin) of a solar cell in space is determined by a balance between the absorbed solar radiation and the thermal radiation emitted by the cell. This is governed by a relationship that depends on the intensity of the incident sunlight, the absorptivity of the cell, and its emissivity, derived from the radiative balance:

$$\alpha I = (\epsilon_f + \epsilon_r)\sigma T^4$$

For simplicity, the absorptivity α is defined as the total energy absorbed by the system, including a factor of $(1 - \eta)$ to account for the portion of the incoming energy that is converted into electricity is not emitted by the cell as radiation. The thermal emissivity is defined by ϵ and the subscripts r and f indicate the emissivity from both the front and rear sides of the solar cell. The Stefan-Boltzmann constant is indicated by σ. Thus the equilibrium operating temperature is:

$$T = \left(\frac{\alpha}{(\epsilon_f + \epsilon_r)\sigma} I\right)^{\frac{1}{4}} = cI^{1/4}, \text{ where } c = \left(\frac{\alpha}{(\epsilon_f + \epsilon_r)\sigma}\right)^{\frac{1}{4}}$$

The intensity I depends on the distance from the Sun and its formula is:

$$I = \frac{I_0}{r^2}$$

where I_0 is the solar intensity at 1 AU (Sun-Earth distance) and r is the distance measured in AU.

The temperature coefficient of efficiency is defined as

$$k = \frac{d\eta}{dT}$$

where η is the conversion efficiency. At high temperatures, solar cells experience a decrease in

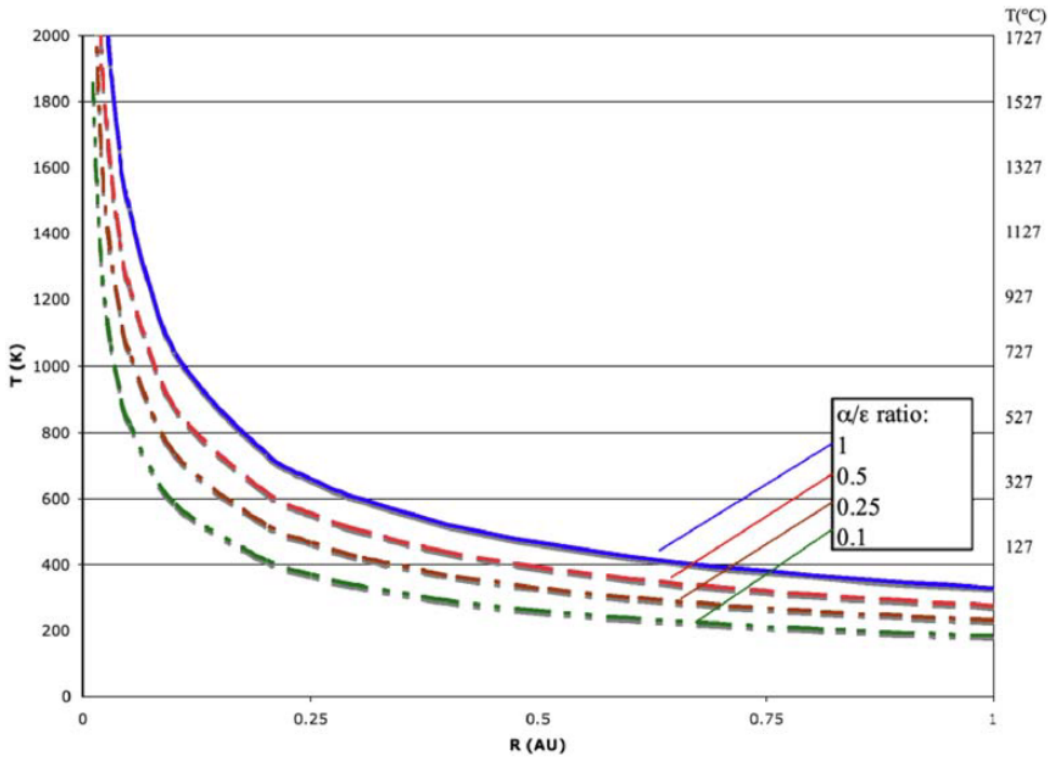

Figure 3.5: Temperature as a function of the solar distance for various α/ϵ ratio, NASA

efficiency due to the negative temperature coefficient of the power output, indeed by a linear extrapolation the power can be compared to the power output from a reference temperature (300 K):

$$P = (\eta_{300K} + k\Delta T)I, \text{ where } \Delta T = T - 300$$

Defining η_0 as the linearly extrapolated efficiency at 0K:

$$\eta_0 = \eta_{300K} - 300k$$

Resulting:

$$P = (\eta_0 + 300k + kT - 300k)I = (\eta_0 + kcI^{1/4})I = I\eta_0 + kcI^{5/4}$$

As the temperature increases, the conversion efficiency of the cells drops. This phenomenon is a result of the increased thermal energy causing electron-hole recombination in the photovoltaic material, reducing the number of charge carriers available for electricity generation.

For any specific solar cell technology, there is a certain incident intensity beyond which the output of the solar cell begins to decline as the intensity increases. In the linear model presented

this intensity is defined as follows:

$$I_{\text{peak-output}} = \left(- \frac{\eta_0}{kc} \right)^4$$

Starting from the basic principles of semiconductor diodes and the relationship between the band-gap and the temperature coefficient, it is possible to estimate how the bandgap of a solar cell influences its efficiency at different temperatures. Figure 3.6 illustrates this effect for a standard single-junction solar cell. As shown, efficiency decreases as the temperature rises. Additionally, it is important to note that the ideal bandgap increases with higher operating temperatures. This is because solar cells with a larger band-gap maintain a higher open-circuit voltage and experience smaller voltage losses as the temperature increases.

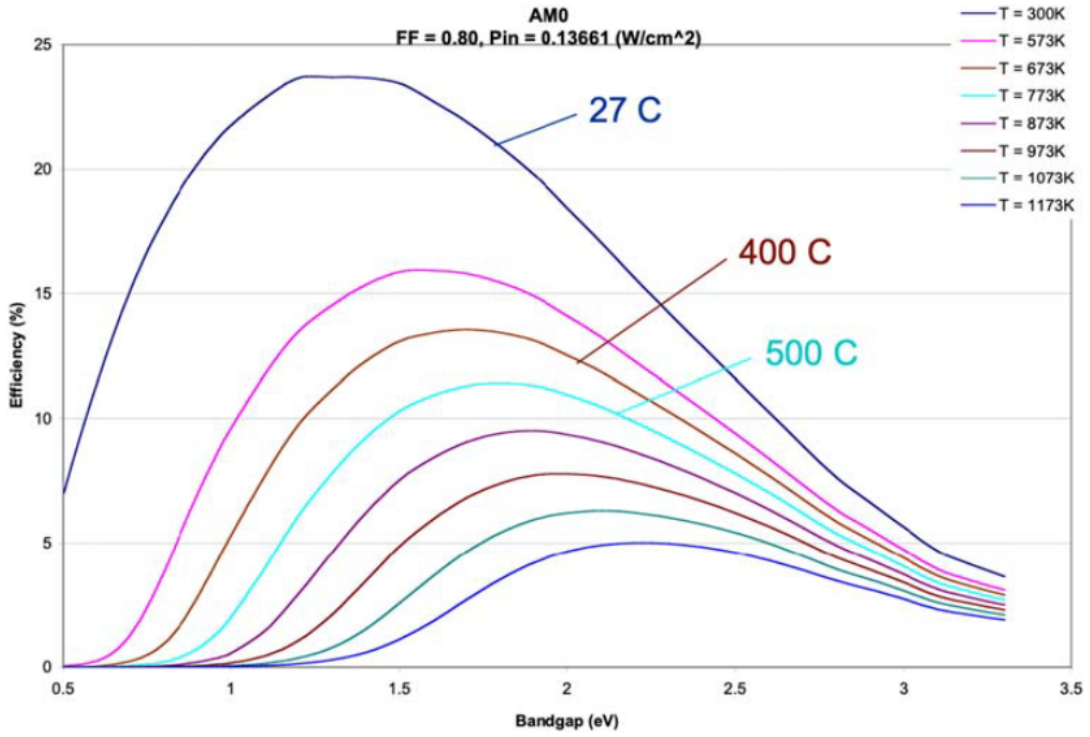

Figure 3.6: Modeled efficiency of a single-junction solar cell as a function of the semiconductor band-gap, for temperatures ranging from 27 to 900 °C, NASA

Innovative Solutions for High-Temperature Environments Several innovative solutions have been proposed to mitigate the temperature-related challenges faced by solar arrays in extreme environments. One key approach involves using high-epsilon, low-alpha coatings on solar cells. These coatings increase the emissivity of the cells while minimizing their absorptivity, helping to reflect excess sunlight and reduce the thermal load on the array.

Another technique is array off-pointing, where the solar array is tilted away from direct sunlight to reduce the incident flux. This method is particularly effective for spacecraft operating in close proximity to the Sun, such as the Parker Solar Probe. By adjusting the angle of the array relative to the Sun, the intensity of sunlight absorbed by the cells can be reduced, thereby lowering the operating temperature and enhancing the overall efficiency of the solar array.

Furthermore, partially populated arrays, where some solar cells are replaced with reflective mirrors, have been used to manage thermal load. These mirrors redirect sunlight away from the solar cells, reducing the amount of heat absorbed by the array. Spectrally selective coatings are also employed to reflect infrared wavelengths that do not contribute to electricity generation, thereby reducing the overall thermal load on the array.

3.1.3 High vacuum

The last additional challenge caused by the space environment is the presence of high vacuum. Many of the materials characteristic of perovskite are volatile. For this reason, the molecules may undergo outgassing once in a vacuum. In doing so, they tend to settle on the cold surface during the thermal cycle, contaminating and affecting the properties of sensitive optics.

Perovskite films generally undergo much more violent degradation under UHV (almost 10^{-9} Torr) than at normal pressure.

Similar phenomena have been observed in more sensitive two-dimensional perovskite films, indicating that vacuum acts as a catalyst during degradation and causes outgassing.

For example, recent studies have highlighted the significant impact of vacuum conditions on the structural integrity and performance of PSCs, especially mixed halide perovskite materials such as $(MAPbBr_3)_{0.17}$ $(FAPbI_3)_{0.83}$[1] (MAFA) [2].

Under vacuum, PSCs undergo severe lattice shrinkage and light-induced phase segregation, resulting in the degradation of their crystalline structure. These structural changes include the segregation of the perovskite layer into a minority $FAPbI_3$ phase and a dominant mixed MAFA phase. This phase segregation is driven by a thermodynamic imbalance, which is more likely to occur in vacuum due to the lower activation energy barrier for lattice strain. The vacuum environment exacerbates strain in the perovskite lattice, resulting in the formation of coherent phase boundaries and grain boundaries due to fractured crystallites. These defects accelerate

[1] $FAPbI_3$ is a perovskite consisting of formamidinium iodide (FAI) and lead iodide (PbI_2). This phase is referred to as a 'minority' phase because it is found in smaller quantities than other phases, such as MAFA, in the material. $FAPbI_3$ has advantageous optical and electronic properties, but can be unstable if not combined with other components, particularly in harsh environments such as vacuum. When phase segregation occurs, small amounts of $FAPbI_3$ separate from the main phase (MAFA) and tend to form separate crystals, leading to stability problems.

[2] The MAFA phase is a mixed perovskite composed of methylammonium bromide (MABr), formamidinium iodide (FAI) and lead iodide (PbI_2). It is called 'mixed' because it contains both methylammonium (MA) and formamidinium (FA) cations, and 'dominant' because it forms the majority of the solar cell's active material. The advantage of the mixed phase is that it offers a combination of structural stability and optical and electronic performance that is superior to the single $FAPbI_3$ phase. However, under extreme conditions such as vacuum, even the MAFA phase can suffer degradation due to phenomena such as phase segregation and crystal lattice shrinkage.

the degradation process by promoting non-radiative recombination pathways and increasing the occurrence of shunt resistances, which directly degrade device performance metrics such as open circuit voltage (VOC) and fill factor (FF).

Furthermore, the migration of excess PbI_2 to the interface between the perovskite and the hole transport layer has been identified as a key factor in reducing the operating efficiency of PSCs in vacuum. PbI_2 accumulation disrupts the energy band alignment at the interface, leading to increased recombination losses and reduced charge extraction efficiency. This migration process also contributes to the formation of pinholes and structural defects in the perovskite layer, further degrading the power conversion efficiency (PCE) of the device. Operando synchrotron radiation-based X-ray scattering techniques have shown that, unlike operation in nitrogen, where lattice shrinkage is minimal and more controlled, vacuum conditions induce significant crystal lattice contraction, leading to spontaneous phase segregation and device instability. As a result, the degradation mechanisms in vacuum suggest the need for encapsulation strategies and atmospheric control to improve the long-term stability of PSCs, particularly for applications in low-pressure environments such as space.

3.2 Silicon solar cells

Silicon is widely used as a semiconductor in solar panels due to its low cost and high energy efficiency. It also offers excellent properties such as superior thermal expansion resistance, exceptional corrosion resistance, long-term durability, high photo-conductivity and low toxicity. Silicon is abundant in nature, ensuring a stable supply of raw materials for the production of silicon crystals.

Pure silicon, the core component of this type of solar cell, has been used in electrical applications for decades. As a semiconductor, it inherently has limited electrical conductivity, but this property is exploited in photovoltaic applications. Silicon solar cells achieve efficiencies in excess of 20%, meaning they can convert more than 20% of incident sunlight into electricity. Its non-toxic nature also contributes to its widespread adoption, minimizing the environmental impact compared to other materials.

Silicon is one of the most common materials used in photovoltaic cells and is abundant in nature as silicon dioxide, which is found in quartz and sand. It is extracted through a process of carbon reduction. Silicon makes up approximately 26% of the Earth's crust, making it an easily accessible resource.

The material's resistance to harsh environmental conditions (including high temperatures, intense sunlight and corrosive seawater) makes it ideal for solar cell applications on Earth. Three main types of silicon are used in solar cells:

- pure crystalline silicon;
- amorphous silicon;

- polycrystalline silicon.

Each type offers distinct advantages depending on the specific requirements of solar technology.

If silicone solar cells are among the most widely used and researched in recent years, they would be an excellent starting point for the construction of a solar cell field on the Moon from which energy could be obtained for the subsequent construction of the different infrastructures required and the panels that would make up the Sunshade itself.

To solve the problem of the poor conduction capacity of pure crystalline silicon (semiconductor in its core), impurities are present inside the solar cell, i.e., other atoms are specifically mixed with silicon to increase its ability to capture energy and convert it into electricity.

Some of the most commonly used atoms are, for example, arsenic and gallium. When arsenic is mixed with silicon, there will be more electrons in the structure, creating an electron-rich layer.

With gallium, on the other hand, the opposite effect will be achieved: there will be a lack of electrons and therefore an electron poor layer will be created.

At the junction between the two semiconductor layers in a solar cell, electrons from the n-type (negative) layer migrate to the p-type (positive) layer to occupy the available holes. This interaction creates a region near the junction known as the depletion zone, where the electrons effectively fill the holes. Once the holes in this zone are fully occupied, the p-type side of the depletion zone, originally characterized by a high concentration of holes, becomes populated by negatively charged ions. Conversely, the n-type side, originally rich in electrons, acquires positively charged ions. The accumulation of these oppositely charged ions creates an intrinsic electric field across the depletion zone, which inhibits further electron movement from the n-type to the p-type layer.

When exposed to sunlight, photons excite electrons in the silicon lattice, causing them to be released, leaving vacancies known as 'holes'. When this excitation occurs under the influence of the internal electric field, the field directs the electrons towards the n-type layer and the holes towards the p-type layer. By connecting the n-type and p-type layers to an external conductive path, such as a metal wire, the displaced electrons cross the depletion zone, flow through the external circuit and return to the n-type layer. This continuous movement creates an electric current, enabling electrical power to be generated.

3.2.1 Production on the Moon

In consideration of the Moon's lower escape velocity in comparison to Earth, the in-situ production of solar cells offers considerable logistical and economic benefits, particularly for missions necessitating large-scale energy generation.The Moon's abundant silicon reserves, in conjunction with recently developed refining methodologies that reduce reliance on non-lunar materials, render lunar-based photovoltaic production a viable proposition.

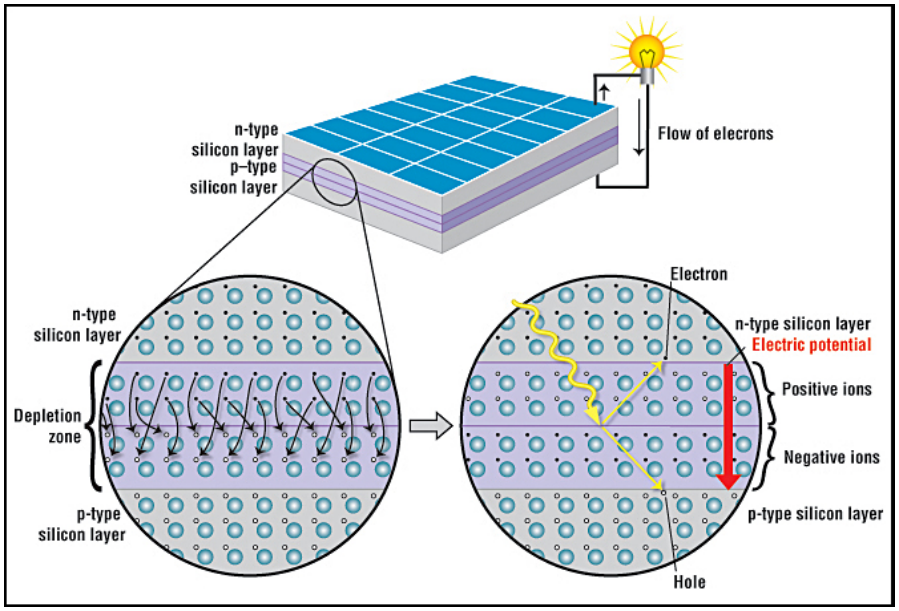

Figure 3.7: Close-up view of the depletion zone around the junction between the n-type and p-type layers

In the subsequent paragraph, both crystalline and amorphous silicon solar cells will be examined, with detailed descriptions of their production methods and evaluations of their specific power levels in the context of lunar and space applications. These data will then be utilized as inputs for the simulation that will be presented in the following chapters. The primary criteria for an effective lunar solar cell production system include the minimization of dependence on Earth-supplied materials, the assurance of low labor demands, the optimization of energy efficiency, and the reduction of equipment mass. A significant energy-intensive step in solar cell production is silicon refining, therefore efficient processing methods are crucial.

Crystalline silicon solar cells

Crystalline silicon solar cells generally demonstrate an efficiency of approximately 15% under space illumination (1.35 kW/m²), with high-performing models attaining 24%.A significant disadvantage of these conventional cells is their comparatively low power-to-weight ratio, attributable to the intrinsic thickness of the silicon substrate.

In order to address this issue, strategies such as the development of ultra-thin cells with light-trapping techniques to enhance optical absorption have been proposed. Additionally, the utilization of lightweight concentrator elements has the potential to significantly enhance specific power.The proposed process sequence for the production of crystalline silicon cells in a lunar environment emphasizes simplicity and the minimization of materials that would need to be imported from Earth. For the purification of silicon, the utilization of multiple vacuum float-zone refining, leveraging the Moon's natural vacuum environment, is proposed as an alternative

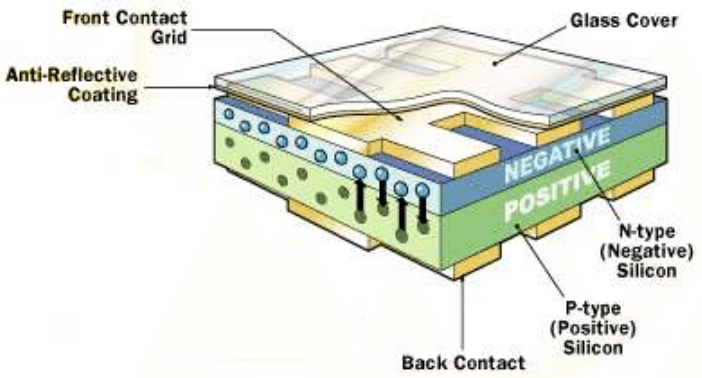

Figure 3.8: Schematic representation of a silicon solar cell

to conventional silane distillation.

The refinement of silicon is followed by a series of processes including single-crystal growth, wafer slicing, and ion implantation for doping. This is then followed by annealing in a solar furnace.While this approach is effective, it requires substantial processing equipment and refined silicon, which pose logistical challenges for lunar operations.

Amorphous silicon solar cells

Amorphous silicon solar cells, with efficiencies ranging from 5% to 6% to 10%, offer a different and alternative approach with respect to crystalline silicon solar cells. Their thin active layers - only 1-2 microns thick - significantly reduce the amount of silicon required, making these cells particularly advantageous. However, light-induced degradation, which can reduce efficiency over time, remains a critical challenge. Despite this, amorphous silicon cells are remarkably radiation tolerant and under proton irradiation, they are up to 50 times more resistant than single-crystal silicon. Furthermore, the ability to repair damage by annealing at temperatures below 200°C is promising.

Of course, the simplicity of the amorphous silicon manufacturing process makes it an attractive option for lunar production. It involves depositing silicon on a substrate using plasma-enhanced chemical vapor deposition (PECVD), a widespread industrial technique that allows automated large-scale production. However, it is necessary to import some key materials from Earth, such as hydrogen and dopants (boron and phosphorus). While indium tin oxide is conventionally used for transparent conductive coatings, alternatives such as zinc oxide (ZnO) - which can be refined from lunar resources - could be used to minimize the need for material imports.

A major consideration in solar cell production is substrate selection. Most high-power-weight amorphous silicon arrays utilize polymer films such as Kapton or Tedlar, which require Earth

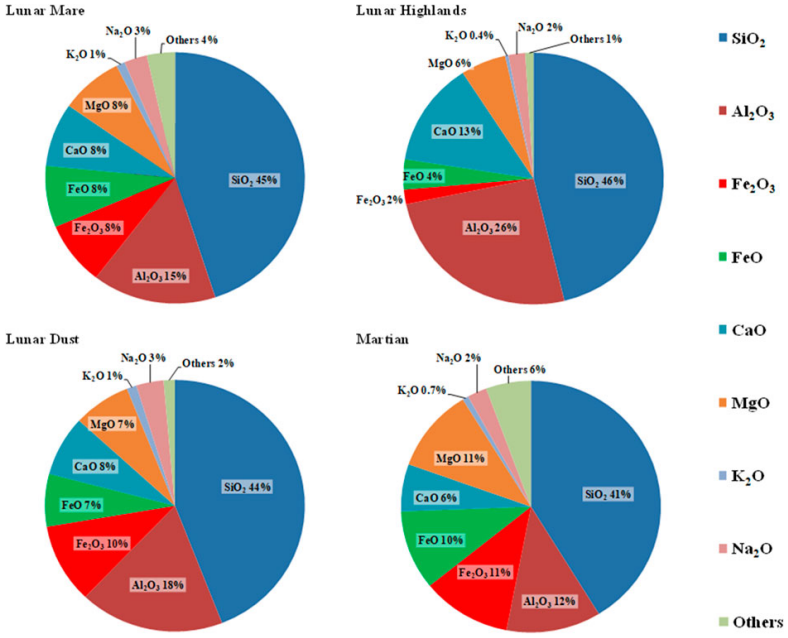

Figure 3.9: Lunar soil main composition [25]

importation due to the Moon's lack of carbon and hydrogen. If weight constraints are less critical, such as for stationary lunar applications, glass or alumina substrates could be used instead. For applications where specific power is paramount (e.g., Sunshade or Mars missions), lightweight metal foils are preferable. Electroformed nickel or stainless steel sheets - potentially refined from lunar meteoric material - could serve as viable substrate options, although Aluminum and Titanium (both available on the lunar soil) remain more desirable due to their lower densities.

Currently, the global output of amorphous silicon solar cells is approximately 10-15 MW per year, with ongoing expansions. The standard plasma-enhanced deposition process operates at pressures between 0.1 and 1 Torr, utilizing glow-discharge techniques for optimal layer formation. A production facility would typically comprise multiple deposition chambers, including those for the transparent conductor and metal contacts, as well as loading and unloading stations. A roll-to-roll system could enable continuous substrate processing, streamlining production. On Earth, such facilities occupy approximately 750 m^2 and weigh around 45,000 kg, although lunar adaptations could significantly reduce these requirements.

The Moon's natural vacuum conditions present a unique advantage for amorphous silicon cell fabrication. Unlike terrestrial operations, where vacuum chambers are required, lunar production could leverage the ambient environment, minimizing equipment mass and complexity. The primary technical requirements include RF generators for plasma excitation, vacuum turbopumps for gas management, and hydrogen recycling systems. The estimated mass of essential equipment is around 600 kg, though automation and additional machinery could increase this figure.

A key metric in evaluating lunar solar cell viability is specific power, expressed in watts per kilogram. For amorphous silicon cells with an assumed efficiency of 5%, an uncovered configuration achieves approximately 1700 W/kg. With a silica cover for radiation protection, this value decreases to 410 W/kg. If the entire cell is fabricated from lunar materials using a steel substrate, specific power drops to 350 W/kg without a cover and 220 W/kg with one. As we will see later we will consider a power production of 0.5 kW per panel, considering a panel around 3.5 kg. Advanced configurations, including thinner substrates and higher efficiencies (10%), could reach 9900 W/kg without cover and 1900 W/kg with a protective layer, but it has been decided to stay as conservative as possible. For all-lunar manufacturing, these values adjust to 2200 W/kg (uncovered) and 1100 W/kg (covered). These calculations suggest that despite efficiency limitations, amorphous silicon cells remain competitive with crystalline silicon counterparts, particularly in applications where specific power is crucial.

Lunar-manufactured solar cells hold great potential for reducing space power system costs. The abundance of lunar silicon, coupled with viable refining and production methods, supports the feasibility of in-situ solar cell fabrication. Given the energy-intensive nature of silicon processing, amorphous silicon technology presents the most promising approach due to its lower material requirements. Structural elements such as array frames and support beams, though not explored in depth, would also play a critical role in deployment. The economic viability of lunar photovoltaics depends on sustained demand, particularly for megawatt-scale power production in space. If solar-electric propulsion gains traction or lunar industrialization accelerates, as it seems to be in the recent years, in-situ solar cell production could become a pivotal component of future space infrastructure.

Examples

There exist different examples that are being studied and implemented by various companies, but they will be presented in more detail in chapter 4.1.

3.2.2 Efficiency

When considering efficiency, we must talk about the Shockley-Queisser limit. William Shockley and Hans-Joachim Queisser were two scientists who first questioned the theoretical limit attainable by primitive single p-n junctions. After years of study, they reported their results in 1961 in the Journal of Applied Physics, Volume 32, pp 510-519, under the name '*Detailed Balance Limit of Efficiency of p-n Junction Solar Cells*'.

The limit was calculated by examining the amount of electrical energy that was extracted for each incident photon, and the value obtained was 33.7 %, considering a single p-n junction with a band gap of 1.4 eV, using an Air Mass of 1.5 solar spectrum. Consequently, an ideal solar cell with incident radiation would generate $337\,\mathrm{W/m^2}$, and as we can see in figure 3.10, the radiation is maximum when the bandgap is $E_g = 1.4$ eV, if the solar radiation is modelled as a 6000 K blackbody radiation.

The flux of blackbody photons above the band gap energy was calculated as:

$$Q_c = \int_{\nu_g}^{\infty} \frac{1}{e^{(h\nu - qV)/(kT_c)} - 1} \frac{2\pi\nu^2}{c^2}\, dx$$

The most popular solar cell material, silicon, that's also the one that's being taken into consideration for this project, has a less favorable band gap of 1.1 eV, resulting in a maximum efficiency of about 32%.

For years, single silicon solar cell technology did not allow for more than 10 to 15% efficiency, whereas with modern studies we have reached even 24 %. On the Moon there are AM0 conditions, and as can be seen once again from the graph below, the maximum achievable efficiency is even lower than 33%.

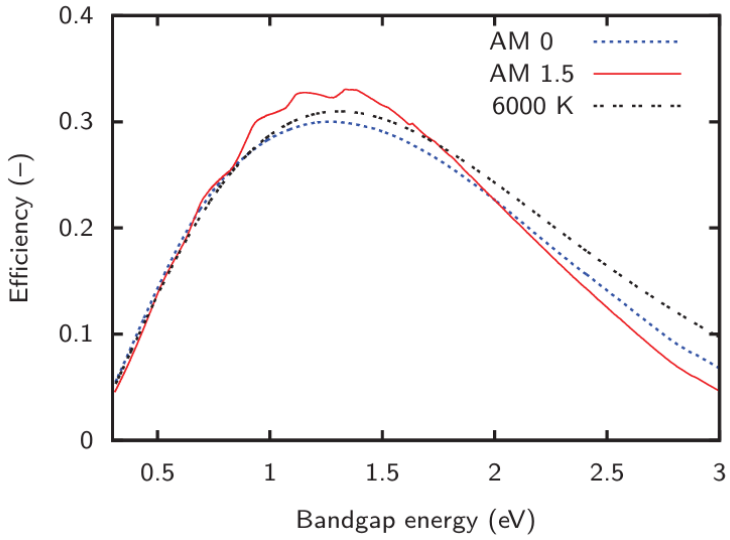

Figure 3.10: The Shockley - Queisser efficiency limit for the black body spectrum at 6000 K, and the AM0 and AM1.5 solar spectra

Recent studies show that this limitation can be overcome by using multi-junction solar cells, also known as tandem cells. These cells use multiple p-n junctions, and each junction is connected to a particular frequency of the spectrum. Since a material with a single given band-gap would have suffered from the problems discussed above, this solution solves the situation. Generally a high band-gap is placed on top as it absorbs high-energy, shorter-wavelength light and transmits the rest. Below this layer is another layer that absorbs some of the lower-energy, longer-wavelength light. There may also be other solar cells, up to a maximum of four layers.

The efficiency of these multi-junction cells is calculated in a similar way to single junction cells, thus reworking the original Shockley-Queisser method. It has been shown that a two-layer cell can reach 42% efficiency, a three-layer cell 49% up to 86% for a cell with infinite multi-layers.

They are generally produced using three layers, blue on top, yellow in the middle and red on the bottom. The semiconductors used are set to specific frequencies, mostly using GaAs (gallium arsenide) compounds, often $GaInP_2$ for blue, GaAs for yellow and germanium for red. At the moment, they are very expensive and require construction techniques similar to those of microprocessors, and although they are already tested for the space environment because they are mounted on several satellites, as the power-to-weight ratio is certainly one of the main drivers of the design of space objects, they are certainly difficult to implement in a lunar facility, given the technological difficulty of their realization.

In any case, this technology is certainly important and to be kept in mind for the future because of the excellent possibilities and scenarios it could generate. In fact, in 2023, Chinese manufacturer LONGi Green Energy Technology Co. announced a tandem silicon/perovskite cell that achieved 33.9% efficiency, the first time a silicon-based cell has exceeded the S-Q limit.

In order to maximize the output of the panels, it is necessary to try to maximize the hours of light available on the panel itself. This is why it was decided by Tharshan Maheswaran's thesis to stack the Lunar Solar Park in the vicinity of Shackleton Crater.

The average solar irradiance on the lunar surface is approximately 1356 W/m^2. In Shackleton Crater, effective solar irradiance can reach around 1153.6 W/m^2, assuming an average illumination level of 85% due to its geographic features and position. Peaks along the rim of Shackleton are almost continually illuminated by sunlight, spending about 80–90% of each lunar orbit exposed to the Sun.

Another important factor to consider in order to maximize efficiency is to raise the panels to a certain height to avoid as much as possible the shadows created by the irregularity of the moon's promontories. There are various proposals in this regard from various companies, including, for example, Astrobotic's Vertical Solar Array Technology (VSAT). They are studying vertical solar arrays to avoid 12 hours of light and 12 of day in the Moon.

Figure 3.11: Render of the VSAT model

3.2.3 Sustainability

As seen in the preceding paragraphs, the creation of amorphous silicon solar cells can take place on the Moon using only material extracted from the regolith present on the lunar soil, reducing the climate impact to almost zero. The only climatic impacts that the project could have on Earth are, however, connected to the launches of the initial phases of the project, to bring to the Moon the material needed to build the first infrastructures and panels to kick-start the construction of the system. it has been calculated that to transport all the material needed with Starship, it would take about 1500 launches, including rovers, landers and various infrastructures (see chapter 4.6). If we compare this number with that of previous projects, such as '*Realistic Sunshade system at L1 for global temperature control*' by Christer Fuglesang and María García de Herreros Miciano (Acta Astronautica, Volume 186, September 2021, Pages 269-279), the impact applied is considerable. By previous authors, the proposed solution was for between 330 thousand and 830 thousand launches. Considering an average of about 580 thousand. The reduction applied is approximately 99.9%. As further evidence of this, companies such as Blue Origin and Astrobotic confirm that their proposed electrolysis processes, using only photovoltaic energy, produce no carbon emissions as waste.

A Starship flight with the Super Heavy booster emitted 2683 tonnes of CO_2, plus 1.7 tonnes of nitrous oxide. This greenhouse gas is 298 times more harmful than CO_2, which means that over one flight, the rocket will release 3189.6 tonnes of carbon dioxide equivalent. But it has to be compared with other transportation systems and the impact that it could have on Earth pollution. In figure 3.12 it can be seen that transports are responsible for 7.29 billion tonnes of GHG (GreenHouse Gases) emissions per year, mainly divided in road, aviation, shipping and rail. The emission of 1500 launches are around 4.8 million tonnes of carbon dioxide equivalent, so compared to the transport pollution in one year it is around the 0.0656%. considering that launches will take place over a period of 60 years it is therefore safe to say that the polluting impact of this project on the earth's climate is very close to zero.

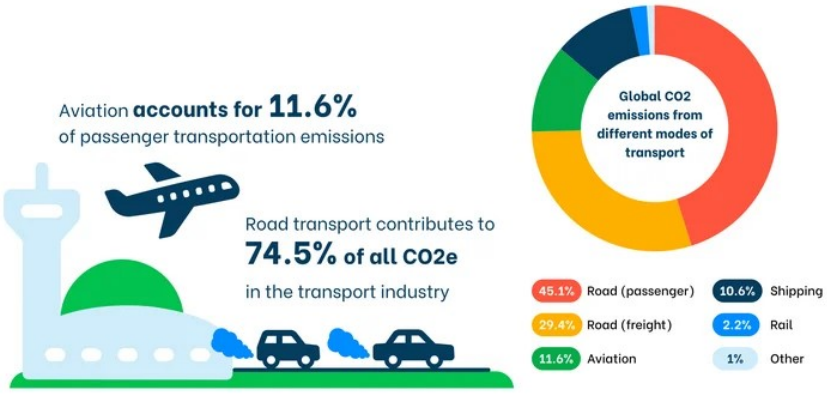

Figure 3.12: Transport pollution on Earth per year

3.3 Perovskite solar cells

Perovskites are a family of materials that have shown great potential in photovoltaics in recent years due to their high performance and low production cost. The perovskites generally used for photovoltaic applications take the more specific name 'metal-halide perovskites' because they are composed of a combination of organic ions, metals and halogens. The generic formula ABX_3 is similar to that of the mineral $CaTiO_3$, first discovered in 1839 by Gustav Rose, who named it after the Russian minerologist L. A. Perovski.

'A' and 'B' refer to cations while X refers to an anion, bound to both positive ions. Often the cation is an oxide and the ideal form it takes is a cubic structure.

Metal-halide perovskites are used as the main absorber material, or active layer, in perovskite solar cells, and are also called 'thin-film' because they are much thinner than the crystalline silicons mentioned above. The thin layer derives from their particular ability to absorb certain colors very effectively. To absorb the remaining color part of the light spectrum, a layer of silicon is often applied underneath the perosvskite, resulting in tandem solar cells with higher efficiency.

The big innovation that perovskitic solar cells introduce compared to silicon ones is that they can be produced by means of an ink-based and roll-to-roll printing process, which will be presented in the next sections.

Specifically with regard to the roll-to-roll application, there are two possibilities. The first one is to bring them directly up from Earth by Starship and then store them in hubs on the Moon and eventually build tandem with silicon extracted from the Moon while the second one could be producing them on the Moon thanks to recent techniques and studies (for example Katriin Kristmann and others, *Pyrite as promising mono-grain layer solar cell absorber material for in-situ solar cell fabrication on the Moon*, or other similar), who show how it is possible to use Lunar Regolith, not only to build silicon solar panels, but also Perovskitic or tandem.

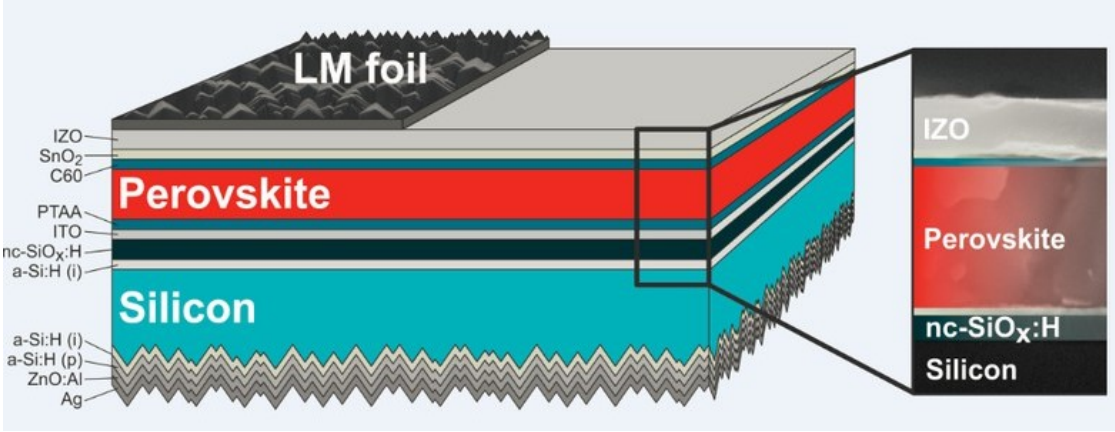

Figure 3.13: Example of a Perovskite Solar panel structure (LM stays for Light Management, IZO for indium zinc oxide, ITO indium doped tin oxide)

Upon comparison with a silicon based solar cell, the Perovskite cell has a number of advantages:

- it is economical and cheaper to produce in comparison to conventional solar cells;
- it absorbs wide range of visible light frequencies;
- it is thin and superior for large scale commercial production and installations;
- it is translucent, flexible, durable and, last but not least, aesthetically appealing;
- it is ideal for both large scale grid applications and for stand-alone applications.

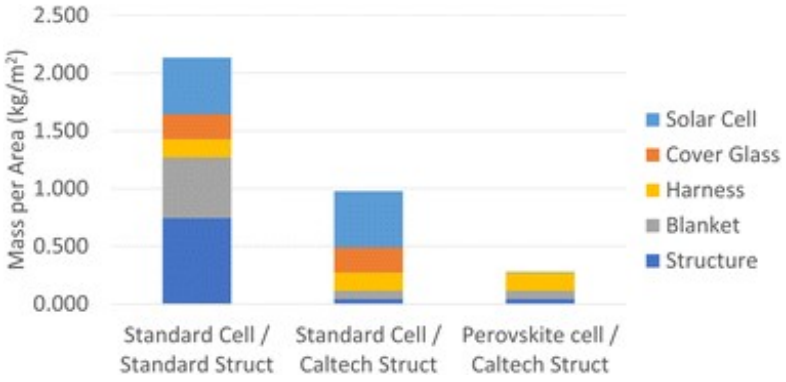

Figure 3.14: Mass per Area ratio of some type of solar cells

Anyway there are several challenges that need to be addressed before commercialization will be possible. Perhaps most significantly, OMHPs (organo-metal halide perovskites) have not yet demonstrated the long-term stability that is necessary to compete with the 30-year lifetime of commercially available Si and CdTe solar panels. Second, there are questions about the current-voltage (J-V) hysteresis during voltage scanning, which could be problematic for large-scale deployment. There are also concerns associated with potential environmental impacts due to the fact that OMHPs contain Pb, and it is toxicological and associated to environmental effects.

However, there are recent studies (as we can see in the figure 3.15) showing that Tin, Germanium, Antimony or Bismuth can be used instead of Lead. Germanium in particular is readily available on lunar soil.

3.3.1 Standard qualification for space operations and test

Perovskite solar cells need to successfully pass the qualification test for space operations (AIAA-S111 space qualification testing). It is critical to understand space environment interactions not only on the PV components, but also on the array substrate materials, wiring harnesses, connectors, and protection circuitry (e.g. blocking diodes).

Key elements of the space environment which must be accounted for in the PV system design include: Solar Photon Radiation, Charged Particle Radiation, Plasma, and Thermal Cycling. While solar photon radiation is central to generating power in PV systems, the complete spectrum includes short wavelength ultraviolet components, which photo-ionize materials, as well as long wavelength infrared which heat materials. High energy electron radiation has been demonstrated to significantly reduce the output power of III-V type PV cells and proton radiation damages material surfaces, often impacting cover-glasses and anti-reflective coatings. Plasma environments influence electrostatic charging of PV array materials, and must be understood to ensure that long duration arcs do not form and potentially destroy PV cells. Thermal cycling impacts all components on a PV array by inducing stresses due to thermal expansion and contraction. Given such demanding environments, and the complexity of structures and materials that form a PV array system, mission success can only be ensured through realistic testing in the laboratory.

Perovskites, moreover, have unique qualities and characteristics, so existing standards are often not suitable for their testing. A striking example is in the radiation standards. AIAA S-111 standards require solar cells be exposed to 1×10^{16} fluence of 1MeV electrons per square cm (e-/cm^2) and 1×10^{13} fluence of 3MeV protons per square cm (p+/cm^2). These values were chosen so that the particles can impart energy into the absorbing layer of the material, to give a reliable indication of the material's response.

Unlike conventional silicon solar cells, which are typically thick, rigid wafers, perovskite cells are implemented as ultra-thin films. The perovskite semiconductors are intrinsically "soft" (low in density and mechanical hardness) compared to crystalline silicon. This softness means that high-energy charged particles (like those used in standard radiation tests, as mentioned above) tend to pass through a thin perovskite layer with minimal interaction, causing little immediate harm. As a result, early irradiation experiments showed perovskite devices hardly degrading, which led to the perception that they were extremely radiation-resistant. In reality, the material was simply not absorbing the full brunt of energetic particles under those test conditions. More importantly, when perovskites do incur radiation-induced defects, they can recover remarkably quickly by reordering their crystal lattice, effectively "self-healing" the damage. This self-healing behavior stems from the ionic, liquid-like nature of the perovskite structure: radiation may momentarily disorder the lattice, but the displaced ions can migrate and relax back into an ordered state, restoring performance. Sellers et al. liken this effect to splashing a tub of water. The water is disturbed by an impact but soon returns to a calm state once the disturbance stops. Thus, perovskite solar cells can be considered radiation-hard not because they incur no damage, but because any damage is rapidly annealed by the material itself.

However, the apparent radiation hardness of perovskites was initially overstated due to limitations of traditional testing protocols. Standard space qualification tests for solar cells, developed with robust silicon or gallium arsenide cells in mind, employ very high-energy protons and electrons to simulate years of cosmic radiation in a short time. For a thin-film perovskite device,

such high-energy particles often deposit only a fraction of their energy in the active layer, or miss it altogether, leading to negligible performance loss during tests. In other words, perovskite cells seemed to be extraordinarily radiation tolerant because the tests were not appropriately designed for a soft, nanoscale-thickness material. Recognizing this discrepancy, researchers pinpointed that new test conditions were required to truly assess how perovskites behave under relevant space radiation environments.

A collaborative team including Brandon K. Durant, Bibhudutta Rout, Ian Sellers, and others set out to develop more suitable radiation testing methods for perovskite solar cells. Instead of relying solely on very high-energy particles, the team designed experiments using low-energy protons that stop within the perovskite layer, thereby depositing their energy directly into the cell's active region. Protons in the low keV to MeV range are abundant in space (for instance, in solar winds and magnetospheric radiation) and are known to cause displacement damage in solar cell materials. By controllably adjusting the proton beam energy, the researchers could target the damage to specific depths (e.g., the perovskite absorber vs. underlying layers) and observe the effects on device pholeerformance. These targeted irradiation tests revealed that perovskite cells do suffer performance drops when the radiation is absorbed in the film, disproving the notion that they are inherently immune to space radiation. Crucially, the experiments also confirmed the fast self-recovery of perovskite devices: after exposure, the cells showed a significant rebound in efficiency as the induced defects healed. The soft perovskite lattice tolerated the introduction of proton-induced point defects without permanent damage, in contrast to rigid semiconductors that accumulate damage over time. This work demonstrated that low-energy protons (a prevalent source of damage in actual space environments) are a critical test of a perovskite's radiation tolerance, and that these solar cells can indeed survive such irradiation through self-healing.

As an outcome of these studies, the research consortium proposed a standardized protocol for qualifying perovskite solar cells under space-like radiation conditions. This new protocol specifies using radiation sources and energies that are relevant to orbits and mission profiles of interest – for example, including a spectrum of proton energies that peak in the perovskite layer, rather than exclusively ultra-high-energy particles. By defining a consistent set of test conditions (particle types, energies, fluences, and testing sequences), the protocol ensures that laboratories around the world can evaluate perovskite space durability on an equal footing. Such standardization is crucial; it prevents mischaracterization and enables more direct comparison of results across studies. NASA researchers have underscored the importance of this advancement. "Space qualification of a new material is driven by mission requirements," notes Lyndsey McMillon-Brown of NASA's Glenn Research Center, emphasizing that the team's work probes perovskites' response to the types of radiation most relevant to actual missions. In collaboration with the broader space power community, the team's guidelines have gained traction as a significant step toward allowing perovskite photovoltaics to be reliably used in space. In essence, by "coming together and defining protocols," the community is paving the way for perovskite solar cells to move from experimental status to flight-ready technology.

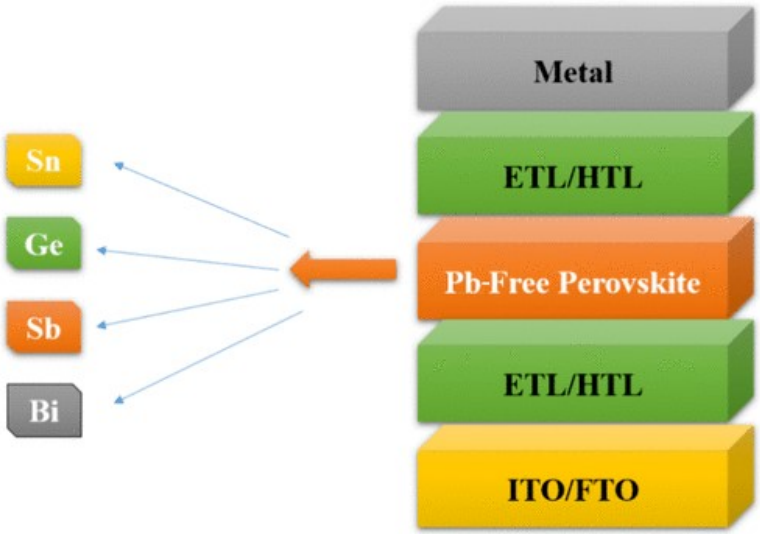

Figure 3.15: Example of substitution of Pb in a Perovskite solar cell: ETL electron transport layer, HTL hole transport layer, ITO indium doped tin oxide, FTO fluorine doped tin oxide

3.3.2 Production on the Moon

Beyond radiation tolerance, perovskite solar cells offer a range of practical benefits for off-Earth deployment, from the Moon to Mars. Their unique combination of material characteristics and processing methods aligns well with the stringent mass and volume limitations of space missions and the desire for on-site manufacturing of infrastructure.

Several key attributes of perovskite solar cells make them well-suited for such applications

First of all they are ultra-lightweight and compact. Perovskite solar cells are deployed as thin-film coatings only hundreds of nanometers thick, on lightweight flexible substrates. This leads to extremely low mass per unit area compared to silicon panels. Large-area perovskite arrays can be folded or rolled up for launch and then unfurled or adhered to surfaces at the destination. The reduced weight and volume could translate into significant savings in launch costs and easier handling during spacecraft deployment. Traditional solar panels, by contrast, require careful packaging to avoid cracking.

They have a really high mechanical flexibility. Because they are not built on brittle wafers, perovskite devices can bend and conform to curved surfaces. For instance, a perovskite power sheet could line the contours of a lunar habitat or be integrated into deployable structures like solar sails or tents. This flexibility also means the cells are more resilient to vibrations and mechanical stresses during launch.

Uniquely, perovskite solar cell material can be transported as a liquid solution “ink” and printed on demand at the remote site. NASA envisions using an inkjet-like electrospraying technique to spray-coat perovskite films onto substrates on the Moon or Mars. This method, developed by researchers at the University of California, Merced, uses a small nozzle and electric

fields to deposit a uniform thin layer of perovskite (about 250 times thinner than a human hair) quickly and efficiently. By carrying just a few liters of perovskite ink, vast solar arrays could be generated vast solar arrays. It is estimated that 12 kg of condensed absorber can produce on the order of a megawatt of solar-generating capacity. After deposition, the wet perovskite film must convert into a crystalline perovskite layer.

Last but not least the fundamental ingredients for many perovskites are common elements that exist in lunar regolith. A prototypical perovskite crystal structure is calcium titanate ($CaTiO_3$), comprising calcium, titanium, and oxygen – notably, all three of these elements are present in Moon rocks in significant quantities. Lunar soil samples indicate roughly 4–6% Ca and 1–2% Ti by weight (mostly in oxides like ilmenite), and about 40–45% oxygen (bound in minerals). This opens the possibility, in the long term, of sourcing some raw materials for perovskite solar cells directly on the Moon, leveraging in-situ resource utilization. To create substrates or electrodes lunar metals can be used for example thin aluminum for the foil (from lunar aluminum extraction) as a substrate/electrode, or deriving glass from regolith to use as a flexible glass substrate. The Moon offers an ultra-dry, vacuum environment which eliminates moisture completely. The absence of water means a major degradation pathway for perovskites (moisture-induced breakdown) is removed. However, printing can't be done in hard vacuum because liquid inks would boil off and not coat properly, requiring perform the roll to roll process inside a pressurized lunar module or an enclosed fabrication chamber. This chamber can have a controlled atmosphere (like inert gas at partial pressure) optimized for ink drying. A lunar factory might use a nitrogen or argon environment at low pressure to allow solvent evaporation in a predictable way. Alternatively, NASA has envisioned a scenario where printer heads "vapor-deposit" solar cell layers onto a substrate in vacuum but that implies using vapor deposition (evaporation or sputtering) instead of liquid inks.

Low gravity (1/6 g) could affect coating flows slightly, thinner fluid films might behave a bit differently, and sedimentation of any particles in the ink is reduced. Generally, coating in lunar gravity is expected to be manageable, but it may require re-tuning of parameters like coating speed or drying time compared to Earth's gravity. The thermal environment is another factor: the Moon has no atmosphere to transfer heat by convection, so cooling of the printed film must rely on conduction through the substrate or radiation. The roll to roll system on the Moon might need more sophisticated thermal management to ensure the perovskite crystallizes correctly, like cooling rollers or heaters. The dust on the lunar surface is a notorious issue; however, if printing is done inside a sealed module, dust contamination during fabrication can be prevented.

As we have seen, launching liquid perovskite from the Earth to be printed on the Moon would probably be the fastest way to produce solar panels on the Moon and the number of launches to be carried out would be similar to the one mentioned above. But after analyzing the time frame that the testing and qualification phases of this new type of panel require, the use and printing of such panels in this thesis was considered only for the Sunshade, and not for the Lunar Solar Park. As will be seen in the following chapters, the Lunar Solar Park will require approximately 35 years

for its full production and operation. During the early stages of the simulation, silicon panels will be produced to ensure efficient and fast production, without waiting time for qualification, and thus lay the foundation for a Lunar Solar Park that will provide enough energy for the extraction of the material required to complete it and, in the meantime, ensure the construction of the coilgun, the printing of the perovskite panels for the Sunshade and the start of the launch phase.

Recent experiments give cause for optimism: a perovskite film tested on the International Space Station for 10 months remained functional, keeping its dark black color (indicating it did not decompose to PbI_2) despite exposure to vacuum, temperature swings, and cosmic UV. This suggests that with proper encapsulation, perovskite PV can survive at least months in space; the goal is to extend that to years or decades. For lunar deployment, regular maintenance or module replacement might be considered. The advantage of an R2R lunar factory is that it could continually produce new solar sheets to replace ones that degrade, creating a sustainable supply of power-generating material for the Sunshade.

In any case, these arguments will be taken up later, when we get into the specifics of the simulation.

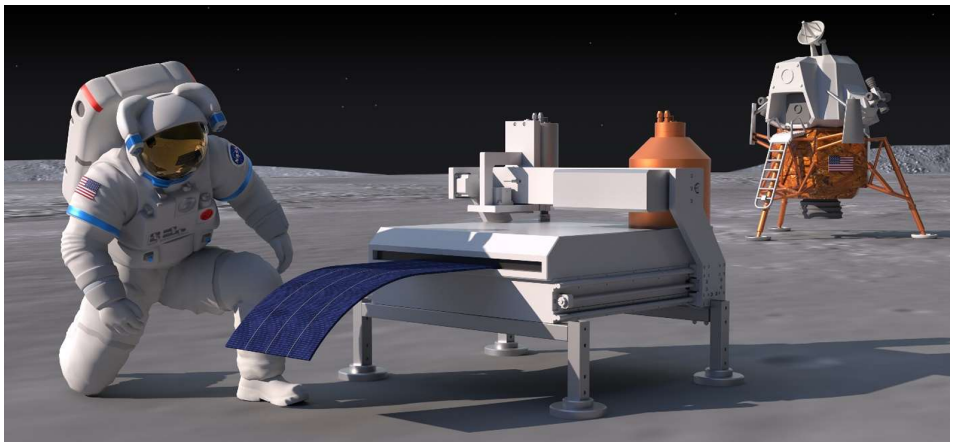

Figure 3.16: Render of a Lunar lander vehicle with sequential in-space printing of perovskite solar module

3.3.3 Efficiency and Sustainability

As previously discussed, the efficiency of perovskite solar cells is higher than silicon solar cells but lower than the tandem. The technology we have today doesn't allow us to go over about the 35% of efficiency for perovskite tandem, as shown in figure 3.17.

Perovskite shows high absorbance, possible long carrier lifetime, higher mobility, and low-temperature processing makes them stand out among all others, better than dye-sensitized solar cell (DSSC), quantum dot solar cell (QDSC), and organic solar cell (OSC). Thus, they are

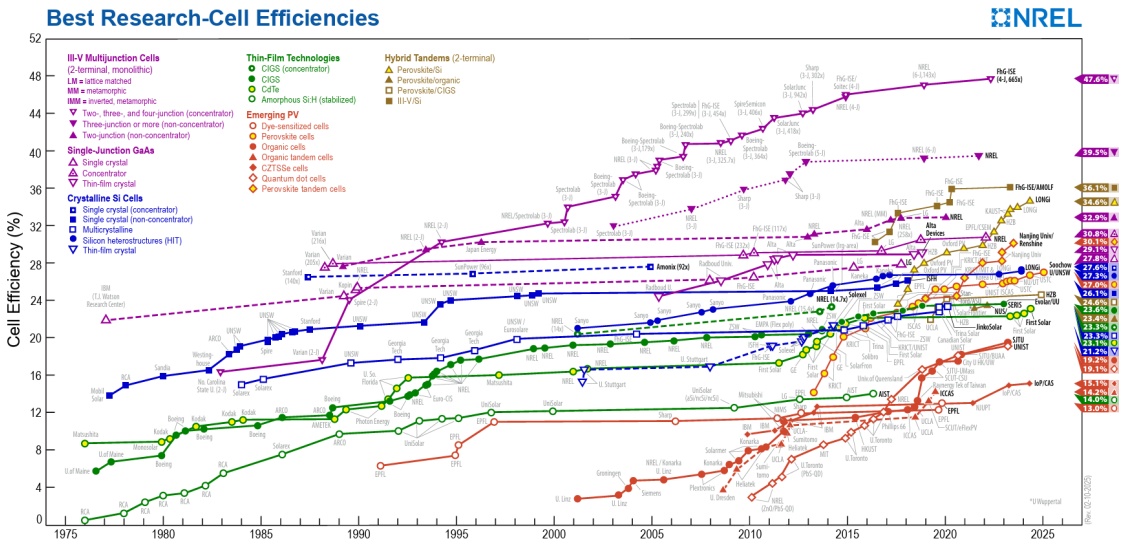

Figure 3.17: Best efficiencies of the Solar Cells divided by type during the years

between the best choices suitable for the absorber layer of solar cells.

But there could be a problem as briefly discussed above, because of the green purpose of this project: toxicity of lead (Pb).

An example of some Eco-friendly alternative could be Germanium, $CsSn_{0.5}Ge_{0.5}I_3$. It is highly stable, air-tolerant, and has a similar absorption coefficient and band-gap as $MAPbI_3$). Mixed Tin-Germanium based perovskite is used as the absorber layer for PSC. The structure is made of ZnO NR (natural rubber).

Over the top of this contains a capping layer of perovskite and HTL (hole transport layer) material. The initial dimension for the length and the diameter of ZnO NR (Natural Rubber), the thickness of the perovskite shell, the thickness of HTL and thickness of perovskite cap are taken as 800 nm, 80 nm, 40 nm, 80 nm and 40 nm.

Perovskite absorber layer and the effect of interface defect density on the performance of this cell are also studied. It was obtained power conversion efficiency (PCE) of 14.50%, the open-circuit voltage (VOC) of 0.96 V; short-circuit current density (JSC) of 18.11 mA/cm^2 and Fill factor (FF) of 83.35%. It was also analyzed the effect of tilt or inclination of NR on the performance of the cell which is a crucial factor toward achieving high performance. By optimizing the device parameters, we have achieved a PCE of 21.27%, VOC of 0.97 V, JSC of 29.56 mA/cm^2, and FF of 84.15% at an inclination of 10-degree tilt with respect to the incident light under AM 1.5 illumination.

Another example is the efficient Cesium Tin–Germanium Tri-iodide ($CsSn_{0.5}Ge_{0.5}I_3$) based perovskite solar cell and attain PCE of 24.51%. Some parameters were studied, such as influence on the thickness of electron transport layer (ETL), doping concentration of charge transport layers and defect density of absorber layer on the performance parameters of the perovskite solar

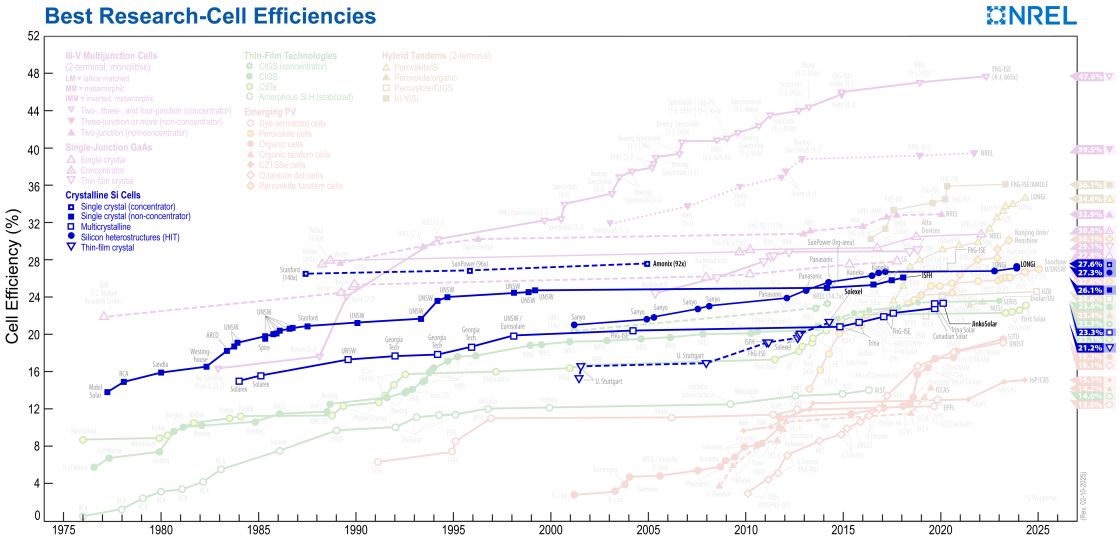

Figure 3.18: Best efficiencies of the Crystalline Silicon Solar Cells divided by type during the years

cell.

It was demonstrated an efficient and non-toxic n-i-p PSC with 24.51% PCE. This work suggests CuI and ZnO-NP as potential HTM and ETM for $CsSn_{0.5}Ge_{0.5}I_3$ based PSC. The impact of absorber layer defect density, ETL thickness and transport layer doping concentration on the performance of PSC is studied. It was concluded that absorber defect density must be as minimum as possible and when defect density reaches beyond $10^{17}/cm^3$ the performance of the cell degrades too heavily. The appropriate ETL thickness when ZnO-NP is used is 20 nm, fabricating thin layer will not only provide lower series resistance but also will reduce the cost of cell due to less material requirement. The appropriate doping concentration suggested by results is $10^{18}/cm^3$ and $10^{17}/cm^3$ for ETM (ZnO-NP) and HTM (CuI) respectively.

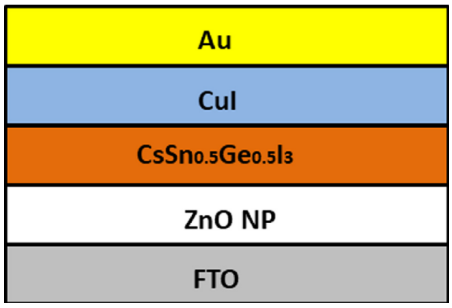

Figure 3.19: Device configuration of the simulated PSC

Titanium (Ti) being Moon-abundant (the ninth element most present in the known universe), non-toxic, thermally stable, and bio-compatible could be another solution. Ju et al.

made a theoretical prediction and experimental synthesis of all inorganic Pb free Ti-based halide perovskites, namely Cesium Titanium halide (Cs_2TiX_6 where X = F-, Cl-, Br-, I-). For these advantages, Chen et al. reported a representative thin film deposition of Cesium Titanium Bromide (Cs_2TiBr_6) for the first time and found an optical bandgap of about 1.8 eV with valance electron/hole diffusion lengths exceeding 100 nm. Like organic-inorganic hybrid absorber materials, organic charge transport materials become unstable in the presence of oxygen, light, and moisture, but the only thing we have to handle with on the Moon is the light. Besides that, several organic charge transport materials react with perovskite material, show hostile behavior due to hygroscopic materials, and have high preparation costs. For these disadvantages, researchers are looking forward to inorganic charge transport materials as they provide good transparency in ultra-violate, visible and infrared spectrum, wide band-gap, high charge carrier mobility, superior thermal and chemical stability, and simple synthesizing process.

Last but not least due to the thinness of perovskite devices, a 1 MW solar array could be printed in space while transporting a modest 12kg of condensed absorber material to orbit. That mass,combined with the recent vast reduction in launch costs of materials (3500 $/kg), results in a mere 0.10 $/W cost for theabsorber material if a module-level efficiency of only 15% could be produced at scale. It is feasible that high power conversion efficiency PSCs can be fabricated via vapor deposition in space. In-space evaporation of PSCs would leverage the existing vacuum of space in which the perovskite absorber layer would be crystallized and passively annealed from exposure to sunlight to reach 120 °C, achieving a high-quality film. Subsequent layers would follow sequentially, and laser scribing could be used to define cell areas and sinter-printed electrical interconnects to create high-voltage arrays. Target substrates are flexible and have high light transmission and thus can be rolled and stowed in a launch vehicle, and then engage with the in-space deposition system to be unfurled for PSC fabrication processes.

3.4 Final comparison

The establishment of photovoltaic (PV) systems on the Moon is essential for supporting long-term lunar missions by providing a sustainable energy source for habitats, scientific instruments, and other technologies. This summary focuses on the potential for developing a photovoltaic space park (referred as Lunar Solar Park) in Shackleton Crater, located near the lunar south pole, known for its favorable illumination conditions.

We have seen lunar regolith contains several materials that can be utilized in the production of photovoltaic panels:

- Silicon Dioxide (SiO_2): Abundant in lunar soil and can be processed to extract silicon;
- Aluminum Oxide (Al_2O_3): Present in regolith and can be used in various applications;
- Iron and Titanium Oxides: Useful for creating conductive materials and other applications;

- Water Ice: Found in permanently shadowed craters. It can be converted into hydrogen and oxygen for fuel or other uses.

While some materials are available on the Moon, others will need to be transported from Earth like dopants for Silicon and specialized equipments. Elements like phosphorus and boron are essential for enhancing silicon's electrical properties but are not readily available on the Moon and machinery required for processing lunar regolith into usable materials must likely be brought from Earth due to their complexity.

Establishing photovoltaic systems in Shackleton Crater presents a viable solution for sustainable energy production on the Moon. Silicon PV panels require more energy and power to produce than perovskite panels but utilize readily available lunar materials. The choice between these technologies will depend on mission objectives, resource availability, and technological advancements in manufacturing processes. In fact, as we will see through this thesis it has been decided to build the "Lunar Solar park" with silicon photovoltaic panel, and the Sunshade with perovskite ones.

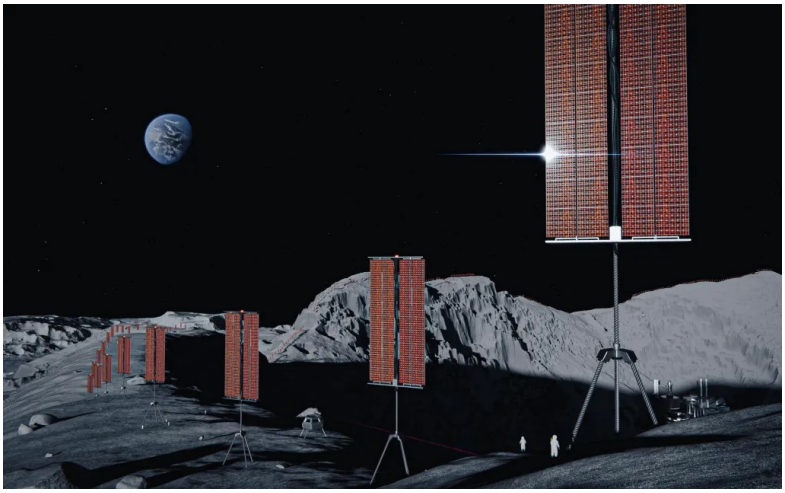

Figure 3.20: Software simulation of how solar panels can appear on the Moon surface

3.5 Nuclear energy

It is also possible (and it is a clean way to do it) to bring nuclear reactors from the Earth to the Moon to produce much energy in less time, but there are problems connected to the safety and politics/bureaucracy topic the will not be further investigated in this thesis work.

To mention some project, the Russian space agency Roscosmos has announced its intention to build a nuclear reactor on the lunar surface in collaboration with the China National Space Administration. According to Roscosmos director general Yury Borisov, "Today we are seriously considering a project - somewhere at the turn of 2033-2035 - to deliver and install a [nuclear] power

unit on the lunar surface together with our Chinese colleagues." The reactor would apparently be used to supply power to the Russian-Chinese International Lunar Research Station (ILRS), plans for which the two nations unveiled in 2021.

These plans come on top of previously announced plans of the United States and United Kingdom for lunar nuclear reactors.

A nuclear reactor could be placed in permanently shadowed areas (where there may be water ice) or generate power continuously during lunar nights.

The thermodynamic characteristics of the nuclear reactor are presented in figure 3.21. It is assumed that the efficiency and structural material for the primary loop are available.

Primary loop	
mass flow rate	7 kg/s
reactor inlet temperature	1030 C
reactor outlet temperature	1100 C
Secondary loop	
mass flow rate	9.4 kg/s
turbine inlet temperature	1040 C
turbine inlet pressure	385 kPa
turbine outlet temperature	656 C
turbine outlet pressure	35.5 kPa
turbine efficiency	78%
Heat rejection system	
Condensation rate	2 MW
Radiation panel	
thickness	6 mm
average temperature	600 C
total surface	80 m^2

Figure 3.21: Software simulation of how solar panels can appear on the Moon surface

Chapter 4: Input analysis

4.1 Introduction: Existing Projects

First of all, to demonstrate the qualitative feasibility of this project, it is important to take a walk among the other existing projects that aim to build solar panels on the Moon, and to show that this is really possible. These projects are going ahead and are also receiving substantial funds from entities such as NASA. This shows not only that the studies are promising, but also that the direction and will of political governments is to move in this direction. Having a continuous source of energy on the Moon would not only ensure greater possibilities for this project, but also the construction of future human lunar bases. This would open up the opportunity to use the Moon as a starting point and return location for possible missions to Mars (allowing our species to become interplanetary) or even become a source of energy and materials for planet Earth, without being disfigured and above all without further polluting our planet. Let's briefly present these projects.

Artemis: NASA is launching a solar power experiment called the Photovoltaic Investigation on the Lunar Surface (PILS) on Astrobotic's Peregrine lander. This experiment aims to demonstrate advanced solar cell technologies, including multi-junction solar cells made from gallium arsenide and silicon, as discussed above, which are designed to efficiently convert sunlight into electricity under lunar conditions. The PILS project will also assess the electrical environment of the Moon, focusing on how solar cells perform in terms of current and voltage outputs over an 8 to 10 day period. The experiment addresses challenges such as radiation exposure and extreme temperatures, with protective measures like reflective films to shield electronics from heat damage. Future solar installations are expected to be strategically located at the lunar poles, where sunlight is nearly constant for extended periods, enhancing energy generation capabilities. NASA plans to establish an Artemis Base Camp at the Moon's south pole. This base will feature essential infrastructure such as habitats, power systems, and rovers designed for exploration and resource utilization. The site is chosen for its favorable conditions, including abundant sunlight and potential water resources, which are critical for long-duration missions. The Base Camp will support longer expeditions by providing necessary facilities for astronauts conducting scientific studies on the lunar surface and its locations on the South Pole is perfect to combine it with our

project.

Blue Alchemist: The core technology of Blue Alchemist involves molten regolith electrolysis. This method extracts essential elements such as silicon, iron, and aluminum from lunar regolith, while also generating oxygen as a byproduct (useful both to be inhaled by humans and guarantee survival on the Moon and as an oxidizing for a propellant). The extracted silicon is purified to over 99.999%, making it suitable for high-efficiency solar cells. The project is designed to be an end-to-end, scalable solution that can autonomously produce solar cells and electrical transmission systems on the Moon. Blue Origin has been experimenting with a reactor, named 'Blue Alchemist,' which is powered solely by electricity and could facilitate the development of a human colony on the Moon. This is because, to survive here, a lot of energy has to be produced, but it can be done in only two ways: by converting sunlight through solar panels, or by using nuclear fission micro-reactors, as previously discussed. In October 2023, Blue Origin was awarded a 35 million dollar Tipping Point partnership from NASA to advance this technology. The funding will support the development and testing of a prototype system, with plans for demonstration in a simulated lunar environment by 2026.

Lunar Resources, Inc.: As a spin-out of NASA's Wake Shield Facility program, Lunar Resources focuses on developing breakthrough technologies to enable the large-scale commercialization of space. They use Molten Regolith Electrolysis (MRE) to extract high-purity oxygen and metals such as magnesium, calcium, and aluminum from lunar regolith without the need for consumable reagents. Currently, Lunar Resources is developing a prototype oxygen capturing, filtering, and storage system (OxPS) capable of processing 3650 kg of oxygen annually at an industrial scale. In addition to MRE, Lunar Resources is advancing Regolith Additive Manufacturing through its Pulsed Electrical Discharge Additive Manufacturing (PE3D) system. This innovative technology allows for the construction of complex structures using lunar regolith without binders or reagents. The low-power PE3D system can fabricate both vertical and horizontal structures on the Moon, which will be essential for supporting future lunar bases. The company is also exploring the feasibility of a Lunar South Pole Oxygen Pipeline in collaboration with Wood. Funded by NASA's NIAC program, this study aims to build a pipeline that would transport gaseous oxygen from extraction sites to lunar bases, thereby supporting sustainable human operations on the Moon. In terms of metallurgy, Lunar Resources is advancing technologies that enable the casting and alloying of metals in low-gravity and vacuum environments. These metals could be utilized for structural elements, cables, and other manufacturing needs. The company specializes in producing atomically ordered thin-film materials and additively manufacturing large metal structures in space. It is also developing technologies for vacuum deposition and welding in space environments. Furthermore, Lunar Resources has proposed the construction of a large radio observatory on the Moon called the FarView Observatory, utilizing its additive manufacturing technologies.

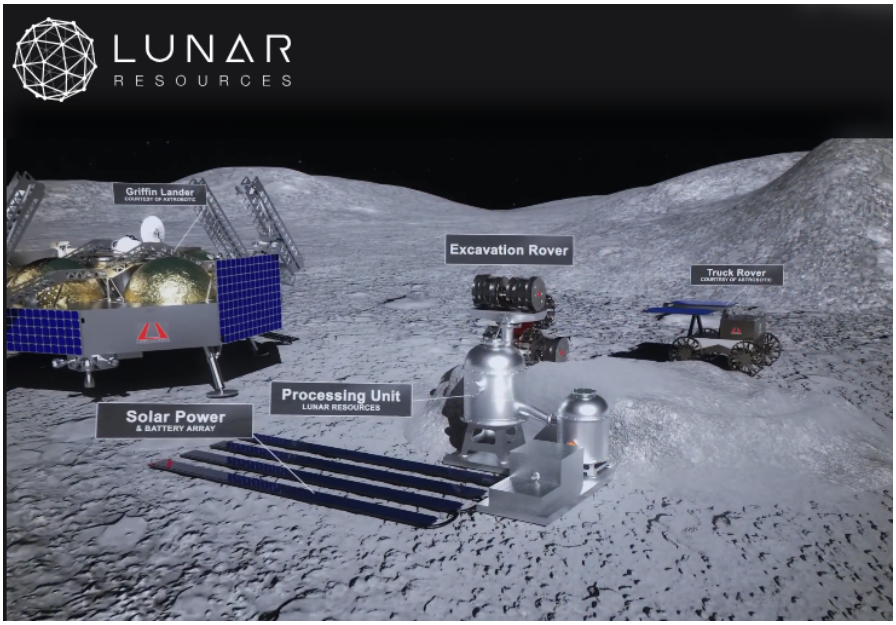

Figure 4.1: Lunar Resources, Inc. regolith excavation simulation 3D-model

4.2 Location

The selection of Shackleton Crater as the location for the Lunar Solar arrays Park was determined by a combination of environmental, logistical and strategic advantages, as seen in Maheswaran thesis. Situated at the lunar south pole, it benefits from distinctive illumination conditions that provide near-continuous sunlight along its rim. It allows us to have a stable and uninterrupted source of solar energy, a prerequisite for in-situ power generation and for supporting infrastructure. At the same time, the interior of the crater is in permanent shadow, a factor that could result in the presence of volatiles such as water ice. The presence of these resources gives us opportunities for in-situ resource utilization, supporting future lunar operations and reducing the need for costly Earth-based supply chains.

The naturally low temperatures in the crater help minimize the need for active cooling, which is typically a major energy requirement for superconducting materials, like the ones needed for the system electromagnetic launcher (the coilgun) studied by T. Maheswaran. It could facilitate a high-frequency, energy-efficient launch system for the transportation of solar panels and other construction materials to the Sunshade at SEL1.

Beyond its energy and launch capabilities, Shackleton Crater is also strategically located because from there it's easily reachable (or at least the access point it's easier from there than from other locations) the Earth-Moon Lagrange Point 2 (EML2), a potential cargo hub for interplanetary material transfer. This proximity significantly enhances the efficiency of processing and launching lunar-derived resources while reducing reliance on Earth-based material transport,

thereby lowering overall mission costs.

The site is also within a region identified as a prime candidate for future lunar exploration bases, including NASA's Artemis program and other international lunar initiatives.The establishment of solar infrastructure in this area could provide long-term energy solutions for both robotic and crewed lunar missions, contributing to the sustainability of human activities on the Moon.

The lunar south pole offers increased protection from solar wind and micro-meteoroid impacts compared to equatorial regions. This relative stability renders the crater particularly well-suited for long-term infrastructure deployment, ensuring that solar arrays, power storage systems, and launch facilities experience less degradation over time. The relatively flat and stable terrain of the crater's rim further facilitates the deployment of large-scale solar panels, optimizing energy capture while minimizing construction challenges, and that's also why we need vertical solar panels, to avoid the shadow of the crater.

In conclusion, the optimal site for a lunar solar arrays park is Shackleton Crater, given its unique combination of continuous solar exposure, suitability for superconducting mass drivers, proximity to key lunar and interplanetary transport nodes, and stable environmental conditions. The selection of this location enhances the feasibility of lunar-based solar energy production and material transportation, supporting the broader objectives of space-based climate mitigation and sustainable lunar exploration.

4.3 Mass Analysis

For the study of the masses involved in the creation of the Sunshade, a MATLAB script was created that allows the choice of simulation of the possible climate scenarios presented in the 2.1 section. Based on the current climate scenario, it was decided to opt for the simulation of scenario 1, i.e. the one that aims to limit global warming to 1.5 degrees, which is the main goal of the Paris Agreement. The results obtained varied according to the possible efficiencies provided by the perovskite panels (yellow line), a small percentage of the total (blue line), and they can be seen in figure 4.2

It can be clearly observed that the total mass of the sunshade would be at least twice as high if no perovskite panels were used, i.e. in the case where the efficiency is approximately zero. The results on the study of the minimum sunshade mass demonstrated in the thesis by S. Fix et al. shows that the minimum mass required for the construction of the sunshade without the use of panels would be 75×10^9 kg.

From the graph in figure 4.2, it can be seen that with the use of perovskite panels for the composition of the Sunshade, a mass of approximately 25×10^9 kg is required. The perovskite panels used are the minimum necessary to be able to absorb the amount of solar radiation required to satisfy the characteristics of climate scenario 1, in our case:

$$\phi = \frac{R_S^2 \ \sigma \ T_S^4}{(AU - d_{SEL1})^2} = 1391.2 \ \frac{\mathrm{W}}{\mathrm{m}^2}$$

where R_s is the radius of the Sun, σ is the Stefan-Boltzmann constant, T_s is the temperature of the Sun as a black body, AU is the astronomic unit and d_{SEL1} is the distance of the Sun-Earth Lagrange point 1 from Earth. Further calculation for the effective stability of this point considering the mass of the Sunshade needs to be developed.

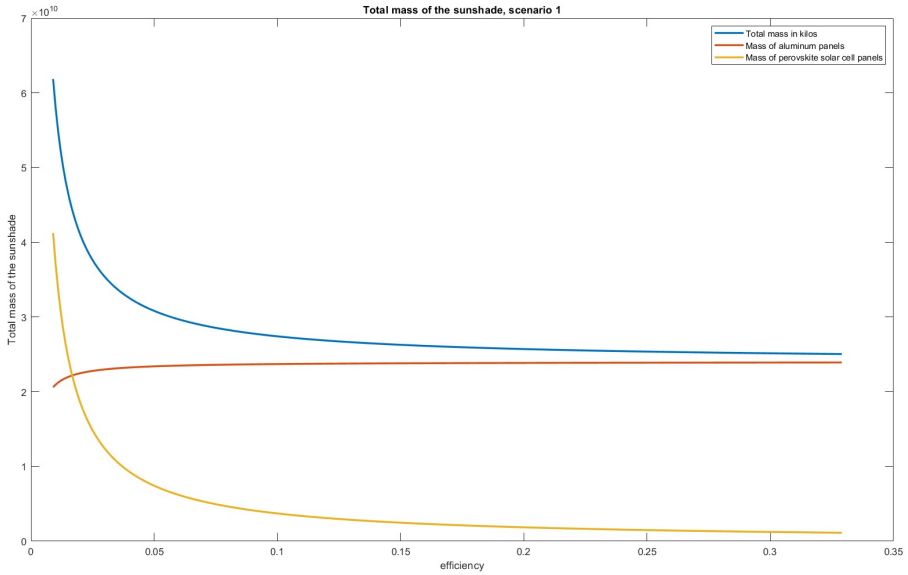

Figure 4.2: Mass needed to build the Sunshade to decrease the Earth's temperature by 1 K

The total area of the Sunshade and therefore the total mass has been determined starting from the amount of radiation that needs to be shielded for every scenario. In tab 4.1 we can see the results of this calculation for every scenario, where RCP is the scenario previously discussed, ΔS is the reduction in solar insulation due to counter radiative forcing, f is the relative fraction of light to be reduced, R_{sh} is the Sunshade radius required and A_{sh} is the area, calculated with the following formulas:

$$\Delta S = \frac{RCP}{1 - \alpha_p} \text{ , where } \alpha_p = 0.313 \text{ is the Earth albedo}$$

$$f = \frac{\Delta S}{S}$$

where $S = 342.75 \ \frac{\mathrm{W}}{\mathrm{m}^2}$ is the average solar insulation on the Earth for the actual surface, $S_0/4$

$$R_{sh} = \frac{R_S d_{SEL1} \sqrt{f}}{AU}$$

$$A_{sh} = \pi R_{sh}^2$$

RCP	ΔS	f	R_{sh}	A_{sh}
1.22	1.78	0.52%	5.3206×10^5	8.8934×10^{11}
1.9	2.77	0.81%	6.6398×10^5	1.3850×10^{12}
2.6	3.78	1.10%	7.7672×10^5	1.8953×10^{12}
3.4	4.95	1.44%	8.8822×10^5	2.4785×10^{12}
4.5	6.55	1.91%	1.0218×10^6	3.2804×10^{12}
6.0	8.73	2.55%	1.1799×10^6	4.3738×10^{12}
7.0	10.19	2.97%	1.2745×10^6	5.1028×10^{12}
8.5	12.37	3.61%	1.4044×10^6	6.1962×10^{12}

Table 4.1: Sunshade parameters divided by scenarios

Obviously, as the efficiency increases, the number of solar panels needed decreases, and in particular, around an efficiency value of 0.20% we have a mass needed for perovskite panels of about 1.8×10^9 kg, while aluminum panels are on the order of 23×10^9 kg.

A silicon solar cell is on average around 0.500 kg/m^2 if we stay conservative and consider the cell around 5 g/m^2, the steel substrate around 200 g/m^2 and the SiO_2 cover around 125 g/m^2, but with the overall mass of the architecture structure it can arrive at 3.5 kg. Considering the base, the density of the surface is a minimum percentage of the total, so the mass between a silicon solar cell and a perovskite one is not so much different. What is different, as seen before in section 3.3, is the energy required to produce them. For the production of silicon solar cells on the Moon, different data can be found on various paper that will be discussed later on this document, but for perovskite, as it is a new technology that still need to be tested, data are not much available. Therefore an assumption has been made, based on on-Earth data production, a roll to roll perovskite Panel can be printed with about 13 kW/m^2.

In figure 4.3 a 3D-perspective of the dimensions of the project is rendered, scaled to make the Sunshade visible, which otherwise would have been an almost invisible dot due to the great distance separating it from the Earth in relation to its size. The proportions of the Sunshade's dimensions for an efficiency of 20 per cent in climate scenario 1 are shown in figure 4.4, while the division between photovoltaic and aluminum panels for the same case is illustrated even more precisely in the graph in figure 4.5.

In particular, the figure 4.5 is not to be considered representative of the arrangement of the panels in the actual construction of the Sunshade. They will be arranged in a pattern that ensures the highest efficiency, so the photovoltaic panels will be scattered throughout the Sunshade amidst the aluminum panels rather than placed all in one place.

Figures 4.6 and 4.7 show how the sunshade mass would increase in the second and fifth climate scenarios (RCP 1.9 and RCP 4.5), respectively. It can easily be seen how the masses increase by one order of magnitude in the first graph and two orders of magnitude in the second,

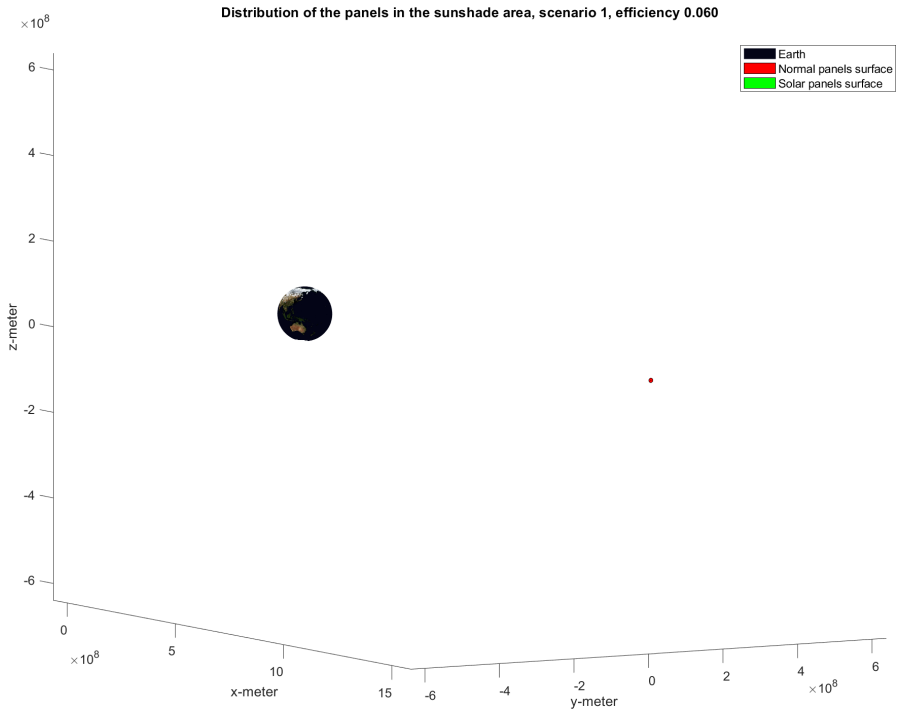

Figure 4.3: Scaled 3D-distance between Earth and Sunshade

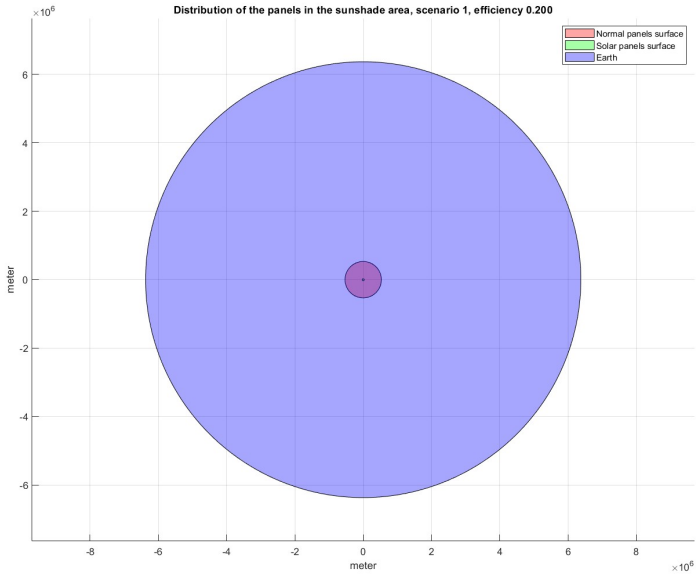

Figure 4.4: Comparison between the area of the Earth and the Sunshade

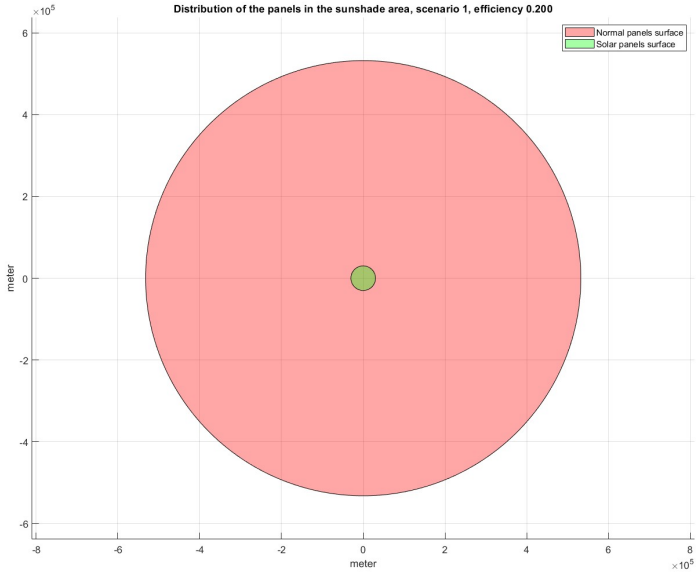

Figure 4.5: Zoomed area of the Sunshade divided between photovoltaic and aluminum panels

with a shift forward in efficiency of the meeting point between the weight of photovoltaic and aluminum panels.

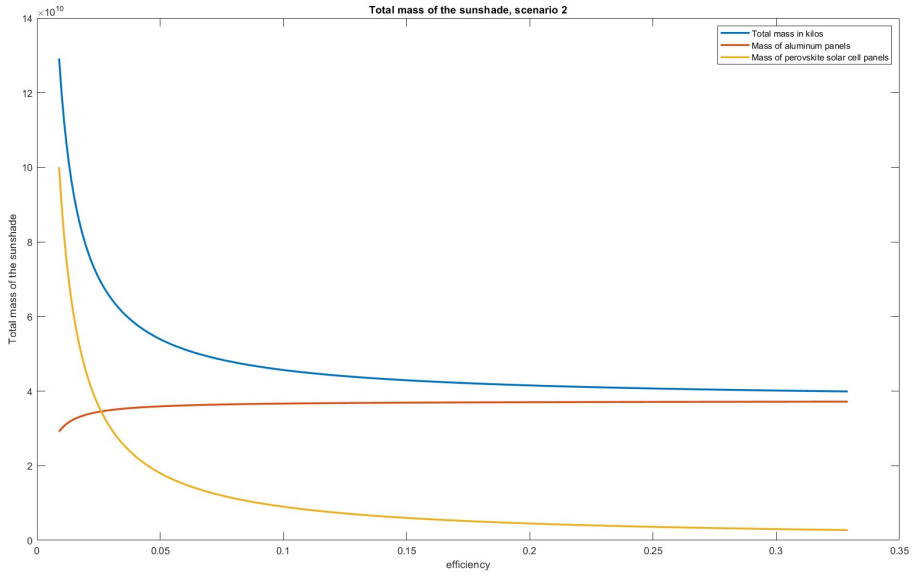

Figure 4.6: Mass needed to build the Sunshade in the RCP 1.9 scenario

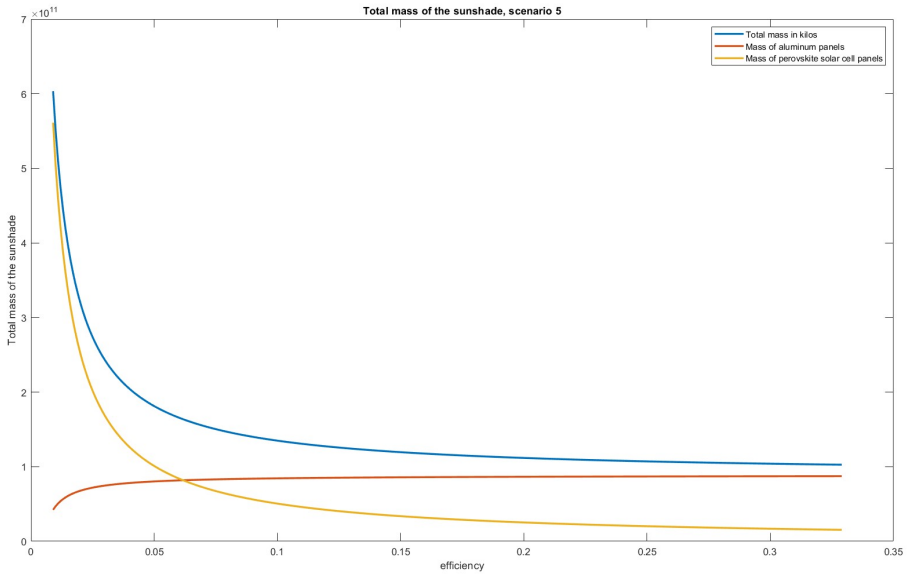

Figure 4.7: Mass needed to build the Sunshade in the RCP 4.5 scenario

4.4 Mining and materials transportation

Among the most important inputs of the energy simulation, apart from the data concerning the masses involved, are undoubtedly those concerning the extraction of material and its transport.

The data-sheets of the Lunar Resources project are unfortunately not known either for the excavation machine in the figure 4.8 or for the transport rover in the figure 4.9, due to the fact that the project is still in the development phase, which is covered by industrial secrecy.

For this reason, the Bucket ladder was selected as the data concerning the mining system on the Moon, as previously suggested in S. Fix's thesis. The table with the data concerning the operation of the Bucket ladder is shown in figure 4.10.

The Bucket Ladder appears to be the best of the means known today due to the favorable ratio between excavation capability and power requirements. It is capable of excavating 2400 kg/h with a power requirement of less than 200 W per machine, i.e. 4.8 kWh per day.

The excavation process for the simulation is divided into two main phases: the first 35, where approximately 15 excavators will be used to extract the material necessary for the creation of the panels that will form the Lunar Solar Park, and the second 35, where approximately 600 excavators will be used to procure the material necessary for the production of the aluminum panels (counting on having 192.5 kg of aluminum per hour per mining unit, see chapter 4.5). During this second phase, the launching phase of the photovoltaic panels already prepared in phase 1 will also begin, ready to be launched from the coilgun, followed gradually by the aluminum panels

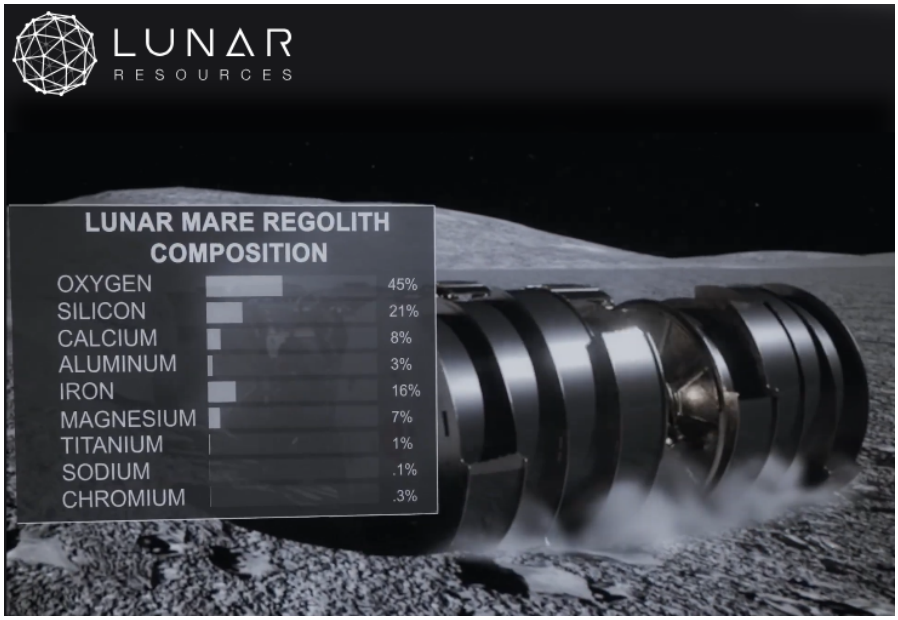

Figure 4.8: Materials percentage distribution in lunar regolith, rendering of a lunar mining system

that are being prepared.

For the transport phase, there are two modes of operation: one is a rover that can operate using solar panels and autonomous batteries, the other is a railway transport system.

Also part of NASA's moon landing program is the FLOAT (Flexible Levitation system On A Track) project to ensure a reliable, autonomous and efficient method of transporting payloads to the lunar surface. It would be essential for transporting excavated regolith to the reactors to obtain consumable in-situ resources for both panel production and infrastructure, for transporting payloads from the landing sites to the lunar base and back, as well as transporting the material needed for excavations.

The FLOAT system uses non-powered magnetic robots levitating on a three-layer flexible film track: the first of graphite allows the robots to passively float on the tracks using diamagnetic levitation, the second of flexible circuits generates an electromagnetic thrust to propel the robots in a controllable manner along the tracks, and the optional third layer of thin-film solar panels could generate power for the base when in sunlight. FLOAT robots have no moving parts and levitate on the tracks to minimize abrasion and wear from moon dust (a major cause of wear and tear on the Moon), unlike lunar robots or rovers with wheels, legs or tracks, panels and batteries.

The FLOAT tracks roll out directly onto the lunar regolith to avoid the need for large on-site constructions. Individual FLOAT robots will be capable of transporting payloads of various shapes/sizes (up to 33 kg/m^2) at useful speeds (>0.5 m/s), and a large-scale FLOAT system will be able to move up to 100,000 kg of regolith/ payload for several kilometers per day, consuming

Figure 4.9: Render of a transportation rover on the Moon

<40 kW of energy. FLOAT will operate autonomously in the dusty and inhospitable lunar environment with minimal site preparation. Another of its great strengths is that its track network can be rolled up/reconfigured over time to meet the mission requirements of the evolving lunar base.

In Phase 1, the fundamental feasibility of designing a FLOAT system with meter-scale robots and km-scale tracks to support human exploration activities (HEO) on the Moon will be established by completing the following four main tasks.

The first is the definition of the mission requirements, mainly mass, size, payload quantity, transport distance and power. Then we need to perform simulations of the FLOAT system with meter-scale robots and km-scale tracks under lunar conditions to refine performance estimates. Then conduct experiments on existing cm-scale robots, similar to FLOAT, to study the most pressing questions on the feasibility of the FLOAT system, and finally size the FLOAT system according to mission requirements, using the lunar performance predicted by the simulations and experiments.

4.5 Production and refining

This section will mainly deal with two methods for extracting material from the lunar soil, of which only one will be chosen to be applied in the energy budget simulation. The two approaches are Molten Regolith Electrolysis (MRE) and fluoridation-based refining. Both approaches have advantages and disadvantages, which will be discussed after they have been presented.

Process	Excavation capability	Depth of Excavation or cut	Mass of system	Power/energy requirements	Traverse speed	Simulant/ analogue used	Comments	Reference
Pneumatic	6 kg/h[a]	Not applicable	–	20 W 2 Wh/kg	–	GRC 1	Operated with NASA Ames K10 mini robotic platform; tested in vacuum chamber; partially tested on parabolic flight	(Zacny et al., 2008b & 2009 & 2012)
Bucket ladder	800 kg/h[b] 1500 kg/h[b] 2400 kg/h[b]	10–15 cm (maximum reach)	76 kg	<200W	8 m/min	–		van Susante and Dreyer (2010)
Bucket drum (RASSOR)	90 kg per trip[c]	–	67 kg[d]	0.761 Wh/kg	30 m/min	Sand KSC crawler way fines BP-1	Tested with gravity offload and in icy BP-1	Mueller et al. (2013 & 2016), Schuler et al. (2019), & Townsend et al. (2017)
Bucket wheel (Polaris)	1050 kg/h[e]	–	200 kg	470 W	24 m/min	GRC 1		Skonieczny et al. (2016a & 2016b)
Bucket wheel (Scarab)	180 kg/h	5 cm (single cut)	312 kg	–	1.62 m/ min	GRC 1	Tested with gravity offload	Skonieczny et al. (2016a & 2016b)

[a] with 1g of compressed gas.
[b] 1st generation (2006); 2nd generation (2008); 3rd generation (2009).
[c] 20 trips of 100 m per charge.
[d] each drum has a mass of 7 kg.
[e] with 14 m driving operation; 17 dig-dump task cycles.

Figure 4.10: Main extraction systems technology on the Moon

The MRE method involves heating the lunar regolith to a molten state, whereby its intrinsic ionic conductivity allows for direct electrolysis. In this process, a voltage is applied between the two electrodes immersed in the molten regolith.

At the anode, oxygen is released in gaseous form, a valuable resource both for life support systems and as a fuel oxidant for rocket propulsion. At the cathode, at the same time, the electrochemical reduction of metal oxides produces reduced metals, including iron, silicon and aluminum, along with other elements such as titanium. One of the key advantages of the MRE method is its high efficiency in extracting oxygen, having demonstrated that up to 95 per cent of the oxygen contained in the regolith can be released.

Scaling up the process from a laboratory-experimental scale, which considers small currents, to a near-industrial production scale will require great attention to the reactor design process. In particular, one aspect to which attention must be paid is the containment of corrosive regolith at high temperature. To address this, innovative designs such as the 'joule heated cold wall' have been proposed, whereby the reactor walls are insulated by a thin, frozen layer of regolith maintained by the heat generated through the electrolysis process itself.

This not only protects the structural materials, but also extends the operational lifetime period, a critical prerequisite for lunar ISRU systems.

The second method is using fluorine-based chemistry to refine lunar regolith. Fluorine is introduced into the regolith as potassium fluoride (KF), which, however, needs to be produced and transported directly from Earth, thus undermining the project's intention to be autonomous in using only lunar resources.

Through electrolysis, KF releases potassium and fluorine as individual elements. The free fluorine then reacts with oxygen in various metal oxides in the regolith displacing oxygen and forming volatile metal fluorides. For example:

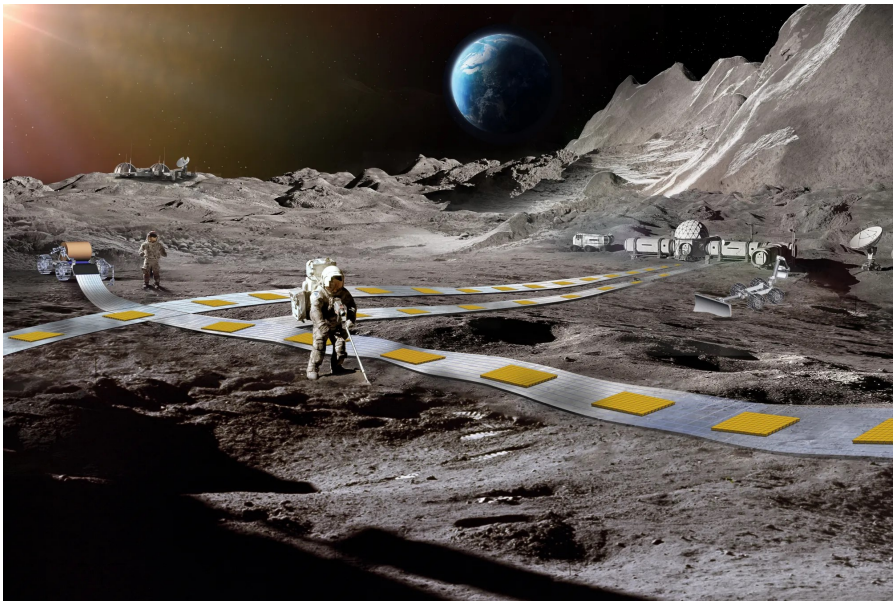

Figure 4.11: Artist concept of novel approach for a Flexible Levitation System on a Track on the Moon

$$SiO_2 + 2F_2 \rightarrow SiF_4 + O_2$$

producing tetrafluorosilane (SiF4) and oxygen. Similarly, metal oxides such as Al_2O_3 undergo fluorination:

$$Al_2O_3 + 3F_2 \rightarrow 2AlF_3 + \frac{3}{2}O_2$$

The volatile tetrafluorosilane, once produced, can be separated from the reaction mixture through fractional distillation owing to its distinct liquefaction temperature ($-86\,^{\circ}C$), and subsequently reduced to elemental silicon using a reducing agent such as potassium:

$$SiF_4 + 4K \rightarrow Si + 4KF$$

Analogous reactions are employed to recover other metals, such as the reduction of aluminum fluoride and iron fluoride to yield aluminum and iron, respectively:

$$AlF_3 + 3K \rightarrow 3KF + Al$$

$$FeF_3 + 3K \rightarrow 3KF + Fe$$

This fluoridation process offers the benefit of producing multiple high-purity products including oxygen, silicon, and metals, while working directly with unpurified regolith. Moreover, the

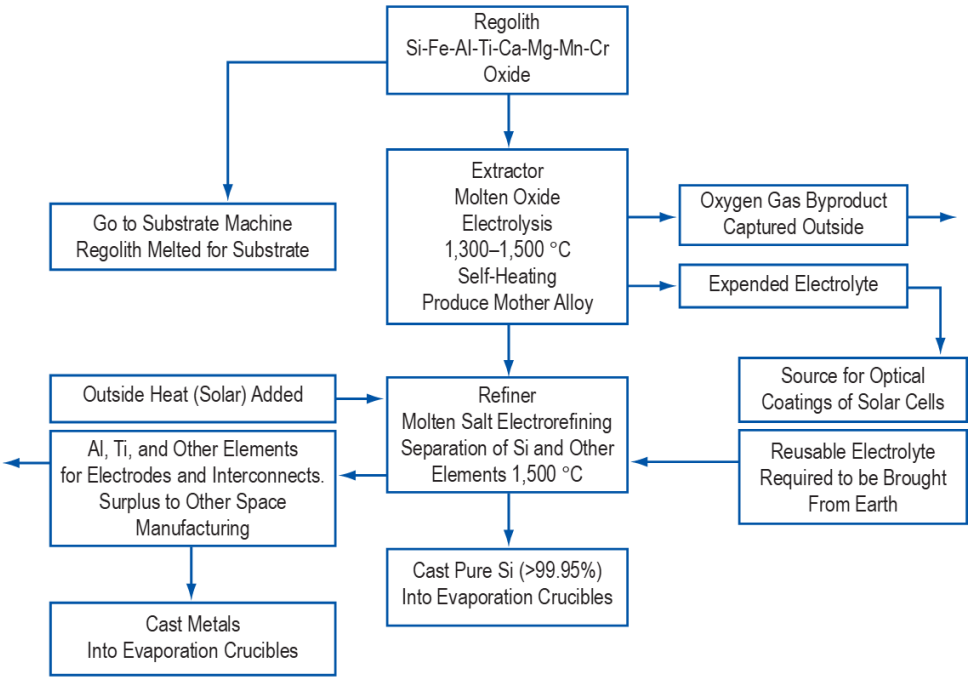

Figure 4.12: Process flow diagram for the Molten Oxide Electrolysis (MOE) - based extraction and refining process

early separation of volatile species facilitates subsequent purification steps that are essential for applications such as semiconductor manufacturing and the production of structural components.

Despite their respective merits, both the MRE and fluoridation-based refining processes face significant challenges. The MRE process, while conceptually straightforward and efficient in oxygen extraction, must contend with the difficulties inherent in high-temperature reactor operation and scaling up to industrial production levels. In contrast, the fluoridation process, although capable of yielding multiple refined products, requires a complex series of chemical reactions and separation steps, as well as the reliable recycling of fluorine reagents to maintain a closed-cycle system.

The choice between these approaches - or the potential development of a hybrid system - will depend on a range of factors, including reactor scalability, energy efficiency, process complexity, and the overall integration into lunar ISRU architectures. Continued research, including the development of parametric models and experimental validation, is essential to advance these technologies from concept to practical application.

A thorough parametric sizing model of an MRE reactor has been set up numerically that provides a database of reactor designs and performance characteristics. For highland regolith, a production rate of 10 t of oxygen, about 2 t of aluminum, 5 t of silicon, and almost 1 t of iron per year for a reactor mass of under 600 kg and an electrical power of 35 kW were achieved within

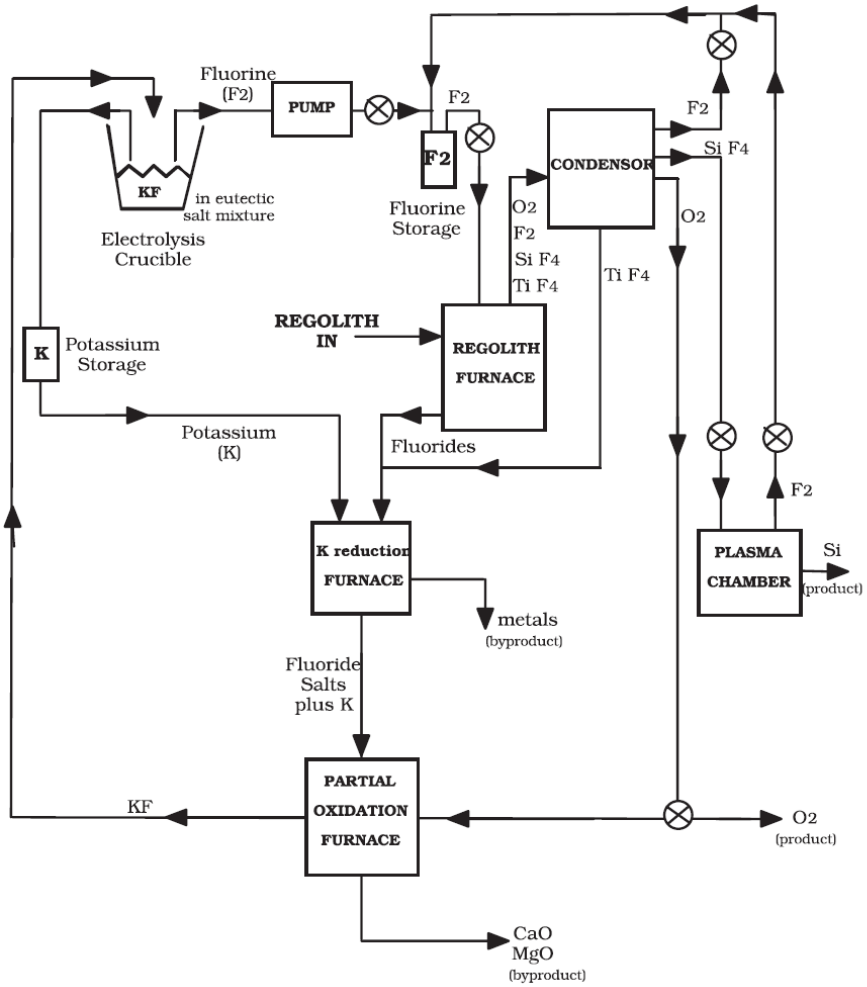

Figure 4.13: Block diagram of silicon and oxygen production steps

the simulations. This means that per day every reactor can produce 27.4 kg of Oxygen, 5.5 kg of Aluminum, 13.7 kg of Silicon and 2.7 kg of Iron. Currently the technology of molten regolith electrolysis is at TRL-4 (Technology Readiness Level).

These reactors have an efficiency of around 30-40%, so from the 2400 kg/h extracted from the mining process, they can process 960 kg of Oxygen, 192.5 kg of Aluminum, 479.5 kg of Silicon and 94.5 kg of Iron per hour. Considering silicon as the limiting factor for the construction of silicon photovoltaic panels, this means that at least 35 reactors are needed to process the 479.5 kg of silicon simultaneously throughout the day. Assuming that the material is mined for 24 hours non-stop, however, the number of reactors must also be multiplied by 24, giving a total of 840 reactors. If each reactor processes 13.7 kg of silicon in one day, this means that it produces the material for approximately 4 panels per day conservatively, i.e. one panel every 6 hours,

requiring 210 kWh of energy per panel.

This means that 137 panels can be produced in one hour, which at the maximum production rate of 3288 per day. In the meantime, as will be seen later in the simulation chapter, another 14 excavators will continue to extract the material and store it in special hubs so that it will be ready when the construction of the Lunar Solar Park is completed in order to start production of the Sunshade panels, which are much thinner and therefore require much less material and energy. It has been estimated, based on the production values of photovoltaic panels on earth, that around 13 kW are required to produce a single perovskite panel. This appears to be a good estimate for an average value, probably even lower considering the roll-to-roll processes bringing liquid perovskite printable from the earth.

The side product of the MRE is that we can produce more than 23 Mg of Oxygen per day, that can be usable both as propellant and, of course, as a fundamental resource to allow human presence on the Moon surface.

In the graph in figure 4.14 it's shown how the possible products from the Electrolysis of regolith can be used for future applications.

Also to be considered is the fact that in any case, the accounts are made with the technologies we have today, but it is to be hoped that technological progress and scientific research will take efficiency levels higher and higher, enabling even greater results than those already achieved. To give an example, the Lunar Resources reactor in figure 4.15 will measure about 1-meter in diameter and height and process scoops of lunar regolith delivered by a small rover. The goal is to process as much as 100 kilograms of lunar regolith during a 24-hour period. Much better then the 70 kg per day considered by this simulation. But if we shows results for a conservative simulation, these results can only be better with better with better performances.

Whereas in the first phase of the simulation 840 reactors were sufficient for 15 mining units, in the second phase of the simulation 600 mining units will be used. The reactors will have to gradually refine the material stored in the hubs during the first 35 years and that extracted by the new mining units. To process the material extracted during the second phase of the mission, while in the first phase 840 reactors were required for 15 mining units (even if only one had been refined), according to a simple proportion, now at least 31920 reactors will be required. The new reactors, according to a study by L. SIbille and J.A. Dominguez, show that it is possible to create reactors for the lunar soil with a power requirement of less than 5 kW and a higher efficiency than before, which is why these were implemented for the second phase of the simulation. In order to be able to complete the project on schedule, an increase from the 5.5 kg per day of aluminum of the first reactors used is expected to 79 kg of aluminum per reactor per day, in order to reach the 24×10^9 kg target.

4.5.1 Solar cells

It's been considered silicon as the "limiting reagent" for the creation process of the panel. As input parameters for the cell we considered the average efficiency of a solar cell around 20%,

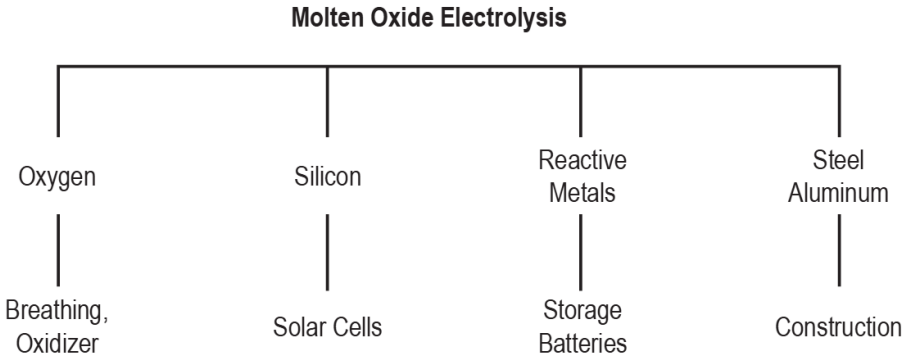

Figure 4.14: Future space resources from the development of MOE

so the production of about 0.3 kW of Power per cell, considering $2\,m^2$ per cell. The extraction process written above, the transportation, the separation and the assembly are all listed in the MATLAB file for a total of 246 kW per cell, considering the really expensive (in power terms) refining process. For the Lunar Solar Park, as said in the previous chapters, the silicon solar cells were chosen because they have been more tested over the years, being safer for the start of such a complex project. Perovskite solar cells were chosen for the Sunshade because by the time its construction will start there are more chances that they will be properly tested for space utilization and the technology of roll to roll printable perovskites will be fully developed.

Last but not least, a really important part in the simulation was considering the degradation of the solar cells in the power budget. It is considered that an average solar cell efficiency degradation is around 0.5-0.9%, it means, considering 0.9% as the worst case and linearizing the problem, a loss in efficiency of the 0.002% per day. The maintenance budget was considered to be the 5% of the total available energy, used to solve the maintenance problem of the various infrastructures and to substitute the old panel with new ones, to always guarantee a high level of power.

The power budget earmarked for maintenance will come into operation from year 10, to replace worn-out panels, once we have already reached maximum daily production. Part of the excess power will then be allocated to the construction of the coilgun.

The Moon has a hostile environment for landers and rovers because of its extreme surface temperature variation (130 °C in the daytime to −170 °C in the night) because the ambient pressure of the lunar surface is a hard vacuum, without atmosphere. The batteries are required as power storage for satellite, rover, and human-crewed missions, as shown in figure 4.16. The desirable battery characteristics for these missions include high power density such as 15 W to 15 kW for satellite, 90 W to 2 kW for rover and 50 kW habitat for manned mission, high cycle life, operating temperature of 0−40 °C for satellite, −233 °C in permanent shadow to 183 °C in sunlight for rover.

Figure 4.15: Rendering of a molten resource extractor under development by Lunar Resources

4.5.2 Infrastructures

Establishing a sustainable presence on the Moon requires the development of several key infrastructure components. These include landing and launch pads, habitation modules, store hubs, and transportation networks. Each of these components plays a crucial role in supporting lunar missions and ensuring the safety and efficiency of operations.

Landing and Launch Pads: Landing and launch pads are critical facilities that must be designed to mitigate the effects of lunar dust and exhaust plume impingement. During landings and launches, the exhaust plume can eject regolith particles at high velocities, posing significant risks to nearby equipment and personnel. To address this challenge, these facilities may incorporate berms or specialized surface treatments to contain and redirect high-velocity ejects. Additionally, using in-situ construction methods, where local resources are utilized to build landing pads, can enhance safety and efficiency. This approach involves using regolith with or without binder additives to create durable surfaces capable of withstanding the harsh conditions of the lunar environment.

The lunar environment lacks an atmosphere, which makes it difficult to dissipate heat and manage debris effectively. Therefore, materials used in the construction of landing pads must be thoroughly tested under simulated conditions to ensure their viability. Despite these challenges, the use of local resources can significantly reduce the reliance on Earth-based supplies and enhance the sustainability of lunar operations.

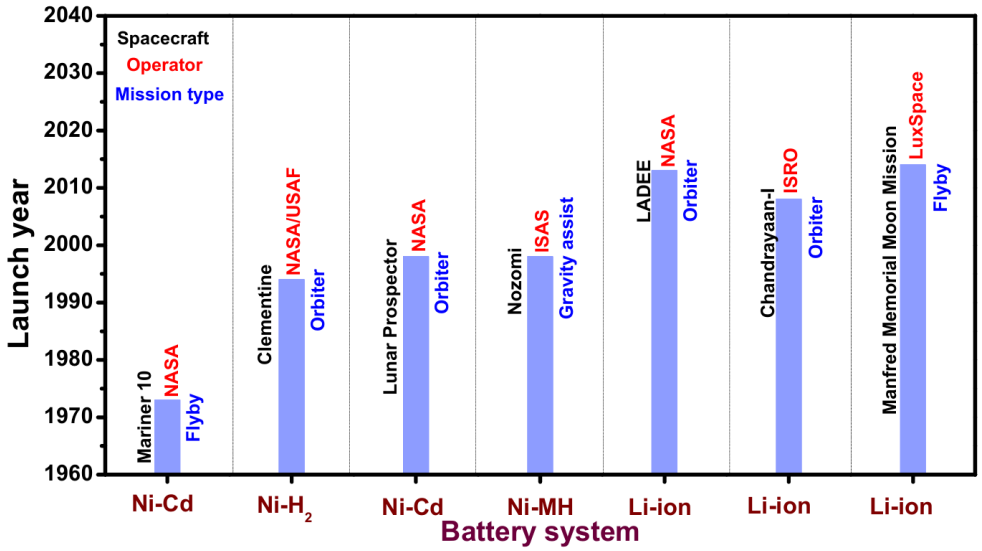

Figure 4.16: Battery system used in Lunar mission

Habitation Modules: Habitation modules are another essential component of lunar infrastructure, designed to provide robust protection for astronauts from radiation, micro-meteoroids, and extreme temperature variations. Long-duration missions require these modules to maintain a stable internal environment and support life for extended periods. This includes air recycling, temperature control, and psychological well-being. Advanced construction techniques, such as in-situ resource utilization (ISRU), can be employed to construct habitats using local materials like regolith. By mixing regolith with polymers, it is possible to enhance radiation shielding while minimizing the need for materials transported from Earth.

Store hub: Store hubs serve as logistical centers for storing supplies, equipment, and resources necessary for lunar operations. These hubs must be strategically located to facilitate easy access for transportation networks and should be shielded from radiation and micro-meteoroids similar to habitation modules. Designing store hubs with ISRU in mind can help minimize reliance on Earth-based supplies, contributing to the sustainability of lunar missions, and especially for this project their importance is maximum to store the lunar regolith excavated that will be processed later.

Transportation Network: A lunar transportation network, including roads and potentially a rail system, will be essential for the efficient movement of personnel, equipment, and resources across the lunar surface. Automated vehicles are preferred for reliability and efficiency in the harsh lunar environment, without placing a burden on energy sources that are already under quota. Robotic construction techniques can be used to build this infrastructure, leveraging in-situ resources where possible. This approach not only reduces the need for manual labor but also

enhances the speed and efficiency of construction processes. By integrating these components effectively, a comprehensive and sustainable lunar infrastructure can be established, supporting both short-term missions and long-term human presence on the Moon, as we have seen before regarding the FLOAT project.

Blast Shield: last shields serve as protective barriers to deflect or absorb the impact of debris and gases expelled by spacecraft, safeguarding nearby infrastructure and personnel from damage. The importance of blast shields cannot be overstated, as they are crucial for protecting lunar bases from the hazardous effects of rocket exhaust and debris. Historical evidence, such as the damage to the Surveyor III probe by the Apollo 12 rocket, underscores the need for such protective measures.

The use of in-situ materials, such as lunar boulders, offers a promising approach for constructing blast shields. Autonomous robotic excavators can collect and stack these boulders to form a protective wall around landing pads or bases. This method is energy-efficient and reduces reliance on materials transported from Earth. Researchers have proposed that such a blast shield could be built in as little as three months, highlighting the feasibility of this approach for rapid deployment.

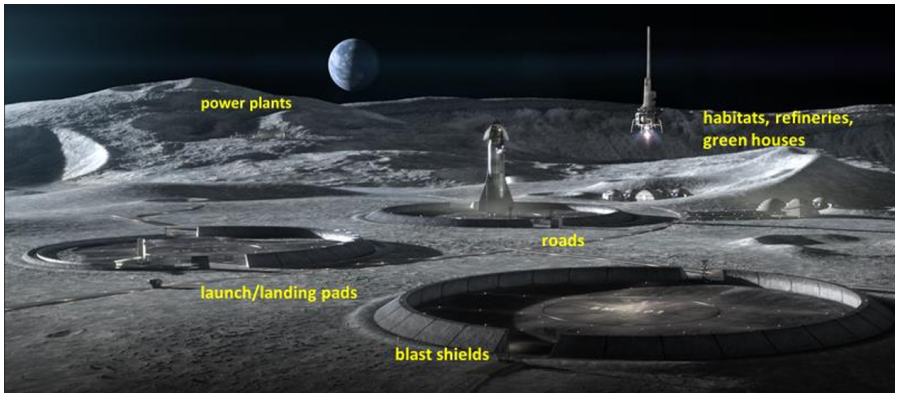

Figure 4.17: Moon infrastructures rendering

4.6 Launch Phase

In this section we will talk about the first launches from Earth with Starship to have a source of starting energy on the Moon and supply the power station with the basic infrastructures. With the launches with Starship we have to bring on the Moon not only the first solar arrays to start the process (at least 1000 kW of power), but also the reactors for the electrolysis of the regolith, the rover for the transportation of the material and the excavators. In the second section we will talk about the coilgun launch phase.

Starship In the previous sections it has been discussed that to start this project we need to bring at least solar arrays for 10^3 kW, 570 mining units, a thousand rovers for the transportation of the material and 840 reactors. In the second phase we will need 585 more mining machines and 31080 more reactors.

Considering that for geostationary orbit Starship carries 27t, we can take it as a good approximation that it can deliver 15t of payload to the Moon, considering the in-orbit refueling system.

For the first panels to be brought from Earth, capable of producing 1000 kW of power, considering a production of about 0.3 kW for a 3.5 kg panel, the weight needed is approximately 12000 kg for the panels that would allow us to easily start the mission, and therefore all of them can be carried in one launch.

The mining systems weigh 76 kg each, so the first 15 can be carried without any problems in one launch, while considering that in subsequent launches a maximum of 197 excavators could be carried per launch, it would take another three launches.

If a reactor of the first type weighs 600 kg, it can carry 25 reactors per launch. So 33 launches at the beginning for the reactors and then another 1244 launches for the next 31080, for a total of 1277 launches for the reactors, considering that they could potentially be less because the new generation reactors could be much lighter.

The Lunar Roving Vehicle weighed 210 kg, but the rovers are the most complex part to calculate as they are very variable in terms of models, weights and characteristics, but above all, there is still not much data available to effectively calculate their transportability to the Moon. Assuming an average of about 100 kg per rover, about seven launches would be needed to transport a thousand rovers.

We thus arrive at a total of about 1289 launches, which, remaining conservative, we can round up to 1500.

Coilgun From the 35th year, we must use some of the energy produced to launch the panels created for the Sunshade.

The coilgun, also referred to as a mass driver, is a crucial component of the lunar-based material transportation system, designed to enable the efficient launch of payloads from the Moon into space. Unlike conventional chemical propulsion systems, which rely on fuel combustion, the coilgun operates through electromagnetic acceleration, utilizing a sequence of superconducting coils along a track to generate a controlled magnetic field. As a payload-carrying platform moves along this track, the coils are activated in a precisely timed sequence, creating a repelling and attracting force that accelerates the payload to the desired velocity. This mechanism allows for a gradual increase in speed over an extended distance, significantly reducing mechanical stress compared to traditional rocket launches.

The choice to implement a coilgun on the Moon is primarily justified by the unique environmental and logistical advantages it offers. The Moon's low gravity and lack of atmosphere

make electromagnetic acceleration particularly efficient, as there is minimal resistance to motion. Furthermore, Shackleton Crater, the selected site for the coilgun, presents ideal conditions for its operation. The crater's interior remains in permanent shadow, providing a naturally cold environment that is highly beneficial for superconducting materials, as they require low temperatures to function efficiently. This significantly reduces the energy demand for active cooling, a major constraint in terrestrial applications of superconducting technology.

The system is designed to support high-frequency launches, facilitating a continuous supply chain from the Moon to key orbital staging points such as Earth-Moon Lagrange Point 2 (EML2), where materials can be assembled into larger structures before being transported to their final destination. Additionally, its modular nature allows for future upgrades and expansions, making it a long-term asset for lunar and deep-space logistics.

The efficiency of the launch system in terms of power per mass presented in T. Maheswaran's thesis is 5 Wh/kg. This will be the main electromagnetic launch system used to launch the panels from the lunar south pole to the gravitational balance point SEL1.

4.7 Power beam back from the Sunshade

The transmission of energy from the Sunshade at the SEL1 position to the Moon can be achieved primarily by laser or microwave teleportation, two methods with different technical characteristics and challenges.

Laser Transmissions Lasers use a coherent optical beam which, because of its relatively low divergence, can maintain a high energy density over long distances. This allows the energy to be concentrated on a compact receiver with high conversion efficiency, making it an attractive option for applications where precision is critical. However, the precise orientation and alignment of the beam is critical to the effectiveness of a laser-based system. Any misalignment could result in significant losses or safety hazards, given the high intensity concentrated in a small area. In addition, advanced thermal management may be required to manage the concentrated beam, as laser energy generation and conversion typically require conversion efficiencies in the order of 30-40%.

Microwave Transmissions Microwave power transmission uses electromagnetic waves in the microwave frequency range, which naturally have a greater beam divergence. This characteristic means that the transmitted beam is spread over a larger area, which necessitates the use of larger transmitter apertures and receiver antennas (often in the form of rectennas) to effectively capture the energy and convert it back into electricity. Microwave systems are generally more tolerant of pointing inaccuracies due to their wider beam, and have demonstrated relatively high conversion efficiencies, sometimes reaching 50-60% in rectenna designs. However, the wider beam also means that a larger receiving area is required to achieve the same energy density as a laser

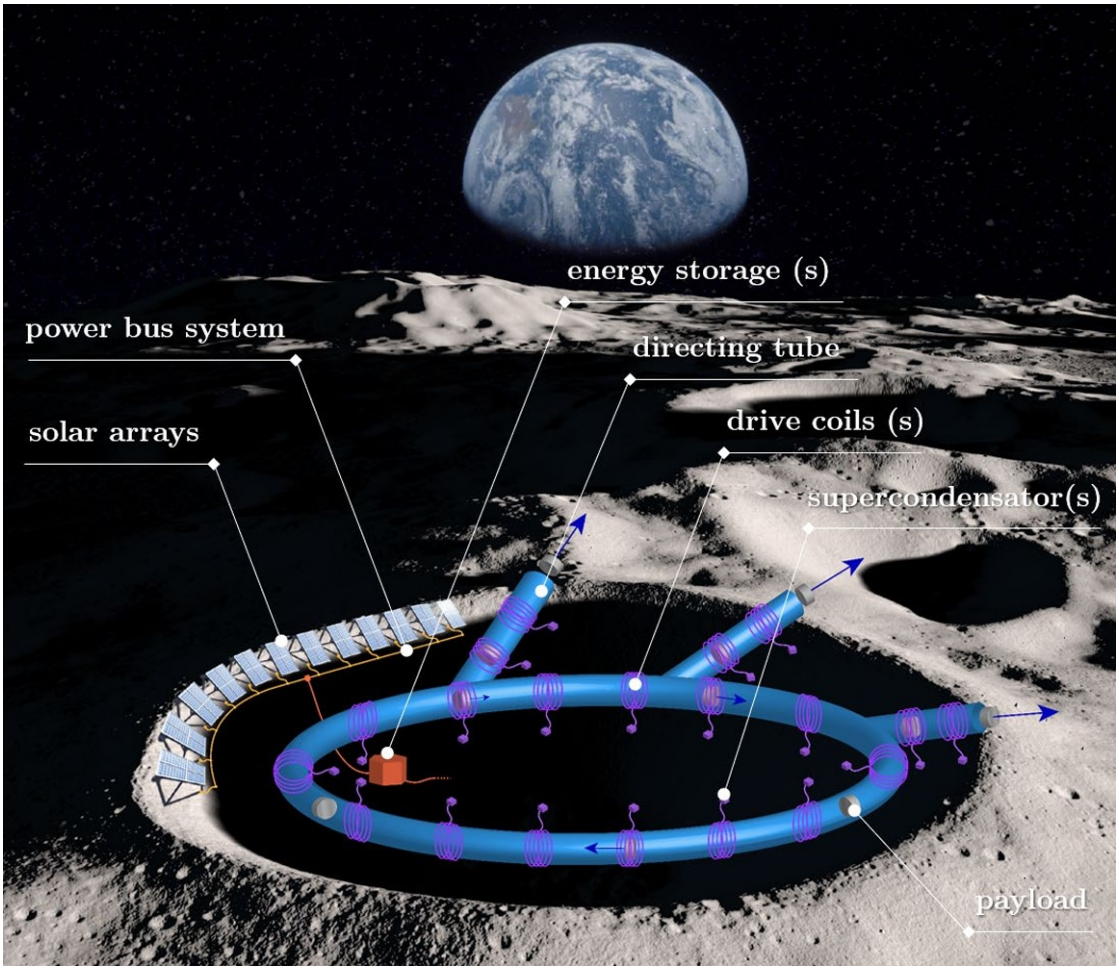

Figure 4.18: Coilgun model in Shackleton crater

system, potentially increasing the infrastructure required.

Anyway both methods benefit from the Moon's lack of atmosphere, which eliminates beam attenuation and scattering issues, allowing more efficient transmission than it would be possible on Earth. The choice between laser and microwave energy delivery therefore depends on a trade-off between the need for precise targeting and high energy concentration versus a more robust, less alignment-sensitive system with larger receiver requirements. For missions where high energy density is critical and the technological challenges of precise beam control can be overcome, laser-based systems may offer superior performance. Conversely, for applications where system robustness and reduced precision requirements are a priority, microwave energy delivery is a compelling alternative.

For this problem specifically, more detailed future studies are postponed as to which method-

ology can be chosen, knowing that on average for the areas shown in figure 4.5 we have 0.25×10^5 radius, i.e. approximately 1.96×10^9 m^2, capable of producing 2.7×10^9 kW of power. We must now take into account the efficiency of the panels, which, being about 20%, yields 5.32×10^8 kW, and the efficiency of the transport motion, which further lowers the value obtained to about 1.9×10^8 kW for laser transmission and 2.9×10^8 kW for microwave transmission, guaranteeing a good power base that can be exploited both on the Moon and on Earth.

Chapter 5: System Modeling

It is now well known how systems engineering is increasingly used from the early stages of missions, supporting their development throughout the entire life cycle, helping to reduce costs, but also to avoid possible risks, failures and schedule delays. For this reason, part of the development of this paper has been focused on the study of processes, architectures and, for those more familiar with the term, state machines, covering the four identified project phases.

To ensure clarity and consistency in the representation of mission subsystems, a structured legend has been adopted. Metamodels are categorized by sectoral areas, with operational states visually encoded: inactive operations are marked in black, while active operations transition from light yellow to intense orange to reflect increasing levels of activity. Additionally, mass exchanges are represented by red arrows, while power and energy exchanges are denoted by purple arrows. The thickness of these arrows is directly proportional to the intensity of the exchange, allowing for an intuitive understanding of the system interactions.

5.1 Metamodel Structure

To systematically represent and analyze the exchanges between the various subsystems of the mission, six distinct meta-models were developed. Each meta-model focuses on a specific functional domain, further subdivided into relevant subcategories. The six identified meta-models are:

- Launch Systems: covers transportation and mobility mechanisms;
- Facilities and Infrastructures: includes the essential structures for mission operations;
- Materials: focuses on regolith processing and material transformation;
- Production and Assembly: involves manufacturing and integration of components;
- Energy gain: pertains to energy production and transmission;
- Operations: covers maintenance, orbital adjustments, and logistics.

Launch Systems Launch systems are all those systems involved in transporting and moving payloads, materials, and components from one location to another, whether from Earth to the Moon or across lunar terrain. Among them there is obviously the launcher that will be used to send the initial loads from Earth, as presented earlier, i.e. Starship, which has been selected due to its high payload capacity and full reusability. Then there is the other major launch mechanism, i.e. the electromagnetic Coilgun realized by T. Maheswaran, designed to provide a sustainable method of launching materials from the lunar surface into space. Additionally there are the electric or chemical propulsion systems (if any) of the previously presented lunar transport systems, such as rovers or railways, that will facilitate the movement of components across the lunar landscape.

Facilities and Infrastructures This sub-category includes some of the infrastructures identified in the 4.5.2 section, thus: Landing and launch pads, designated for spacecraft arrival and departure, habitation modules, built like small living quarters for crewed operations, store hub, centralized facilities for material and equipment storage, while the transportation network is included in the above meta-model.

Materials It includes all operations that have to do with the materials involved, to transform lunar regolith into usable materials for the constructions we need. These include in particular the aforementioned extraction, the process of mining regolith from the lunar surface, pre-processing by removing the unwanted elements, and separation and isolation of silicon, alumina, iron and other materials, using the methods seen in 4.5. Together with infrastructures, these are the only operations that work throughout the whole process life cycle, ensuring a continuous supply of raw materials.

Production and Assembly Once raw materials have been processed, they undergo manufacturing and assembly to form mission-critical components. This model represents the fabrication, assembly and integration of the materials processed and reworked to create the panels that will make up first the Lunar Solar Park and then the Sunshade. Photovoltaic cells and structural elements will be manufactured, integrated into deployable modules and prepared for installation.

Energy gain In this sub-category, the structures that after being assembled will be able to produce and transmit energy are analyzed, i.e. the Lunar Solar Park and, of course, the actual Sunshade that will send the collected energy in the form of laser or microwave transmission, as presented in the 4.7 section.

Operations Under the name "operations" there are all the activities that will begin once production is well underway and assembly has begun, to maintain and adjust mission systems after initial deployment. The maintenance concerns the panels of the Lunar Solar Park, which will be repaired or replaced after years of activity, wear, tear and damage due to dust on the

lunar soil. De-orbiting maneuvers will be used to safely remove outdated units and replace them with new ones in the Sunshade, and orbital maneuvers, which can adjust the position of the Sunshade by solar sailing or alternative propulsive techniques.

5.2 Phase 1

The first phase is the crucial start of the mission, when the process officially begins with the delivery of essential infrastructure to the lunar surface. During this initial phase, the activity of the launches from Earth is particularly intense, as they must transport not only the necessary equipment for the extraction and processing of materials, but also the tools for the production and assembly of the solar panels. The success of this phase depends heavily on the ability to quickly establish a self-sufficient base of operations, gradually reducing dependence on ground supplies.

After deployment, the infrastructure begins to interact with the lunar environment: regolith mining and processing systems are installed and tested, but the actual production process is still in its infancy. At the same time, solar panel production will begin, albeit at a reduced rate. During this period, the main source of power for all operations comes from the pre-assembled solar panels transported from Earth aboard the launch rocket. These panels provide the initial energy support for critical infrastructure, allowing the first stages of extraction and refining to begin with a minimum of self-sufficiency.

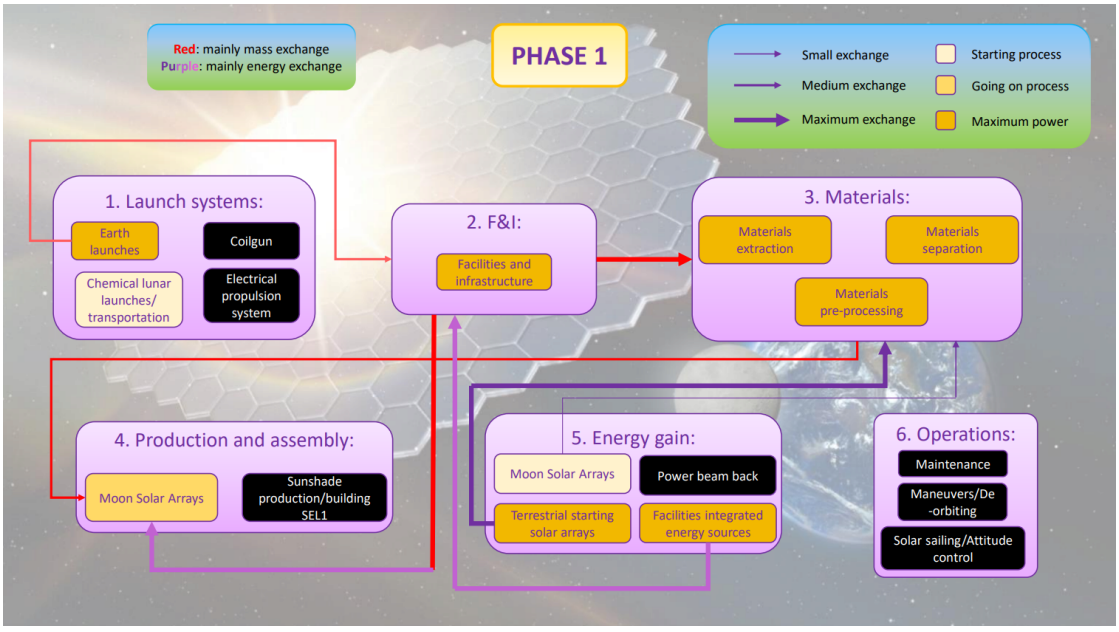

Figure 5.1: Model of the first phase

Infrastructure, such as housing modules, control centers and hubs, are designed to be partially

autonomous, thanks to integrated energy sources. However, as the local production of solar panels is still in its infancy, the amount of available energy remains limited, which affects the pace at which the entire production ecosystem can develop. Indeed, the extraction and processing of materials depend on the available energy, and only when panel production reaches higher levels it will be possible to sustain the lunar industrial processes on a large scale.

At this early stage, mission operations cannot yet become fully operational, as they require an established infrastructure before they can be active. Initial operations are therefore focused on commissioning the facilities and starting production of essential materials, which will form the basis for building further facilities, more panels and expanding production capacity.

Looking at the graphical representation of the model, it is evident that the first phase of the mission is mainly characterized by mass exchanges between the Earth and the lunar infrastructure. Material flows transported by the launchers are predominant, while energy exchanges are limited and restricted to the few solar panels initially available. The progression of the mission will see a gradual increase in local energy production, marking the transition to the second phase, in which energy self-sufficiency will become an increasingly concrete goal.

5.3 Phase 2

In the second phase of the mission, the most obvious change concerns the role of the launch systems. Whereas in the initial phase, launches from Earth were crucial for the transport of infrastructure and initial resources, in this new phase, these operations are progressively exhausted, leaving room for more efficient and autonomous internal logistics. In Box 1, devoted to launch systems, it can be seen that the contribution of ground launchers becomes marginal, while lunar transport vehicles come into play with greater intensity. The latter assume a crucial role in the transfer of processed materials to the solar panel production and assembly sites, as well as to the coilgun, which is being built but still inactive at this stage.

The focus then shifts to the large-scale production of the solar panels for the Lunar Solar Park. Thanks to the increased efficiency in the regolith extraction and processing cycle, the pace of panel production and assembly becomes faster, allowing for a significant increase in power generation capacity.

This step is decisive for the completion of the self-sustaining production process: the energy generated by the solar panels is no longer just a support, but becomes the primary source to power all extraction, pre-processing and material separation operations. In particular, the MRE method comes into full swing, ensuring a constant flow of raw materials processed and ready to be used in the construction of new infrastructure and components.

Another significant aspect of this phase is the start of maintenance operations. As shown in Box 6, dedicated to mission-critical operations, maintenance becomes the first operational activity to be activated. Since by this time the mission will have been underway for several years, the effects of wear and tear and the hostile lunar environment begin to become more

apparent. The accumulation of lunar dust on the solar panels, prolonged exposure to radiation and thermal stresses all contribute to degraded performance of the power systems, necessitating repair and replacement operations. For this reason, a portion of the energy produced is directly allocated to maintaining the operational efficiency of the Lunar Solar Park, ensuring that energy production remains constant over time and does not drop significantly.

This phase therefore marks the transition from a system still dependent on ground supplies to an increasingly autonomous reality, in which the local production of energy and materials becomes the focus of operations. The progressive activation of infrastructures and logistical support mechanisms represents a fundamental step towards achieving the full operability of the mission and its long-term sustainability.

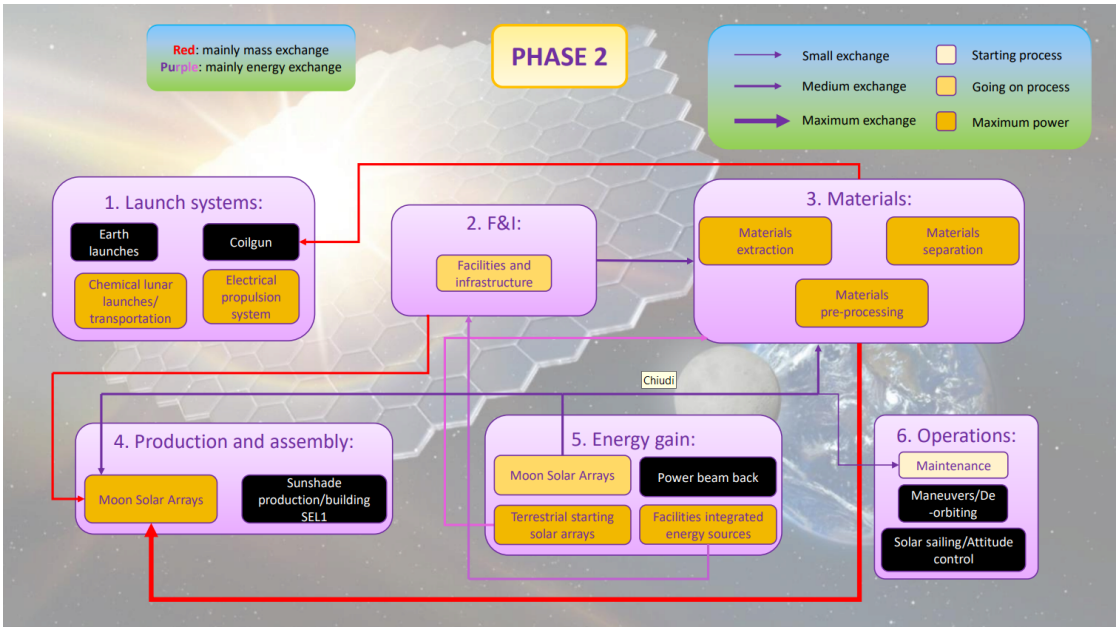

Figure 5.2: Model of the second phase

5.3.1 Phase 2 - closed loop

Phase 2 is the first time that a closed loop is manifested within the system, marking the progressive shift towards energy and material self-sufficiency. This loop highlights the direct link between the extraction, processing and production processes and shows how the flow of materials is continuously reinvested within the system. Specifically, extracted and refined raw materials are sent to production and assembly centers where they are transformed into solar panels. Once installed, these panels begin to generate energy, which in turn is used to power both the extraction and refining operations and the further construction of new solar panels.

This mechanism creates a self-sustaining cycle that feeds itself and allows for the gradual

expansion of the power plant. As new panels are produced and installed, the energy capacity grows in a non-linear manner, allowing the overall process to be accelerated. The energy available not only covers the initial production requirements, but also allows the scale of the operation to be increased, improving efficiency and reducing dependence on external energy sources.

The most important aspect of this model is that the growing energy capacity does not follow a linear trend, but tends to become exponential. As can be seen from the graphs resulting from the implemented simulation, the system is designed to reach energy production peaks much faster than in a constant growth scenario. This phenomenon makes it possible to speed up the entire expansion process and quickly reach a production threshold that guarantees the system's complete self-sufficiency.

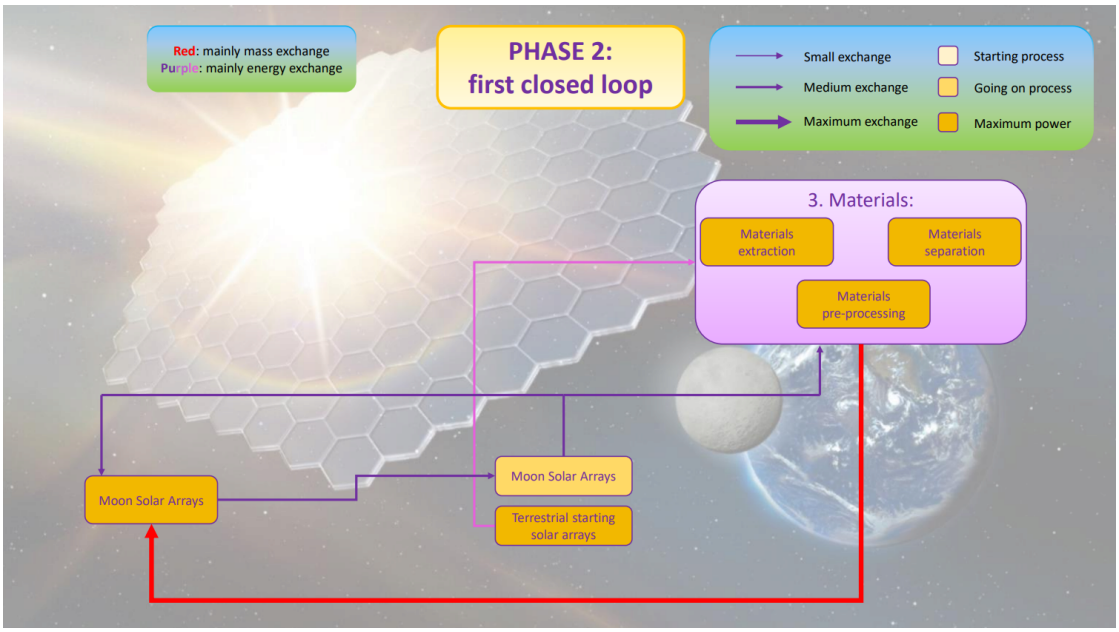

Figure 5.3: Clean vision of the second phase - closed loop

5.4 Phase 3

In phase 3 of the project, there is an intensification of exchanges between the various subsystems, as we are now at the crucial moment of the entire mission, when all the key elements come into operation and the system reaches its maximum level of operability. In terms of visual representation, it is immediately noticeable that the only subsystem that remains inactive is that of the ground launches, which are now exhausted, while all the other compartments of the system are active, with clear connections between them.

One of the key aspects of this phase is the operational activation of the coilgun, which finally comes into operation after having been built and tested in the first two stages of the mission.

The coilgun represents the logistical heart of the system, as it enables the transfer of the solar panels assembled on the Moon to the SEL1 point, where they will form the Sunshade structure. However, its operation requires a significant amount of energy, which is why it is entirely powered by the Lunar Solar Park, which is now fully operational and able to sustain the energy impact of launch operations.

Activation of the coilgun results in a significant increase in mass exchanges, particularly between the extraction facility and the assembly system itself. This steady flow of materials ensures a continuous and sustainable rate of shipments to space, thus accelerating the Sunshade construction process. In parallel, the Lunar Solar Park continues to receive a steady supply of solar panels, increasing its production capacity and ensuring that there is enough energy available not only to maintain production but also to activate new support systems.

Another important innovation introduced at this stage is the start of energy production in space as well, thanks to the first Sunshade panels that, once placed in SEL1, begin generating and transmitting energy back to the Moon. This step represents a crucial milestone for the mission, as it allows an external energy source to be integrated into the lunar system, progressively reducing dependence on the initially carried terrestrial panels and the Lunar Solar Park alone. While in later phases such energy can be harnessed to support Earth as well, in this initial deployment it will be allocated entirely to lunar infrastructure, contributing to the further growth of the project.

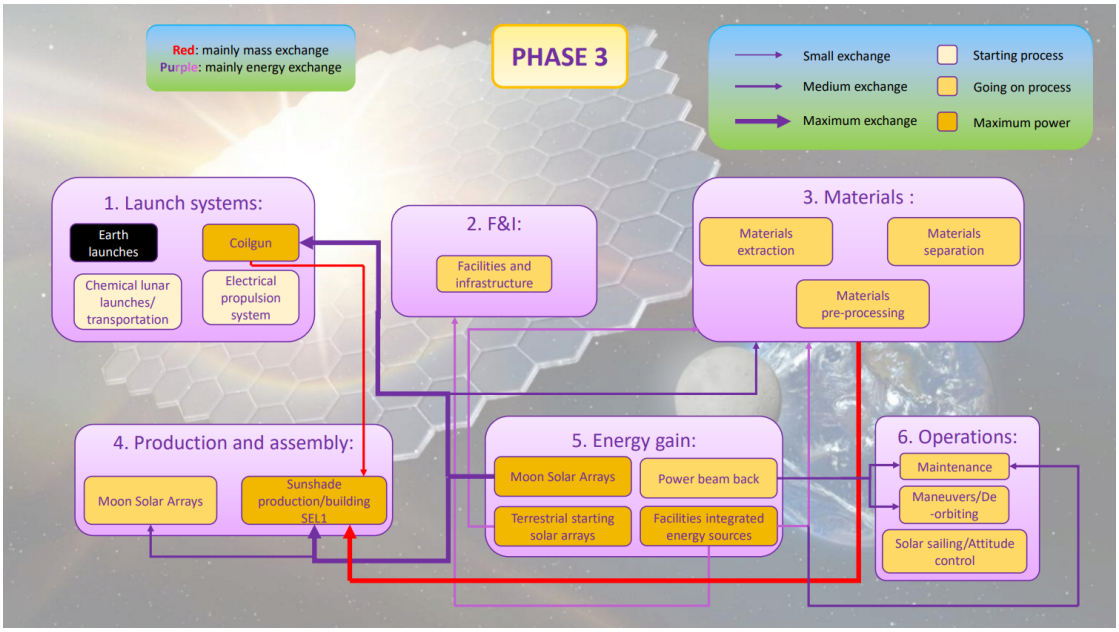

Figure 5.4: Model of the third phase

In parallel, the activation of the Sunshade and the increase in operational activities lead to the need for a greater commitment to maintenance operations. While up to this point maintenance

mainly concerned the Lunar Solar Park panels, at this stage it also becomes essential to intervene on the lunar infrastructure, which after years of use begins to require repairs and interventions to ensure their efficiency. In addition, a portion of the energy collected from the Sunshade's perovskite panels is allocated not only to support lunar operations, but also to manage the orbital maneuvers required to maintain position and de-orbiting any damaged panels.

This phase thus marks the point of maximum development of the system before the final stabilization planned in the next phase. The integration of all the components allows us to move ever closer to the final stages of project optimization and management.

5.4.1 Phase 3 - closed loop

In this second closed loop, the system becomes even more complex than in the previous phase, as a new key player comes into play: the coilgun. The introduction of this element brings with it additional exchanges of mass and power, as the solar panels produced and assembled no longer remain exclusively on the Moon, but must be transferred to the designated point in orbit, namely SEL1. This phase marks a crucial step for the mission, as it marks the actual transition from lunar self-sufficiency to the project's expansion into deep space.

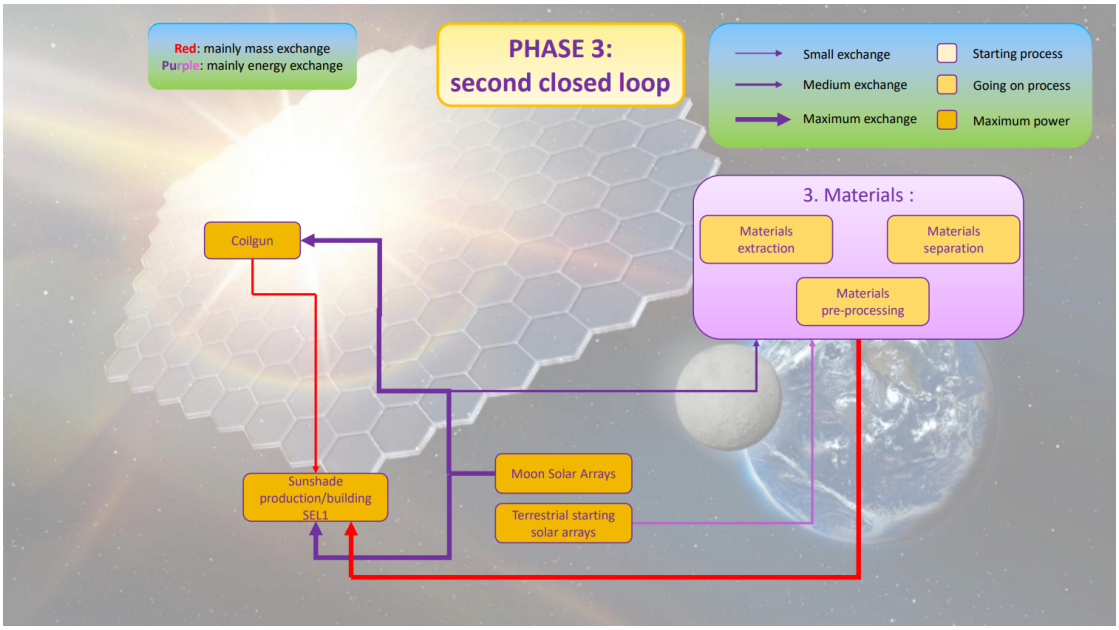

Figure 5.5: Clean vision of the third phase - closed loop

Energy-wise, the coilgun is powered entirely by energy generated by the Lunar Solar Park panels, which are operating at full capacity at this point in the mission. Their production is now well established, and the power generated is sufficient not only to support the launch operations of the new panels to SEL1, but also to keep the entire production cycle active on the Moon.

Indeed, at this stage, the extraction and processing of materials continue without interruption, ensuring a steady flow of resources for the construction of new panels.

The need for a continuous cycle of production, launch, and replacement thus marks a new phase in the self-sufficiency of the system, which is no longer just limited to exponential growth, but must also be able to maintain efficiency in the long run.

In this way, the closed loop of the mission reaches a level of maturity that will allow not only the stabilization of the project, but also its future expansion, which will be made possible through the continued optimization of production, transportation and maintenance processes, both on the Moon and in space, including with the implementation of the new technologies discussed in the previous chapters.

5.5 Phase 4

In the last phase of the mission, Phase 4, there is a significant change in the nature and intensity of operations from previous phases. Many of the activities that until recently were operating at full capacity, such as the production and assembly of solar panels, slow down dramatically. However, this does not mean that they will come to a complete halt: production will no longer take place on a daily, continuous basis, but will be activated only intermittently, in response to the need to replace panels that are damaged or have now reached the end of their life-cycle. At the level of representation, this operation could be indicated with a light yellow color to highlight its transition from an intensive to a more sporadic, maintenance phase.

At the same time, the intensity of panel assembly activities for the Sunshade also decreases, as most of the PV structure has already been completed in the previous stages. At this point, it is no longer necessary to produce new panels to power the Sunshade, other than to fill any small remaining gaps with the last aluminum modules, the production of which had been started and largely completed already in Phase 3. Therefore, the main mass exchange no longer takes place between the production and assembly facilities on the Moon, but directly between the coilgun and the SEL1 point, where the panels are sent and placed in orbit.

While production and assembly activities slow down, other operations become more crucial and reach their maximum operation. In particular, the focus shifts to Sunshade operation and maintenance maneuvers, which will need to be conducted regularly to ensure the long-term stability and efficiency of the structure. These operations will be powered by the energy provided by the Sunshade itself, which now generates sufficient energy to support monitoring, position correction, and replacement of degraded panels.

Meanwhile, the energy produced by the Lunar Solar Park, which is no longer needed to support intensive panel production, is being redirected to new infrastructure on the lunar surface. Indeed, the ultimate goal of this phase is to upgrade existing installations and lay the groundwork for the construction of a permanent colony. This step marks a key moment in the mission: it is no longer just about building a facility to mitigate global warming, but also about harnessing

the technology and resources developed to facilitate the expansion of human activity in space. The Moon, in this perspective, is no longer just a foothold for the Sunshade project, but becomes a strategic platform for long-term settlement, paving the way for future exploration and colonization missions.

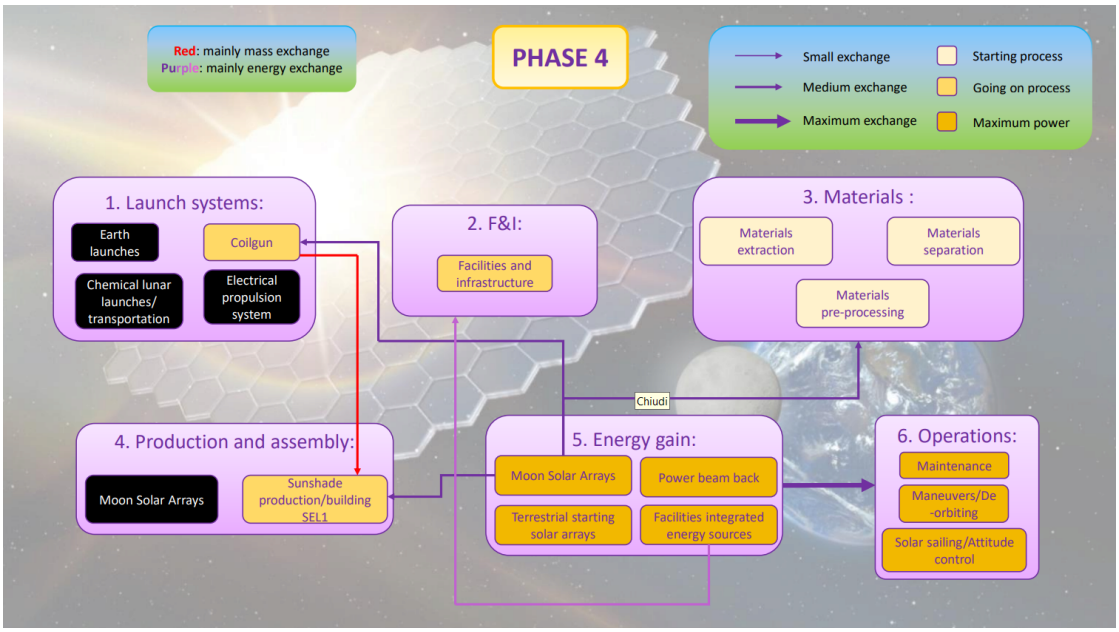

Figure 5.6: Model of the fourth phase

Mission evolution is not simply a sequence of independent operations, but an interconnected process in which each phase lays the foundation for the next, generating a positive feedback mechanism that leads to exponential growth in available energy and operational capabilities.

The four phases of the project, ranging from initial dependence on the Earth to achieving full autonomy, were carefully designed and planned, starting with the need to manage and optimize resources to achieve maximum performance and self-sufficiency.

In conclusion, the entire process demonstrated the effectiveness of a systems-based approach that could integrate, optimize, and monitor the different phases of the mission, from production to maintenance to achieving self-sufficiency. Each phase is designed as part of a continuous cycle that reinforces and evolves over time, allowing initial challenges to be overcome and long-term goals to be successfully addressed. This approach not only allows the mission's goals to be achieved, but has also paved the way for future technological applications that could be used for space exploration and colonization, positioning the Moon as a crossroads for the expansion of human activity beyond Earth's borders.

Chapter 6: Power and Mass budget

6.1 Scenarios analysis (MATLAB)

In order to verify the feasibility of the solar panel manufacturing system directly on the lunar surface, a MATLAB code was developed to simultaneously analyze the evolution of power availability and mass resource management over time. The approach taken is not limited to an analysis of available power, but also integrates an assessment of the amount of material extracted, processed and used to manufacture the panels, so as to ensure an overall view of the sustainability of the system.

The input parameters used in the model are derived directly from the analyses conducted in the previous chapters, in which the energy requirements of the individual stages of the production process, the efficiencies of the extraction and refining systems, and the progressive degradation of the panels over time were defined. In particular, the code considers as main variables the initial available energy transported from Earth, the daily production of PV panels on lunar soil, the energy consumption associated with silicon extraction and processing operations, and the efficiency losses due to module degradation.

The computational implementation makes it possible to simulate the gradual accumulation of panels over time, evaluating the increase in power generated and comparing it with the requirement required to sustain the production process. In addition, the model tracks the amount of material extracted daily and calculates the surplus of available silicon, which can be allocated to the construction of the solar sunshade. An additional aspect analyzed is infrastructure maintenance, the energy impact of which is introduced from a certain number of years of operation to assess the net balance of the system.

In the remainder of this section, the structure and operation of the code will be described in detail, illustrating the logic implemented to manage the key variables and presenting the results of the simulations obtained. These will make it possible to evaluate the time evolution of the system, identifying the moment when panel production reaches a stable balance between consumption and energy generation and ensuring that the available material flow is sufficient to support the construction of the Sunshade.

6.2 Power-Mass budget analysis: 0-35 years

As extensively explained in Chapter 4, all input data analyzed were used to develop the temporal simulation of the mission using MATLAB. The simulation is based on a set of key parameters, including an initial power source provided by photovoltaic panels capable of generating 1000 kW, with a daily efficiency loss of 0.002%. Given these constraints, the results indicate that approximately 35 years are required to reach the desired energy levels, ensuring a self-sustaining power infrastructure for subsequent mission phases.

A fundamental aspect of this simulation is the dynamic interplay between power availability and the number of photovoltaic panels constructed daily. The number of panels produced at each time step depends on multiple factors, including the power required for panel fabrication, the available power at any given time, and the efficiency degradation due to operational wear and environmental factors. The recursive nature of this process establishes a positive feedback loop, where each newly installed panel contributes additional power, thereby accelerating the overall production rate over time.

Initially, the simulation incorporated a discrete panel construction time of approximately 15 days, introducing a phase shift in the panel deployment schedule. However, considering the already substantial complexity of the model and the long operational timescale (spanning 12,775 days, about 35 years) it was determined that a 15-day offset would introduce a negligible 0.11% deviation in the timeline. As such, this temporal delay was considered insignificant and omitted from the final implementation to streamline the computational model.

Since the analysis focuses on Phase 1 of the project, the number of panels produced per day can be determined by the following equation:

$$n_{\text{pan}} = \frac{\text{P}_{\text{available}}}{\text{P}_{\text{production}}}$$

where $\text{P}_{\text{available}}$ represents the total power available at a given time step, and $\text{P}_{\text{production}}$ is the power required to manufacture a single panel. As the number of operational panels increases, so does the totale available power, leading to an exponential growth in production capacity. This iterative expansion can be expressed mathematically for the first three days (for example) as follows:

$$\text{P}_{\text{day1}} = \text{P}_{\text{terrestrial arrays}} + n_{\text{day1}} \cdot \epsilon$$

$$\text{P}_{\text{day2}} = \text{P}_{\text{terrestrial arrays}} + n_{\text{day1}} \cdot \epsilon \cdot (1 - e) + n_{\text{day2}} \cdot \epsilon$$

$$\text{P}_{\text{day3}} = \text{P}_{\text{terrestrial arrays}} + n_{\text{day1}} \cdot \epsilon \cdot (1 - 2e) + n_{\text{day2}} \cdot \epsilon \cdot (1 - e) + n_{\text{day3}} \cdot \epsilon$$

where:

- $P_{\text{terrestrial arrays}}$ accounts for the initial power supply from Earth-deployed solar arrays;
- n_{dayx} corresponds to the number of panels produced on a given day x;
- ϵ represents the power generated by a single panel installed on the Moon;
- e is the daily efficiency loss due to wear and tear.

Another key consideration in the simulation is the long-term effect of panel degradation. It was determined that maintenance operations should begin when efficiency losses become significant enough to impact overall system performance. Based on degradation rates, maintenance activities were scheduled to commence after approximately 10 years, with 5% of the total available power allocated to the replacement or repair of damaged panels. This allocation ensures that the power deficit caused by wear and tear remains controlled, preventing excessive power losses over time.

Finally, to account for physical and logistical constraints in lunar manufacturing, a maximum daily production capacity of about 3300 panels was imposed. This upper bound reflects limitations in material availability, manufacturing throughput, and energy constraints. According to the simulation, this production limit is reached and sustained from approximately day 5500 (year 15) onward, as shown in Figure 6.1. Notably, this milestone coincides with the projected transition toward Phase 2 (in section 5.2), where surplus energy and material resources can begin to be redirected toward the fabrication of perovskite-based photovoltaic panels intended for deployment in the Sunshade structure at the SEL1 point, that will be discussed later.

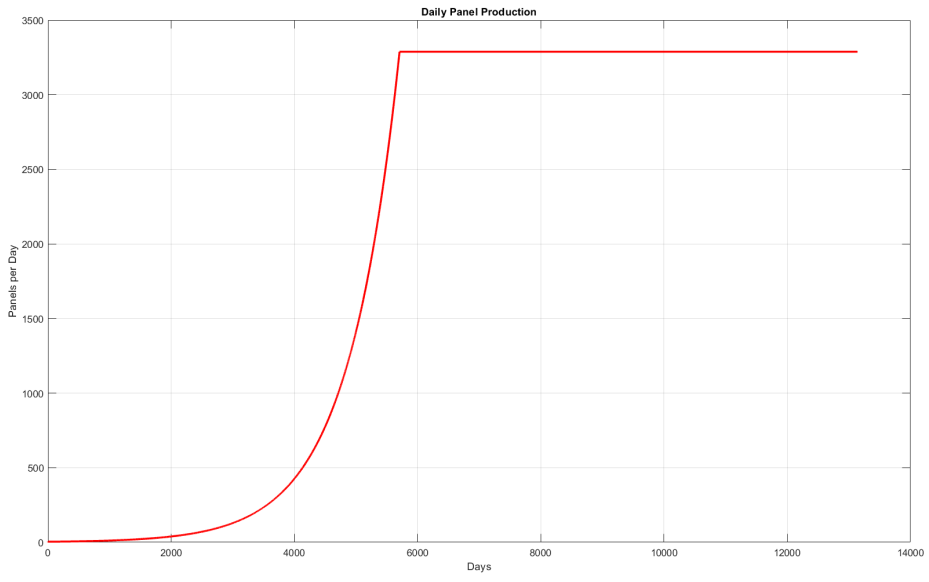

Figure 6.1: Daily number of panels produced for the Lunar Solar Park

From the graphs obtained, it can be seen that the trend of daily panel production follows an exponential trend, highlighting the initial growth phase of the production system until the maximum daily output capacity is reached. This behavior is due to the progressive self-sufficiency of the Lunar Solar Park, which, thanks to the increasing energy availability generated by the panels already installed, is able to fuel the production of new modules without having to draw significantly on the resources initially transported from Earth, as shown in phase 2 of the mission explained in the previous chapter. In parallel, the graph of total available power, depicted in figure 6.3, shows a trend strongly correlated with the increase in the total number of installed panels, shown in figure 6.2, confirming the close relationship between production capacity and energy availability.

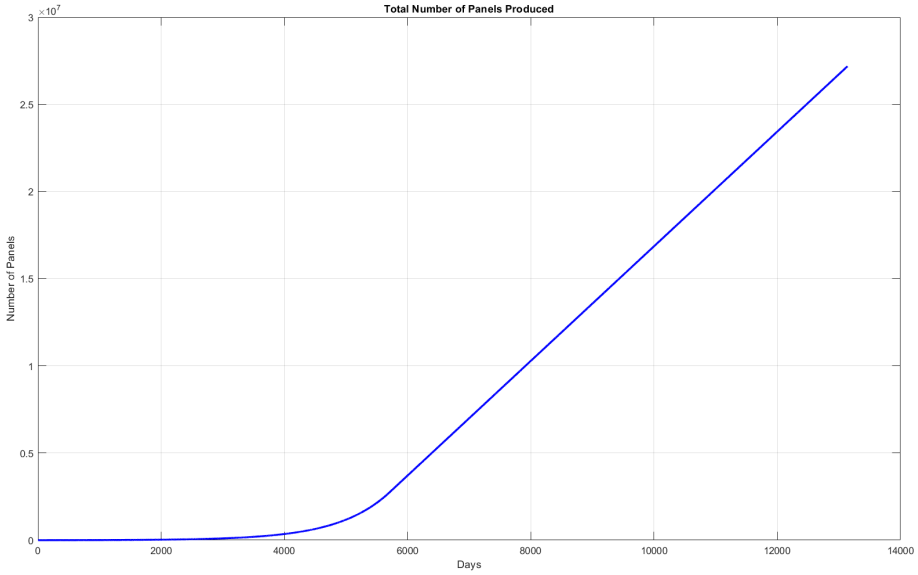

Figure 6.2: Total number of panels produced for the Lunar Solar Park

Beginning in the tenth year of the mission, as mentioned above, a fraction of power allocated to infrastructure maintenance activities is introduced, with a visible impact on the net power available. In particular, it is observed that the maximum value of power generated by the Lunar Solar Park, amounting to about 7.5×10^6 kW, is reduced to a final value of about 7×10^6 kW due to the energy consumption required for the maintenance of the facilities and the replacement of degraded modules. This figure highlights the need for careful maintenance planning to ensure maximum operational efficiency of the entire system in the long run.

The last two graphs related to this section (6.4 and 6.5) provide crucial information on the management of mass and energy resources, demonstrating the amount of mined material that is not immediately used for the production of the Lunar Solar Park panels and that, as a result,

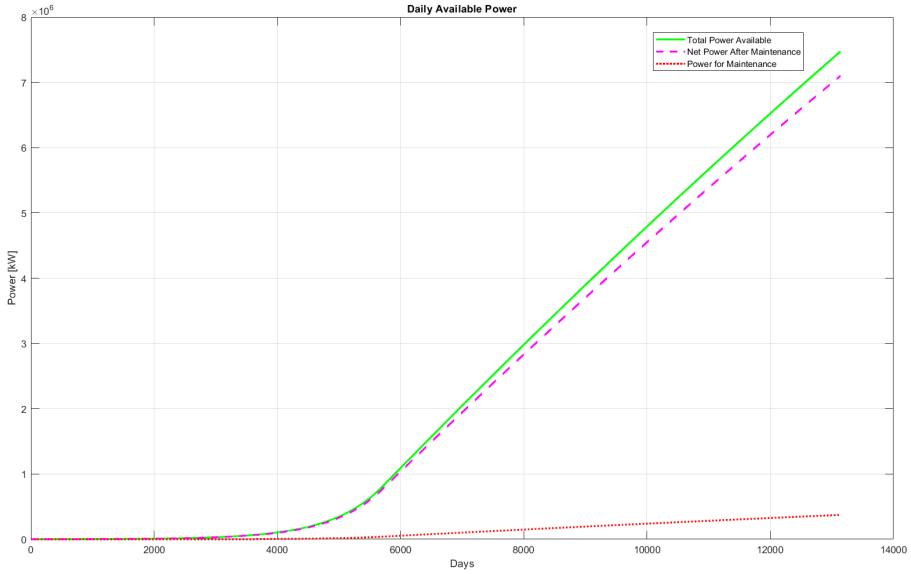

Figure 6.3: Daily amount of power available on the Moon

can be stored in storage hubs during the first 35 years of the mission. In parallel, the amount of energy that, once the needs of the Lunar Solar Park are met, can be allocated to the production of additional panels for the Sunshade is illustrated. These results highlight a key turning point in the mission: as panel production for the Lunar Solar Park comes into full swing, operating at maximum daily capacity, a fraction of both the extracted material and the available energy can be progressively redirected toward the manufacture of the perovskite panels destined for the Sunshade.

A key moment in this transition is around 15 years from the start of the mission. At this time scale, Perovskite/Silicon tandem panel fabrication technologies are expected to be sufficiently mature to be implemented directly on the lunar surface, allowing the technology based solely on silicon cells to be progressively surpassed. This technological evolution represents a critical point in the mission roadmap, as perovskite panels offer the potential for higher efficiency and better adaptability to space environmental conditions than conventional silicon cells. Thus, the energy and mass balance analysis confirms that it is feasible to begin construction of the panels for the Sunshade without compromising the functionality and sustainability of the Lunar Solar Park, paving the way for the implementation of the Solar Sunshade.

The results obtained from the simulation demonstrate that the total mass of unused materials stored in the lunar hubs over the mission's 35-year duration amounts to approximately 2.0241×10^9 kg. This value represents the cumulative excess material that remains available after accounting for the production demands of the Lunar Solar Park. On the other hand, the effective

mass of materials allocated for the fabrication of perovskite-based photovoltaic panels for the Sunshade, considering the power constraints associated with their production, is estimated at 1.8348×10^9 kg.

This result is highly significant, as it confirms that the available stored mass aligns remarkably well with the projected material requirements for the Sunshade. Specifically, the total required mass for the Sunshade's photovoltaic panels, as analyzed in chapter 4.3 and illustrated in figure 4.2, was determined to be approximately 1.8×10^9 kg. The close agreement between these values validates the feasibility of leveraging surplus lunar manufacturing capacity for the production of the Sunshade's panels without exceeding the expected resource constraints.

Moreover, this mass balance analysis further supports the assumption that, once the Lunar Solar Park reaches full operational capacity and material production stabilizes, a significant portion of the available resources can be efficiently re-purposed toward the Sunshade project.

These results reinforce the validity of the assumptions made regarding in-situ resource utilization (ISRU) and lunar-based industrial processes. The mass estimates confirm that the established supply chain can sustain large-scale panel production while maintaining a sufficient buffer of raw materials to accommodate potential inefficiencies or losses. This highlights the robustness of the proposed production model, ensuring both the Lunar Solar Park and the Sunshade can be developed in parallel without requiring additional terrestrial supply missions beyond the initial infrastructure deployment phase.

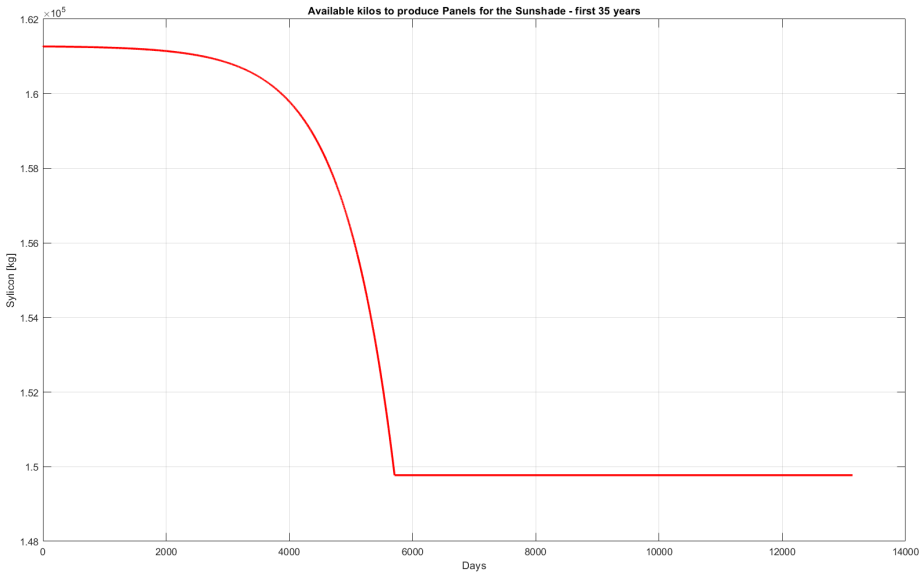

Figure 6.4: Available kilos to produce Panels for the Sunshade - first 35 years

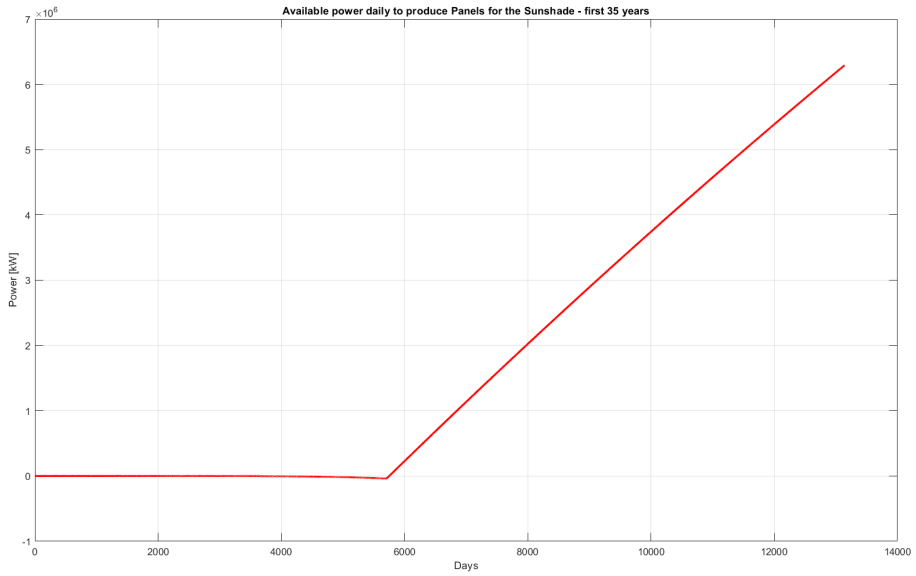

Figure 6.5: Available daily power to produce Panels for the Sunshade - first 35 years

6.3 Power-Mass budget analysis: 35-70 years

The second stage of the simulation is relatively simpler than the first, as the system is now fully operational and running at its maximum efficiency. Consequently, the data-set exhibits a more linear and predictable behavior, significantly simplifying the computational complexity of this stage.

To determine the required daily output of aluminum production and launch cadence, a reverse engineering approach was applied. Given the total aluminum mass needed, as extensively analyzed in chapter 4.3 and illustrated in figure 4.2, the simulation was designed to calculate the required daily production and launch rates. This ensures the successful completion of the mission within the planned 35-year time-frame, avoiding any delays or resource shortfalls.

At full operational capacity, the daily available power supplied by the Lunar Solar Park is approximately 7.1008×10^6 kW. However, in this Phase (Phase 3 previously discussed), the system benefits from an additional energy return from the Solar Sunshade itself. By averaging the power transmission efficiencies between microwave and laser-based energy transfer, the estimated additional power return is approximately 2.4×10^8 kW, while under worst-case transmission conditions, it is expected to be around 1.9×10^8 kW.

A portion of this energy is allocated to the continuous manufacturing and replacement of photovoltaic panels for the Solar Sunshade. This process must also account for the daily replacement of over 3000 panels from the Lunar Solar Park, ensuring that power generation remains at peak

efficiency. The estimated power required for this continuous panel production is 8.0892×10^5 kW per day.

Additionally, the energy required for aluminum panel production was calculated based on the need to manufacture a total of 24×10^9 kg within the 35 year mission duration. This translates to a required daily production rate of approximately 1.88×10^6 kg of aluminum, demanding an estimated 3.8×10^6 kW per day to sustain the necessary industrial processes, and 2736 kWh for the daily mining process.

The system also accounts for the power consumption of next-generation reactors used for various refining and manufacturing operations. Each reactor consumes approximately 3 kW, and given that the system in the second stage operates 31920 reactors, the total power requirement for this subsystem amounts to 95760 kW per day.

Furthermore, the coilgun launch system, designed by T. Maheswaran, was assessed for its operational feasibility. The system is theoretically capable of launching mass payloads at rates ranging from 421 to 1632 tons per hour. However, to meet the mission's material transport requirements, a much lower launch rate of 78.2 tons per hour is sufficient. At this rate, the energy required for the coilgun's daily operation is approximately 9393.34 kWh, a value that remains well within the available energy budget. If it were not possible to finish launching the perovskite panels in the first stage of the simulation then there would still be room in terms of power and mass to complete the launch in this stage. In fact, to complete the launch of the perovskitic panels in the first 5 years of the second stage would be sufficient to increase the daily launch capacity by 986.3 tons, or another 41.1 tons per hour, reaching a total (between perovskite and aluminum) of 119.3 tons per hour, also well within the margins, and increasing energy consumption by an additional 4932 kWh.

By analyzing these power consumption figures relative to the total available power from both the Lunar Solar Park and the Solar Sunshade, it becomes evident that the system is fully self-sustaining in its second stage. This is further reinforced by the integration of advanced energy transmission technologies, ensuring that power deficits do not emerge as a limiting factor in mission execution.

It is also crucial to highlight that the simulation results remain conservative, adhering to a safety-first approach. At every stage of the analysis, the worst-case among the available data points was selected, and the simulation avoided reliance on unverified, highly experimental, or speculative technologies. Instead, the model strictly incorporates technologies that have either received formal research funding or have already entered initial testing phases. This methodological rigor enhances the realism and reliability of the entire system's simulation performance projections.

This approach ensures that if the mission remains viable under the worst-case scenario, it will perform even more efficiently under more favorable conditions. This provides a strong margin of confidence in the feasibility and long-term sustainability of the mission, further reinforcing the robustness of the proposed infrastructure and its capability to achieve the intended objectives

within the planned timeframe.

Chapter 7: Conclusions

The analysis conducted in this thesis allowed for the determination of the technical feasibility of the space solar Sunshade design, evaluating the balance between energy availability and mass management in the long run. A key aspect of the work performed was the detailed input analysis, discussed in Chapter 4, which allowed the definition of key parameters necessary for model development. Constraints related to lunar energy production, material availability and transportation capabilities were identified, elements that directly affect the sustainability of the project. In particular, characterization of the extracted resources and their actual usability formed the basis for subsequent modeling, ensuring consistency between theoretical assumptions and numerical simulation.

In Chapter 5, the construction of the power-mass balance model was developed, which divided the time horizon into two main phases: 0-35 years and 35-70 years. In the first 35 years of the mission, the total amount of materials mined and stored in the lunar stores is 2.0241×10^9 kg, representing the excess accumulated after the Lunar Solar Park requirements. The amount of mass actually destined for the manufacture of photovoltaic panels for the Sunshade is estimated to be 1.8348×10^9 kg, being in line with the projected material requirements for the project.

The Lunar Solar Park achieves a maximum daily power output of 7.5×10^6 kW, which stabilizes around 7×10^6 kW after the introduction of maintenance and replacement activities for degraded panels. Panel production capacity is limited to a maximum of about 3300 units per day, constrained by the availability of energy and materials. This limit is reached and maintained from the 15th year of the mission, coinciding with the start of panel production for the Sunshade. The model made it possible to highlight the gradual energy transition of the system, with increasing autonomy of the lunar network and a reduction in the impact of the early stages of development on overall energy availability.

The coilgun launch system, based on T. Maheswaran's design, was evaluated to ensure efficient transport of materials. The theoretical launch capacity varies between 421 and 1632 tons/hour, but a rate of 78.2 tons/hour is sufficient to meet mission requirements, with an energy consumption of 9393.34 kWh/day. Should the launch rate need to be increased to complete panel deployment in a shorter time, a launch capacity increase of 986.3 tons/day would be sufficient, with an additional impact of 4932 kWh on energy consumption. The integration of an attitude and orbit control system (AOCS) derived from existing satellite technologies is crucial

to maintain the stability of the sunshade in SEL1.

The analysis confirms that after the Lunar Solar Park reaches full operation, a substantial portion of the available resources can be effectively redirected to the production of the panels for the Sunshade, without negatively impacting the energy balance of the system. The energy return from the Sunshade itself, via laser or microwave transmission, will provide an additional contribution to the lunar grid, estimated to be between 1.9×10^8 kW and 2.4×10^8 kW, further reducing dependence on primary energy sources and providing the possibility of using this energy for other lunar projects or even terrestrial applications.

The results show that the solar shielding system can be implemented without exceeding the resource and power constraints imposed by the project, having to revise the road-map proposed in the figure 2.5, shifting it forward a few years, as time is one of the major concerns and critical aspects. Lunar panel production, supported by a progressively self-sufficient energy infrastructure, ensures a sustainable approach to building the Sunshade. The data confirm that integration between Lunar Solar Park and Sunshade is possible without requiring additional resupply missions from Earth, solidifying the long-term viability of the project.

But beyond data and simulations, this thesis represents more than just a technical assessment. It is a step towards a new vision of our existence in the cosmos, a revolutionary idea that is part of the great flow of human knowledge that does not bend to destruction, but seeks in science and technology the way to preserve our planet. Climate change is the greatest challenge of our time and we have a moral duty to respond with intelligence, with creativity and with courage.

Perhaps this will not be the project that saves the world, perhaps it will take decades of research and experimentation before we find the ultimate solution. But every contribution counts, every step we take in the right direction is a small victory in the battle for the future. Believing in this project means believing in humanity's ability to rise above its mistakes and use its intelligence to build, rather than destroy. To be part of this process of transformation means not standing still in the face of decline, but being pulled along by the unstoppable flow of progress that propels us, powerfully, towards a better tomorrow.

Geoengineering is not just a scientific possibility, it is a necessity. The time to act is now, and research is our most powerful weapon. Every idea, every project, every study like this one adds a piece to the complex mosaic that could one day become the key to our survival. And it is with this awareness that we look ahead, determined to be part of the change, aware that history is written by those who dare to imagine a better future.

Chapter 8: Outlook

As this study has demonstrated, the development of a large-scale space-based solar shield involves a complex interplay of engineering disciplines, from materials science to orbital mechanics and long-term maintenance strategies. While the current research provides a solid foundation for the feasibility of such a mission, several aspects require further investigation to refine the concept and ensure its long-term viability. This chapter wants to outline key topics that warrant deeper exploration in future studies. The following areas have been identified as crucial for advancing the design, implementation, and operational effectiveness of the proposed system:

- Encapsulation of solar cells for extreme space temperature ranges;
- Correction maneuvers and orbital regulations;
- In-Orbit assembly after launch via Coilgun;
- Long-term maintenance strategies for the Lunar Solar Park and SEL1 infrastructure;
- Energy storage solutions and battery study for the mentioned space-based photovoltaic systems.

Encapsulation of solar cells for extreme space temperature ranges Photovoltaic systems must withstand rapid temperature fluctuations, prolonged exposure to high-energy radiation, and potential mechanical stresses caused by thermal expansion and contraction. Future studies should explore the most effective encapsulation materials and structural solutions to maximize durability while minimizing degradation over time. Moreover, given the harsh conditions in both lunar and deep-space environments, investigating the resilience of encapsulation layers to micro-meteoroid impacts and space debris will be crucial. The development of self-healing coatings or advanced protective layers could significantly extend the operational lifespan of solar panels deployed on the Moon and at SEL1.

Correction maneuvers and orbital regulations Although the equilibrium point provides a relatively stable location for the structure, perturbative forces (including solar radiation pressure and gravitational interactions) necessitate periodic correction maneuvers. Future work should investigate the optimal propulsion methods for such adjustments, comparing traditional ion

thrusters, solar sails, and other low-thrust propulsion technologies. Additionally, the long-term sustainability of station-keeping operations will depend on the availability of propellant or alternative non-consumable propulsion solutions. Beyond the technical aspects, further research is needed to examine the regulatory and operational framework governing large-scale structures in SEL1, particularly in terms of international space law, collision avoidance strategies, and potential governance mechanisms.

In-Orbit assembly after launch via Coilgun While the Coilgun enables an efficient and cost-effective means of transporting materials from the Moon to SEL1, the subsequent process of constructing the large-scale structure in space remains an open question. Advanced deployment mechanisms must be developed to ensure the seamless integration of individual panels into a coherent and functional system. This raises important questions regarding the role of robotics and automation in the assembly process, as well as the potential application of swarm robotics, autonomous construction techniques, and modular self-assembling structures. Furthermore, while the current project assumes an entirely robotic approach, future studies might explore the feasibility of human-assisted assembly, particularly in the event of future crewed missions to SEL1.

Long-term maintenance strategies for the Lunar Solar Park and SEL1 infrastructure On the Moon, photovoltaic panels will be exposed to lunar dust, which can degrade efficiency over time. Investigating innovative solutions such as electrostatic cleaning technologies, self-cleaning coatings, or automated maintenance systems will be essential for preserving performance. In SEL1, where panels may experience gradual degradation due to space weathering, further research is needed to determine the best methods for panel repair or replacement. The feasibility of self-repairing materials, modular panel swapping, or in-orbit servicing missions should be explored to extend the system's operational lifespan. Additionally, maintenance strategies must consider the logistics and cost of replacing malfunctioning components over decades of operation.

Energy storage solutions and battery study for the mentioned space-based photovoltaic systems While the Sunshade's primary function involves beaming solar energy via laser or microwave transmission, energy storage solutions will still be necessary to buffer fluctuations in power generation and ensure operational continuity. Identifying the most suitable battery technology for deep-space applications will require a dedicated study, comparing lithium-ion, solid-state, and alternative high-efficiency storage solutions. Thermal management will be a critical factor, as extreme temperature variations can degrade battery performance and longevity. Additionally, integrating storage solutions with advanced power distribution networks will help optimize energy efficiency and overall system resilience.

The concepts outlined in this thesis provide a framework for a revolutionary approach to climate mitigation and space-based energy solutions. However, the scale and complexity of such

an endeavor necessitate further refinement and interdisciplinary collaboration. Future advancements in materials science, robotics, artificial intelligence, and space policy will be instrumental in turning this concept into a feasible reality.

By addressing the outlined research areas, the scientific community can progressively build upon the foundation established here, paving the way for the next generation of space-based solutions to planetary challenges. Ultimately, this research not only contributes to the development of the Sunshade project but also lays the groundwork for broader applications in space-based energy, planetary defense, and sustainable exploration beyond Earth's orbit.

Appendices

.1 First Code Trade Off

```
% INPUT:

Area=10; % Area in square meters for every solar panel (average of 1 square meter)
m1=0.027*Area; % kilos according to Sebastian Fix Master Thesis

d2=0.300; % kg/m^-2 average density for a perovskite solar cell (Low-intensity low-temperature analysis of perovskite solar cells for deep space applications Tyler Colenbrander)
RCP=[1.22 1.9 2.6 3.4 4.5 6.0 7.0 8.5]'; % different climate scenarios
v_eff=(0:0.001:0.330); % vector of the efficiencies from 0 to 0.330 according to the Shockley queisser limit for the cell chosen (perovskite this case)
e=0.20; % solar cells efficiency (e>=0.009)   (silicon, perovskite, worst and best case)
sc=1; % climate scenario based on RCP choice

% OUTPUT:

% Sunshade plot with respect to Earth (Earth and sunshade are bigger than the real dimension by a factor f)

%%

if e<0.009
    fprintf('\n please insert a number for the efficiency > 0.009 \n')
end

% vector with Solar sunshade Area for every RCP case:

% constant definition

alphap=0.313; % Earth albedo
S=342.75; % average solar insolation on the Earth for the actual surface, 4 times larger then its projection (Szero/4)
RS=696340000; % radius of the Sun [meter]
dSEL1=1.588*10^9; % distance of the Sun-Earth Lagrange point 1 from Earth: this location could be rearranged, since the force exerted by photons impinging on the occulting disk, i.e. solar radiation pressure (SRP), moves the equilibrium position sunwards from the classical location
au=149.598*10^9; % astronomic unit
sigma=5.670400*10^(-8); % Stefan-Boltzmann constant
Ts=5770; % in Kelvin
Re=6371000; % radius of the Earth [meter]

deltaS=zeros(length(RCP),1); % reduction in solar insolation due to counter radiative forcing
f=zeros(length(RCP),1); % relative fraction of light to be reduced
```

```
Rsh=zeros(length(RCP),1); % shade's radius required
Ash=zeros(length(RCP),1); % shade's Area required

for i=1:length(RCP)
    deltaS(i)=RCP(i)/(1-alphap);
    f(i)=deltaS(i)/S;
    Rsh(i)=RS*dSEL1*sqrt(f(i))/au;
    Ash(i)=Rsh(i)^2*pi;
end

res=[RCP deltaS f Rsh Ash]; % vector with the solutions

Phi=RS^2*sigma*Ts^4/(au-dSEL1)^2; % solar radiation in SEL1 [W/m^2]

% Comparison of the number of solar cells for every case with various efficiencies
    :

% number of panels in the different scenarios

n_pan1=zeros(1,length(v_eff));
n_pan2=zeros(1,length(v_eff));
n_pan3=zeros(1,length(v_eff));
n_pan4=zeros(1,length(v_eff));
n_pan5=zeros(1,length(v_eff));
n_pan6=zeros(1,length(v_eff));
n_pan7=zeros(1,length(v_eff));
n_pan8=zeros(1,length(v_eff));

for i=1:length(v_eff)
    n_pan1(i)=deltaS(1)*Ash(1)/(v_eff(i)*Phi*Area); % Total power/(efficiency*Phi*
        Area)
    n_pan2(i)=deltaS(2)*Ash(2)/(v_eff(i)*Phi*Area);
    n_pan3(i)=deltaS(3)*Ash(3)/(v_eff(i)*Phi*Area);
    n_pan4(i)=deltaS(4)*Ash(4)/(v_eff(i)*Phi*Area);
    n_pan5(i)=deltaS(5)*Ash(5)/(v_eff(i)*Phi*Area);
    n_pan6(i)=deltaS(6)*Ash(6)/(v_eff(i)*Phi*Area);
    n_pan7(i)=deltaS(7)*Ash(7)/(v_eff(i)*Phi*Area);
    n_pan8(i)=deltaS(8)*Ash(8)/(v_eff(i)*Phi*Area);
end

figure()
semilogy(v_eff(2:length(v_eff)-1), n_pan1(2:length(v_eff)-1))
hold on
semilogy(v_eff(2:length(v_eff)-1), n_pan2(2:length(v_eff)-1))
hold on
semilogy(v_eff(2:length(v_eff)-1), n_pan3(2:length(v_eff)-1))
hold on
semilogy(v_eff(2:length(v_eff)-1), n_pan4(2:length(v_eff)-1))
hold on
```

```
84  semilogy(v_eff(2:length(v_eff)-1), n_pan5(2:length(v_eff)-1))
85  hold on
86  semilogy(v_eff(2:length(v_eff)-1), n_pan6(2:length(v_eff)-1))
87  hold on
88  semilogy(v_eff(2:length(v_eff)-1), n_pan7(2:length(v_eff)-1))
89  hold on
90  semilogy(v_eff(2:length(v_eff)-1), n_pan8(2:length(v_eff)-1))
91  xlabel('efficiency')
92  ylabel('number of perovskite solar panels')
93  legend(' 1 = -1 K    ', ' 2 = RCP 1.9', ' 3 = RCP 2.6', ' 4 = RCP 3.4', ' 5 = RCP
        4.5', ' 6 = RCP 6.0', ' 7 = RCP 7.0', ' 8 = RCP 8.5')
94  title('Perovskite solar panels needed to shield solar radiation in all the cases')
95
96  % Comparison of the simple panels for every case:
97
98  % Free area for every case:
99  A_free1=zeros(1,length(n_pan1));
100 A_free2=zeros(1,length(n_pan2));
101 A_free3=zeros(1,length(n_pan3));
102 A_free4=zeros(1,length(n_pan4));
103 A_free5=zeros(1,length(n_pan5));
104 A_free6=zeros(1,length(n_pan6));
105 A_free7=zeros(1,length(n_pan7));
106 A_free8=zeros(1,length(n_pan8));
107
108 % Area occupied by solar panels for every case:
109
110 A_pan1=zeros(1,length(n_pan1));
111 A_pan2=zeros(1,length(n_pan2));
112 A_pan3=zeros(1,length(n_pan3));
113 A_pan4=zeros(1,length(n_pan4));
114 A_pan5=zeros(1,length(n_pan5));
115 A_pan6=zeros(1,length(n_pan6));
116 A_pan7=zeros(1,length(n_pan7));
117 A_pan8=zeros(1,length(n_pan8));
118
119 for i=1:length(v_eff)
120     A_pan1(i)=Area*n_pan1(i);
121     A_pan2(i)=Area*n_pan2(i);
122     A_pan3(i)=Area*n_pan3(i);
123     A_pan4(i)=Area*n_pan4(i);
124     A_pan5(i)=Area*n_pan5(i);
125     A_pan6(i)=Area*n_pan6(i);
126     A_pan7(i)=Area*n_pan7(i);
127     A_pan8(i)=Area*n_pan8(i);
128 end
129
130 for i=1:length(v_eff)
131     A_free1(i)=Ash(1)-A_pan1(i);
```

```
132     A_free2(i)=Ash(2)-A_pan2(i);
133     A_free3(i)=Ash(3)-A_pan3(i);
134     A_free4(i)=Ash(4)-A_pan4(i);
135     A_free5(i)=Ash(5)-A_pan5(i);
136     A_free6(i)=Ash(6)-A_pan6(i);
137     A_free7(i)=Ash(7)-A_pan7(i);
138     A_free8(i)=Ash(8)-A_pan8(i);
139 end
140
141 % Area matrixes:
142
143 Apan=[A_pan1; A_pan2; A_pan3; A_pan4; A_pan5; A_pan6; A_pan7; A_pan8]';
144
145 % real Areas without negative values:
146
147 Ar_free1=A_free1(A_free1>0);
148 Ar_free2=A_free2(A_free2>0);
149 Ar_free3=A_free3(A_free3>0);
150 Ar_free4=A_free4(A_free4>0);
151 Ar_free5=A_free5(A_free5>0);
152 Ar_free6=A_free6(A_free6>0);
153 Ar_free7=A_free7(A_free7>0);
154 Ar_free8=A_free8(A_free8>0);
155
156 Arfree=  [Ar_free1(1+size(Ar_free1,2)-size(Ar_free8,2):size(Ar_free1,2));
157           Ar_free2(1+size(Ar_free2,2)-size(Ar_free8,2):size(Ar_free2,2));
158           Ar_free3(1+size(Ar_free3,2)-size(Ar_free8,2):size(Ar_free3,2));
159           Ar_free4(1+size(Ar_free4,2)-size(Ar_free8,2):size(Ar_free4,2));
160           Ar_free5(1+size(Ar_free5,2)-size(Ar_free8,2):size(Ar_free5,2));
161           Ar_free6(1+size(Ar_free6,2)-size(Ar_free8,2):size(Ar_free6,2));
162           Ar_free7(1+size(Ar_free7,2)-size(Ar_free8,2):size(Ar_free7,2));
163           Ar_free8(1+size(Ar_free8,2)-size(Ar_free8,2):size(Ar_free8,2))]';
164
165 figure()
166 plot(v_eff(2+length(v_eff)-1-size(Ar_free1,2):length(v_eff)-1), Ar_free1(1:size(
        Ar_free1,2)-1))
167 hold on
168 plot(v_eff(2+length(v_eff)-1-size(Ar_free2,2):length(v_eff)-1), Ar_free2(1:size(
        Ar_free2,2)-1))
169 hold on
170 plot(v_eff(2+length(v_eff)-1-size(Ar_free3,2):length(v_eff)-1), Ar_free3(1:size(
        Ar_free3,2)-1))
171 hold on
172 plot(v_eff(2+length(v_eff)-1-size(Ar_free4,2):length(v_eff)-1), Ar_free4(1:size(
        Ar_free4,2)-1))
173 hold on
174 plot(v_eff(2+length(v_eff)-1-size(Ar_free5,2):length(v_eff)-1), Ar_free5(1:size(
        Ar_free5,2)-1))
175 hold on
```

```
176 plot(v_eff(2+length(v_eff)-1-size(Ar_free6,2):length(v_eff)-1), Ar_free6(1:size(
        Ar_free6,2)-1))
177 hold on
178 plot(v_eff(2+length(v_eff)-1-size(Ar_free7,2):length(v_eff)-1), Ar_free7(1:size(
        Ar_free7,2)-1))
179 hold on
180 plot(v_eff(2+length(v_eff)-1-size(Ar_free8,2):length(v_eff)-1), Ar_free8(1:size(
        Ar_free8,2)-1))
181 xlabel('efficiency')
182 ylabel('Area covered by aluminum panels [m^2]')
183 legend(' 1 = -1 K   ', ' 2 = RCP 1.9', ' 3 = RCP 2.6', ' 4 = RCP 3.4', ' 5 = RCP
        4.5', ' 6 = RCP 6.0', ' 7 = RCP 7.0', ' 8 = RCP 8.5')
184 title('Area for which aluminum panels are to be used in all the cases [m^2]')
185
186
187 % comparison between the area covered by solar and simple panels for the selected
        case
188
189 figure()
190 semilogy(v_eff(2+length(v_eff)-1-length(Arfree(:,sc)):length(v_eff)-1), Arfree(1:
        length(Arfree(:,sc))-1, sc))
191 hold on
192 semilogy(v_eff(2+length(v_eff)-1-length(Arfree(:,sc)):length(v_eff)-1), Apan(2+
        length(v_eff)-1-length(Arfree(:,sc)):length(v_eff)-1, sc))
193 xlabel('efficiency')
194 ylabel('area occupied by the panels')
195 legend('Area for aluminum panels','Area for perovskite solar panels')
196 title(sprintf('Distribution of the panels in the sunshade area, scenario %d', sc))
197
198 % raffiguration of the sunshade area (select efficiency at the beginning) for the
        selected scenario:
199
200 C_free  = nsidedpoly(1000, 'Center', [0 0], 'Radius', Rsh(sc));
201 C_solar = nsidedpoly(1000, 'Center', [0 0], 'Radius', sqrt(Apan(e*1000+1,sc)/(2*pi
        )));
202 C_earth = nsidedpoly(1000, 'Center', [0 0], 'Radius', Re);
203
204 % with Earth
205 figure()
206 plot(C_free, 'Facecolor', 'r')
207 hold on
208 plot(C_solar, 'Facecolor', 'g')
209 hold on
210 plot(C_earth, 'Facecolor', 'b')
211 axis equal
212 grid on
213 xlabel('meter')
214 ylabel('meter')
215 legend('Normal panels surface', 'Solar panels surface','Earth')
```

```
216 title(sprintf('Distribution of the panels in the sunshade area, scenario %d,
        efficiency %.3f', sc, e))
217
218 % without Earth
219 figure()
220 plot(C_free, 'Facecolor', 'r')
221 hold on
222 plot(C_solar, 'Facecolor', 'g')
223 axis equal
224 grid on
225 xlabel('meter')
226 ylabel('meter')
227 legend('Normal panels surface', 'Solar panels surface')
228 title(sprintf('Distribution of the panels in the sunshade area, scenario %d,
        efficiency %.3f', sc, e))
229
230
231 % raffiguration 3d of the sunshade area (select efficiency at the beginning) for
        the selected scenario:
232
233 f=10; % scale factor
234
235 C1=[dSEL1 Re 0]; % 1 = aluminum panels
236 r1=f*Rsh(sc);
237 n1=[1, 0, 0];
238
239 C2=[dSEL1 Re 0]; % 2 = solar panels
240 r2=f*sqrt(Apan(e*1000+1,sc)/(2*pi));
241 n2=[1, 0, 0];
242
243 theta=0:0.01:2*pi;
244
245 v1=null(n1);
246 v2=null(n2);
247
248 points1=repmat(C1',1,size(theta,2))+r1*(v1(:,1)*cos(theta)+v1(:,2)*sin(theta));
249 points2=repmat(C2',1,size(theta,2))+r2*(v2(:,1)*cos(theta)+v2(:,2)*sin(theta));
250
251 % Earth graphic
252 figure()
253 set(gca,'FontSize',12);
254 set(gcf,'Color','White');
255 EARTH = imread('planisphererid5.jpg','jpg');
256 props.FaceColor='texture';
257 props.EdgeColor='none';
258 props.FaceLighting='phong';
259 props.Cdata = EARTH;
260 Center = [0; 0; 0];
261 [XX, YY, ZZ] = ellipsoid(Center(1),Center(2),Center(3),f*Re,f*Re,f*Re,50);
```

```
surface(-XX, -YY, -ZZ,props);
clim([-Re/100 Re/100]) % clim or caxis
hold on
fill3(points1(1,:),points1(2,:),points1(3,:),'r-');
hold on
fill3(points2(1,:),points2(2,:),points2(3,:),'g-');
axis equal
xlabel('x-meter')
ylabel('y-meter')
zlabel('z-meter')
legend('Earth','Aluminum panels surface', 'Perovskite solar panels surface')
title(sprintf('Distribution of the panels in the sunshade area, scenario %d,
    efficiency %.3f', sc, e))

% Mass: the magnitude mass of an aluminum solar sail panel, and of a perovskite
    panels should be around 100/200 kilos:

D1=m1/Area; % density of the aluminum solar panels [kg/m^2]
m2=d2*Area+m1;
D2=m2/Area; % density of the solar sail covered by a perovskite solar cell layer [
    kg/m^2]
Mass1=D1*Arfree(1:length(Arfree(:,sc))-1, sc);
Mass2=D2*Apan(2+length(v_eff)-1-length(Arfree(:,sc)):length(v_eff)-1, sc);


Total_mass=Mass1+Mass2;

figure()
plot(v_eff(2+length(v_eff)-1-length(Arfree(:,sc)):length(v_eff)-1), Total_mass,'
    LineWidth', 2)
hold on
plot(v_eff(2+length(v_eff)-1-length(Arfree(:,sc)):length(v_eff)-1), Mass1,'
    LineWidth', 2)
hold on
plot(v_eff(2+length(v_eff)-1-length(Arfree(:,sc)):length(v_eff)-1), Mass2,'
    LineWidth', 2)
xlabel('efficiency')
ylabel('Total mass of the sunshade')
legend('Total mass in kilos', 'Mass of aluminum panels', 'Mass of perovskite solar
     cell panels')
title(sprintf('Total mass of the sunshade, scenario %d', sc))
```

.2 Power-Mass Simulation

```
% Initial parameters
E_0 = 1e3; % Initial power from panels brought from Earth (kW)
epan = 0.3; % Power production of a single panel produced on the Moon (kW per day)
```

```
eloss = 0.00002; % Daily efficiency loss percentage (0.002%)

% Energy cost to produce a single panel (kWh)
n_mining = 15; % dispositivi di mining (1 per la produzione dei pannelli sul Solar Lunar Park principalmente e gli altri per i pannelli del Sunshade)
extraction_energy = 0.00146*n_mining; % we can extract 2400 kg/h of raw material per mining infrastructure, 2400 kg of lunar regolith with 0.2 kWh, in one day. From 2400 extracted we can produce 137 panels, in 24 hours 3288)
transport_energy = 1.0; % we transport the material to the Reactors
separation_energy = 210; % we need at least 35 reactors to process the material extracted in 1 hour, so 840 for one day, with a max production of 3360 panel per day but with one reactor we can process 13.7 kg of sylicon --> there are on average 3.5 kg of sylicon on a PV panel, so 4 panel per reactor. A single reactor needs 6 hours to process a panel, so 35*6 kWh)
assembly_energy = 35; % estimation of the real value
Eprod = extraction_energy + transport_energy + separation_energy + assembly_energy; % the order of 1MWh, it's correct in literature)
% we need 840 reactors to process all the mining material excavate in a day from 1 mining unit to create silicon solar panels

max_daily_output = 3288;  % Maximum limit of panels produced per day with lunar infrastructures
lunarpark_ny = 36;  % Number of years of panel production
lunarpark_days = 365 * lunarpark_ny;  % Panel production period (30 years)
check_interval = 365;  % Interval for energy check

% Maintenance energy consumption (5% of produced energy)
maintenance_fraction = 0.05;
maintenance_start_day = 3650; % Maintenance starts after 10 years

% Simulation settings
days = lunarpark_days;
Estart = zeros(1, days);
E = zeros(1, days);
n = zeros(1, days);
n_daily = zeros(1, days);
E_maintenance = zeros(1, days);
E_net = zeros(1, days);

% Initial conditions
Estart(1) = E_0;
E(1) = E_0;
n(1) = 0;
n_daily(1) = 0;
max_energy_reached = false;
max_energy_level = 0;

for t = 2:days
    % Decay of initial power source
```

```
    Estart(t) = Estart(t-1) * (1 - eloss);

        % Calculate total power available considering panel degradation
    E(t) = Estart(t);
    for j = 1:t-1
        E(t) = E(t) + n_daily(j) * epan * (1 - (t - j - 1) * eloss);
    end

    % Panel power contribution and degradation
    if t <= lunarpark_days
        potential_panels = floor(E(t - 1) / Eprod);
        n_daily(t) = min(potential_panels, max_daily_output);
        n(t) = n(t - 1) + n_daily(t);
    end

    if ~max_energy_reached && E(t) > max_energy_level
        max_energy_level = E(t);
    else
        max_energy_reached = true;
    end

    if max_energy_reached
        E(t) = max_energy_level;
    end

    % Maintenance cost
    if t >= maintenance_start_day
        E_maintenance(t) = maintenance_fraction * E(t);
    end

    E_net(t) = max(E(t) - E_maintenance(t), 0);
end

% Graphs
figure;
plot(1:days, n, 'b', 'LineWidth', 2);
title('Total Number of Panels Produced');
xlabel('Days');
ylabel('Number of Panels');
grid on;

figure;
plot(1:days, n_daily, 'r', 'LineWidth', 2);
title('Daily Panel Production');
xlabel('Days');
ylabel('Panels per Day');
grid on;

% Plot results
```

```
92  figure;
93  plot(1:days, E, 'g', 'LineWidth', 2);
94  hold on;
95  plot(1:days, E_net, 'm--', 'LineWidth', 2);
96  plot(1:days, E_maintenance, 'r:', 'LineWidth', 2);
97  title('Daily Available Power');
98  xlabel('Days');
99  ylabel('Power [kW]');
100 legend('Total Power Available', 'Net Power After Maintenance', 'Power for
        Maintenance');
101 grid on;
102
103 %%
104
105 mining = 2400; % kg/h for one device
106 kg_avanzo = zeros (1,days);
107 extraction_eff = 0.2; % raffination of the materials efficiency. For 2400 kg
        extracted I can use 480 kg of Sylicon, limiting factor
108
109 En_available_daily = zeros (1,days);
110
111 for g = 1 : days
112
113     kg_avanzo (g) = mining * 24 * (n_mining-1) * extraction_eff - n_daily(g) *
            3.5; % kg of mined material left over each day
114     En_available_daily (g) = E(g) - E_maintenance(g) - n_daily(g) * Eprod;
115
116 end
117
118 % Graph of kilograms of material left over (not used for Lunar Solar Park)
119 figure;
120 plot(1:days, kg_avanzo, 'r-', 'LineWidth', 2);
121 title('Available kilos to produce Panels for the Sunshade - first 35 years');
122 xlabel('Days');
123 ylabel('Sylicon [kg]');
124 grid on
125
126 kg_available = sum(kg_avanzo); % this is the material not used in the elaboration
        process
127
128 disp ('kg_available =')
129 disp (kg_available)
130
131 % Graph of power available after production of the Lunar Solar Park panels
132 figure;
133 plot(1:days, En_available_daily, 'r-', 'LineWidth', 2);
134 title('Available power daily to produce Panels for the Sunshade - first 35 years')
        ;
135 xlabel('Days');
```

```
136 ylabel('Power [kW]');
137 grid on
138
139 En_available = sum(En_available_daily);
140 e_foil_perovskite = 13; % kWh for production 1 kg about 13 kWh per kilo (45kWh for
        3.5 kg-1 panel), there will be the technology to do that
141 kg_effective = En_available / e_foil_perovskite; % how many kilos we can produce
        with the energy we have
142
143 %From the 35th year we have to use the energy to launch the created panels
144 % for the Sunshade (coilgun - 5 Wh/kg for Maheswaran thesis) and to
145 % process the aluminum panels (about 5 kWh per kilo, hypothesis
146 % based on fabrication date of perovskite)
147
148 launch_phase = 35; % years for the launch fase
149
150 E35_daily = max(E_net); % we consider the E_net available (without maintenance)
151 E35_available = E35_daily;
152
153 % to produce 24 billion kg how much energy do I need?
154 kg_al = 2.4e10;   % quantity of kg of aluminum required
155 e_foil_al = 2;
156 E35_needed_al = kg_al/365/35 * e_foil_al;
157
158 % Consider that new reactors can be as high as 3 kW of power
159 % needed according to Joule-heated Molten Regolith Electrolysis Reactor
160 % Concepts for oxygen and metal production on the Moon and Mars (2012)
161 Ereactors = 31920 * 3; % number of reactors * kW
162
163 e_coilgun_kg = 0.005;
164 E35_coilgun = e_coilgun_kg * (kg_effective/5 + kg_al/35)/365; % launch all panels
        both photovoltaic and non-photovoltaic
```

Bibliography

[1] Sebastian Fix (2021), *Master Thesis: Feasibility study of a Sunshade in the vicinity of the Sun Earth L1 Lagrange Point*, Stuttgart, DE

[2] Joan-Pau Sánchez, Colin R. McInnes (26 August 2015), *Optimal Sunshade Configurations for Space-Based Geoengineering near the Sun-Earth L1 Point*, Plos One

[3] Jianming Yang, Qinye Bao, Liang Shen, Liming Ding (October 2020), *Potential applications for perovskite solar cells in space*, Nano Energy, Volume 76

[4] Ilaria Cardinaletti, Tim Vangerven, Steven Nagels, Rob Cornelissen, Dieter Schreurs, Jaroslav Hruby, Jelle Vodnik, Dries Devisscher, Jurgen Kesters, Jan D'Haen, Alexis Franquet, Valentina Spampinato, Thierry Conard, Wouter Maes, Wim Deferme, Jean V. Manca, (1 August 2018), *Organic and perovskite solar cells for space applications*, Solar Energy Materials and Solar Cells, Volume 182

[5] Lennart K. Reb, Michael Böhmer, Benjamin Predeschly, Sebastian Grott, Christian L. Weindl, Goran I. Ivandekic, Renjun Guo, Christoph Dreißigacker, Roman Gernhäuser, Andreas Meyer, Peter Müller-Buschbaum (16 September 2020), *Perovskite and Organic Solar Cells on a Rocket Flight*, Joule, Volume 4, Issue 9

[6] Yukinori Nishigaki, Takayuki Nagai, Mitsutoshi Nishiwaki, Takuma Aizawa, Masayuki Kozawa, Kota Hanzawa, Yoshitsune Kato, Hitoshi Sai, Hidenori Hiramatsu, Hideo Hosono, Hiroyuki Fujiwara (21 January 2020), *Extraordinary Strong Band-Edge Absorption in Distorted Chalcogenide Perovskites*, Solar RRL, Volume 4, Issue 5

[7] Advanced Science News with Prof. Hiroyuki Fujiwara at Gifu University contribution (31 January 2020), *Almost 40% conversion efficiency predicted in new perovskite solar cell*

[8] C. Horton, C. Gramajo, A. Alemu, L. Williams, A. Ignatiev, A. Freundlich (13 October 2004), *First demonstration of photovoltaic diodes on lunar regolith-based substrate*, Texas Center for Superconductivity and Advanced Materials, University of Houston

[9] Sebastian F. Hoefler, Gregor Trimmel, Thomas Rath (8 February 2017), *Progress on lead-free metal halide perovskites for photovoltaic applications: a review*, Springer

[10] Atteq Ur Rehman, Sang Hee Lee, Soo Hong Lee (February 2016), *Silicon space solar cells: progression and radiation-resistance analysis*, Journal- Korean Physical Society 68(4)

[11] Dong Yang, Xiaorong Zhang, Yuchen Hou, Kai Wang, Tao Ye, Jungjin Yoon, Congcong Wu, Mohan Sanghadasa, Shengzhong (Frank) Liu, Shashank Priya, (27 February 2021), *28.3%-efficiency perovskite/silicon tandem solar cell by optimal transparent electrode for high efficient semitransparent top cell*, Nano Energy, Volume 84

[12] Team Kalkine Media (23 May 2020) *Perovskite Solar Cells possible solution to inherent problems with Conventional Solar Projects as Global Economy still looks for Solar to Power Future*, Kalkine media, Australia edition

[13] Roni Peleg (01 November 2019), *NASA working to print perovskite solar cells in space*, Perovskite-info

[14] Roni Peleg (01 December 2020), *Perovskite Solar*, Perovskite-info

[15] Roni Peleg (07 August 2020), *Perovskite solar cell production line starts operation in east China*, Perovskite-info

[16] Ron Mertens (01 June 2021), *TCI starts offering new hole selective self-assembled monolayer forming agents to boost perovskite PV performance*, Perovskite-info

[17] Carys Worsley, Dimitrios Raptis, Simone Meroni, Alexander Doolin, Rodrigo Garcia-Rodriguez, Matthew Davies, Trystan Watson (04 May 2021), *γ-Valerolactone: A Nontoxic Green Solvent for Highly Stable Printed Mesoporous Perovskite Solar Cells*, Willey Online Library

[18] Nature (22 January 2020), *Perovskites take steps to industrialization*, nature energy vol. 5

[19] Daniel Kaschubek, Matthias Killian, Laura Grill (September 2021), *System analysis of a Moon base at the south pole: Considering landing sites, ECLSS and ISRU*, Acta Astronautica, Volume 186

[20] Geoffrey A. Landis, Maria Antonietta Perino (10-13 May 1989), *Lunar production of solar cells*, Prepared for the 9th Biennial SSI/Princeton Conference on Space Manufacturing sponsored by Space Studies Institute Princeton, New Jersey

[21] Alex Ignatiev, Alexandre Freundlich, Charles Horton (30 June - 2 July 2004), *Solar cell development on the Moon from in-situ resources*, Texas Center for Superconductivity and Advanced Materials, University of Houston, Houston, Texas

[22] Daniel Pérez-del-Rey,Chris Dreessen,Ana M. Igual-Muñoz,Lennart van den Hengel,María C. Gélvez-Rueda,Tom J. Savenije,Ferdinand C. Grozema,Claus Zimmermann,Henk J. Bolink (23 September 2020), *Perovskite Solar Cells: Stable under Space Conditions*, Wiley Online Library

[23] Planetary Sunshade Foundation, (March 2023), *State of space-based solar radiation management*

[24] Matthew K. Chamberlain, Stephen H. Kiefer, Matt LaPointe, Pete LaCorte, (February 2021), *On-orbit flight testing of the Roll-Out Solar Array*, Acta Astronautica, Volume 179, Pages 407-414

[25] Luigi Giuseppe Duri, Antonio Giandonato Caporale, Youssef Rouphael, Simona Vingiani, Mario Palladino, Stefania De Pascale, Paola Adamo (04 January 2022), *The Potential for Lunar and Martian Regolith Simulants to Sustain Plant Growth: A Multidisciplinary Overview*, Front. Astron. Space Sci.

[26] Ehsan Raza, Zubair Ahmad (November 2022) *Review on two-terminal and four-terminal crystalline-silicon/perovskite tandem solar cells; progress, challenges, and future perspectives*, Energy Reports, Volume 8, Pages 5820-5851

[27] Sven Rühle (June 2016) *Tabulated values of the Shockley–Queisser limit for single junction solar cells*, Solar Energy, Volume 130, Pages 139-147

[28] A. J. De Vos (1980) *Detailed Balance Limit of the Efficiency of Tandem Solar Cells*, Journal of Physics D: Applied Physics, Vol. 13, No. 5, pp. 839-846

[29] Christer Fuglesang, María García de Herreros Miciano (2021) *Realistic Sunshade system at L1 for global temperature control*, Acta Astronautica 186, 269-279

[30] Beth Howell, Tamara Birch (20 March 2024) *Here's the world's top most polluting industries*, theecoexperts

[31] Josh Jackman, Tamara Birch (17 December 2024) *Elon Musk's rocket emitted 358 tonnes of CO_2 in a six-minute flight*, theecoexperts

[32] Brandon S. Phillips, Todd A. Schneider, Jason A. Vaughn, Kenneth H. Wright Jr. *Space Environment Testing of Photovoltaic Array Systems at NASA's Marshall Space Flight Center*

[33] Zhaoning Song, Suneth C. Watthage, Adam B. Phillips, Michael J. Heben (15 April 2016) *Pathways toward high-performance perovskite solar cells: review of recent advances in organometal halide perovskites for photovoltaic applications*, Journal of Photonics for Energy, Vol. 6, Issue 2

[34] Sultan Ahmed, M. A. Gondal, A. S. Alzahrani, M. Parvaz, Ahsan Ahmed, Shahir Hussain (February 2024) *Recent Trends and Challenges in Lead-Free Perovskite Solar Cells: A Critical Review*, ACS Appl. Energy Mater, 7, 4, 1382–1397

[35] Dickinson, T., Newsom, H. (1984) *Ge abundances in the lunar mantle and implications for the origin of the Moon*, Abstracts and Program for the Conference on the Origin of the Moon, p. 16

[36] American Institute of Aeronautics and Astronautics (2014) *Standard: Qualification and Quality Requirements for Space Solar Cells (AIAA S-111A-2014)*, Inc.: Washington, DC

[37] Lyndsey McMillon-Brown, Joseph M. Luther, Timothy J. Peshek (2022) *What would it take to manufacture perovskite solar cells in space?*, ACS Energy Letters (3), 1040-1042

[38] Ershad Parvazian, Trystan Watson (May 2024) *The roll-to-roll revolution to tackle the industrial leap for perovskite solar cells*

[39] Ellen Bausback (May 2023) *10-Month Voyage Proves Solar Cell Material Survives, Thrives in Space*

[40] T. Ibn-Mohammed, S.C.L. Koh, I.M. Reaney, A. Acquaye, G. Schileo, K.B. Mustapha, R. Greenough (December 2017) *Perovskite solar cells: An integrated hybrid lifecycle assessment and review in comparison with other photovoltaic technologies*, Renewable and Sustainable Energy Reviews, Volume 80, Pages 1321-1344

[41] Priyanka Roy, Ayush Khare, (2021) *Analysis of an efficient and eco-friendly $CsGeSnI_3$ based perovskite solar cell: A theoretical study*, materialstoday: PROCEEDINGS, Volume 44, Part 2, Pages 2997-3000

[42] G.H. Just, K. Smith, K.H. Joy, M.J. Roy (2020) *Parametric review of existing regolith excavation techniques for lunar In Situ Resource Utilisation (ISRU) and recommendations for future excavation experiments*, Planetary and Space Science 180, 104746

[43] *Sparkwing - space made easy*, Data Sheet

[44] T. Seyisi, B.G. Fouda-Mbanga, J.I. Mnyango, Y.B. Nthwane, B. Nyoni, S. Mhlanga, S.P. Hlangothi, Z. Tywabi-Ngeva (2025) *Major challenges for commercialization of perovskite solar cells: A critical review*, Energy Reports 13, 1400–1415

[45] Narayana Murty Svs, Sharad Chandra Sharma (February 2022) *Materials for Indian Space Program: An Overview*, Journal of the Indian Institute of Science

[46] Samuel S. Schreiner, Laurent Sibille, Jesus A. Dominguez, Jeffrey A. Hoffman (2016) *A parametric sizing model for Molten Regolith Electrolysis reactors to produce oxygen on the Moon*, Advances in Space Research 57, 1585–1603

[47] Ary Pizarro-Chong, L3 MAPPS, Chuan Wang, Chuang Ma, Lixian Zhang (June 2010) *Development of space nuclear reactors for lunar purposes: Overview of technical and non-technical issues*, 3rd International Symposium on Systems and Control in Aeronautics and Astronautics, Harbin, China, pp. 1339-1344

[48] Tharshan Maheswaran (April 2021) *Analysis of logistical construction aspects of a Sunshade concept in the vicinity of the Sun Earth L1 Lagrange Point*

[49] Geoffrey A. Landis (December 2005) *Materials Refining for Solar Array Production on the Moon*, NASA/TM—2005-214014

[50] David R. Criswell, Robert D. Waldron (June 1993) *International lunar base and lunar-based power system to supply Earth with electric power*, Acta Astronautica, Volume 29, Issue 6, pages 469-480

[51] Geoffrey A. Landis (May-June 2007) *Materials refining on the Moon*, Acta Astronautica, Volume 60, Issues 10–11, Pages 906-915

[52] David Schrunk, Madhu Thangavelu, Bonnie Cooper, Burton Sharpe (April 2012) *Physical Transportation on the Moon: The Lunar Railroad*

[53] P.A. Curreri, E.C. Ethridge, S.B. Hudson, T.Y. Miller, R.N. Grugel, S. Sen, D.R. Sadoway (August 2006) *Process Demonstration For Lunar In Situ Resource Utilization— Molten Oxide Electrolysis (MSFC Independent Research and Development Project No. 5–81)*

[54] Laurent Sibille, Jesus A. Dominguez (January 2012) *Joule-heated Molten Regolith Electrolysis Reactor Concepts for Oxygen and Metals Production on the Moon and Mars*, Conference Paper at the 50th AIAA Aerospace Sciences Meeting including the New Horizons Forum and Aerospace Exposition

[55] Anil D. Pathak, Shalakha Saha, Vikram Kishore Bharti, Mayur M. Gaikwad, Chandra Shekhar Sharma (May 2023) *A review on battery technology for space application*, Journal of Energy Storage, Volume 61

[56] T.S. Balint, J.A. Cutts, E.A. Kolawa, C.E. Peterson, T. Balint (2007) *Extreme Environment Technologies for In-situ Lunar Exploration*, pp. 1–24

[57] Keith Cooper (July 2024) *Moon robots could build stone walls to protect lunar bases from rocket exhaust*, SPACE.com

[58] Oleksandr Burlaka (July 2024) *Lunar base could be protected from debris by a rock wall*, Universe Space Tech

[59] Jonas Walther, Ryan Luke Johns, Hendrik Kolvenbach, Valentin Tertius Bickel, Marco Hutter (June 2024) *Autonomous construction of lunar infrastructure with in-situ boulders*, Front. Space Technol., Sec. Space Exploration, Volume 5

[60] Ambatali Charleston Dale, Nakasuka Shinichi (July 2024) *Microwave wireless power transfer efficiency analysis framework for a thin film space solar power satellite*, Advances in Space Research, Volume 74, Issue 1, Pages 454-470

[61] James Mcspadden, John Mankins (January 2003) *Space Solar Power Programs and Microwave Wireless Power Transmission Technology*

[62] Geoffrey A. Landis, (2023) *Space photovoltaics for extreme high-temperature missions*, Photovoltaics for Space Key Issues, Missions and Alternative Technologies, Pages 393-410

[63] Alex Fedoseev, Yana Gurimskaya, Stanislau Herasimenka, Michael Moll, Mikhail Reginevich, (20 June 2023) *Photovoltaics for space*, 42nd RD50 Workshop, Tivat, Montenegro

[64] Nadim Maraqten, Andrea Bari, Conall De Paor, Zoe Ashford, Yakov Bobrov , Anna Dietz, Daniel Cantos Gálvez, Inês Carriço, Daniel Friedrich, Juan Manuel Martinez Rossi, Michele Nigro, Lina Salman, Maximilian Schneider, Isabel Pitz, Tharshan Maheswaran, Prof. Dr. Gisela Detrell (2-6 October 2023) *Paradigm Change in Space Utilization: Conceptual Design Study of a Lunar Space Station for In-Space Manufacturing*, 74th International Astronautical Congress (IAC), Baku, Azerbaijan

[65] Geoffrey A. Landis (September 1994) *Review of solar cell temperature coefficients for space*, NASA Lewis Research Center, Proceedings of the 13th Space Photovoltaic Research and Technology Conference (SPRAT 13)

[66] Dechan Angmo, Shiqin Yan, Daniel Liang, Andrew D. Scully, Anthony S. R. Chesman, Michael Kellam, Noel W. Duffy, Nick Carter, Regine Chantler, Cherry Chen, Mei Gao (2024) *Toward Rollable Printed Perovskite Solar Cells for Deployment in Low-Earth Orbit Space Applications*, ACS Appl. Energy Mater., 7, 1777-1791

[67] Tharshan Maheswaran, Sebastian Fix (October 2021) *Roadmap for an International Planetary Sunshade (IPSS)*, 72nd International Astronautical Congress (IAC), Dubai, United Arab Emirates

[68] Tharshan Maheswaran, Denis Acker, Stefanos Fasoulas, Uwe Brauer (September 2022) *The International Planetary Sunshade - An Umbrella Project to Foster International Collaboration to Mitigate Global Warming*, 73rd International Astronautical Congress (IAC), Paris, France

[69] Martin Kaltenbrunner, Getachew Adam, Eric Daniel Głowacki, Michael Drack, Reinhard Schwödiauer, Lucia Leonat, Dogukan Hazar Apaydin, Heiko Groiss, Markus Clark Scharber, Matthew Schuette White, Niyazi Serdar Sariciftci, Siegfried Bauer, (August 2015) *Flexible high power-per-weight perovskite solar cells with chromium oxide–metal contacts for improved stability in air*, Nature Materials

[70] Yongguang Tu, Jiang Wu, Guoning Xu, Xiaoyu Yang, Rong Cai, Qihuang Gong, Rui Zhu, Wei Huang (April 2021) *Perovskite Solar Cells for Space Applications: Progress and Challenges*, Advanced Materials

[71] W. Z. Sadeh, M. E. Criswell (1996) *Infrastructure for a Lunar base*, Advances in Space Research, Volume 18, Issue 11, Pages 139-148

[72] Ahmad R. Kirmani, Brandon K. Durant, Jonathan Grandidier, Nancy M. Haegel, Michael D. Kelzenberg, Yao M. Lao, Michael D. McGehee, Lyndsey McMillon-Brown, David P. Ostrowski, Timothy J. Peshek, Bibhudutta Rout, Ian R. Sellers, Mark Steger, Don Walker, David M. Wilt, Kaitlyn T. VanSant, Joseph M. Luther (May 2022) *Countdown to perovskite space launch: Guidelines to performing relevant radiation-hardness experiments*, Joule, Volume 6, Issue 5, Pages 1015-1031

[73] Lyndsey McMillon-Brown, Kyle M. Crowley, Kaitlyn T. VanSant, and Timothy J. Peshek (2021) *Prospects for Perovskites in Space*, IEEE 48th Photovoltaic Specialists Conference (PVSC), Fort Lauderdale, FL, USA

[74] F. Lang, N. H. Nickel, J. Bundesmann, S. Seidel, A. Denker, S. Albrecht, V. V. Brus, J. Rappich, B. Rech, G. Landi, H. C. Neitzert (August 2016) *Radiation Hardness and Self-Healing of Perovskite Solar Cells*, Advanced Materials

[75] John F. Geisz, Ryan M. France, Kevin L. Schulte, Myles A. Steiner, Andrew G. Norman, Harvey L. Guthrey , Matthew R. Young, Tao Song, Thomas Moriarty (April 2020) *Six-junction III–V solar cells with 47.1% conversion efficiency under 143 Suns concentration*, Nature Energy

[76] Zhaoning Song, Suneth C. Watthage, Adam B. Phillips, Michael J. Heben (February 2016) *Pathways toward high-performance perovskite solar cells: Review of recent advances in organo-metal halide perovskites for photovoltaic applications*, Journal of Photonics for Energy

[77] Gulnara Ganieva (May 2024) *Silicon and its application in solar cells*, University Chemistry

[78] Alex Ignatiev, Alexandre Freundlich, Micheal B. Duke, S. Rosenberg (January 2020) *The fabrication of silicon solar cells on the moon using in-situ resources*, 40th AIAA Aerospace Sciences Meeting & Exhibit

[79] Xiangyu Li, Joseph Peoples, Peiyan Yao, Xiulin Ruan (2021) *Ultrawhite BaSO4 Paints and Films for Remarkable Daytime Subambient Radiative Cooling*, ACS Applied Materials and Interfaces, 13, 21733-21739

[80] Sebastian F. Hoefler, Gregor Trimmel, Thomas Rath (March 2017) *Progress on lead-free metal halide perovskites for photovoltaic applications: a review*, Monatshefte für Chemie/-Chemical Monthly, Volume 148, pages 795–826

[81] Lewis M. Fraasa, Mark O'Neillb (October 2019) *A Solar Power Satellite Sending an Infrared Beam from GEO to 40% Efficient Concentrating Solar Power Modules on the Ground 24 Hours per Day*, 70th International Astronautical Congress (IAC), Washington D.C., United States

[82] Lukas Hoffmann (October 2017) *O'Moon: Power production and storage for a lunar modular power infrastructure*, Master Thesis, Universität Stuttgart

[83] Shubham Bhatt, Raghvendra Shukla, Chetan Pathak, Saurabh Kumar Pandey (2021) *Evaluation of performance constraints and structural optimization of a core-shell ZnO nanorod based eco-friendly perovskite solar cell*, Solar Energy 215, 473-481

[84] Saif Ahmed, Farihatun Jannat, Md. Abdul Kaium Khan, Mohammad Abdul Alim (2021) *Numerical development of eco-friendly Cs_2TiBr_6 based perovskite solar cell with all-inorganic charge transport materials via SCAPS-1D*, Optik - International Journal for Light and Electron Optics 225, 165765

[85] Riming Nie, Aarti Mehta, Byung-wook Park, Hyoung-Woo Kwon, Jino Im, Sang Il Seok (2018) *Mixed sulfur and iodide-based lead-free perovskite solar cells*, Journal of the American Chemical Society, Vol 140, Issue 3

[86] Diego Colombara, Hossam Elanzeery, Nicoleta Nicoara, Deepanjan Sharma, Marcel Claro, Torsten Schwarz, Anna Koprek, Max Hilaire Wolter, Michele Melchiorre, Mohit Sood, Nathalie Valle, Oleksandr Bondarchuk, Finn Babbe, Conrad Spindler, Oana Cojocaru-Miredin, Dierk Raabe, Phillip J. Dale, Sascha Sadewasser Susanne Siebentritt (July 2020) *Chemical instability at chalcogenide surfaces impacts chalcopyrite devices well beyond the surface*, Nature Communications

[87] Lea Beatriz Dai-Pra, Joao Batista Dias, Amanda Gonçalves Kieling (June 2015) *Comparison between the Energy Required for Production of PV Module and the Output Energy Througout the Product Life Time*, Journal of Power and Energy Engineering 9(6)

[88] `https://sedac.ciesin.columbia.edu/ddc/ar5_scenario_process/RCPs.html`

[89] `https://www.eoportal.org/satellite-missions/iss-rosa#technology-testing`

[90] `https://www.energy.gov/eere/solar/perovskite-solar-cells`

[91] `http://www.esa.int/Enabling_Support/Space_Engineering_Technology/Building_a_lunar_base_with_3D_printing`